PLGA Implants for Controlled Release of Immune Checkpoint Inhibitors, Cpg, and Docetaxel for the Treatment of Glioblastoma

by

Jennifer M. Walker

A dissertation submitted in partial fulfillment
of the requirements for the degree of
Doctoral of Philosophy
(Pharmaceutical Sciences)
in the University of Michigan
2020

Doctor Committee:

Professor Steven P. Schwendeman, Chair
Professor Maria G. Castro
Associate Professor James Moon
Associate Professor Anna Schwendeman

Jennifer M Walker

marchijm@med.umich.edu

ORCID ID: 0000-0002-1211-6161

Dedication

To my parents, sister, Nono, and Eric. Thank you for your constant support and love. You have been my motivation and confidence in everything I do.

Acknowledgements

I would like to thank my advisor, Dr. Steve Schwendeman. Thank you for giving me the opportunity and support at UM and in your lab for the past four years. I have grown as a scientist and a person through every experience and have always been appreciative of your knowledge and your guidance on approaching problems and finding the best way to figure out a solution. I know that I have gained skills that I will take with me in my future. Thank you to Dr. Anna Schwendeman for serving on my committee and giving guidance on my project. You always go out of your way to offer advice for students in your lab and outside of your lab and we are all very lucky to have your support. To my committee members, Dr. Moon and Dr. Castro, thank you for your support and advice on my project throughout my PhD and for your work on our collaborative projects.

To my Mom and Dad, thank you for always supporting me. You have always loved me unconditionally and supported all of my ventures. I would not be who I am today without your love and your example of hard work and selflessness. I have always worked hard to make you proud and would not be here without you. To my sister, Danielle, thank you for always making me laugh, I am lucky to have a sister that is always there for me. To my husband, Eric, I cannot begin to thank you enough. This past 5 years has been a true team effort. Thank you for bearing with me on the worst and most stressful of days and being there to celebrate the good ones. You are always there to make me laugh and take a moment to put everything into perspective. I am so lucky to have you.

I have had a great time working with everyone in the Schwendeman Labs. Our lab is truly a fun and friendly group to work in, and I have been lucky to get the opportunity to work with all of you. Each of you has made an impact on my life, scientifically and personally, whether it was collaborating on a project or experiment together, travelling at conferences together, or simply waving hello every day. Thank you to Morgan and Jia for your help and for allowing me to shadow you when I joined the lab. To Rae Sung for showing me everything to do with PLGA implants and working with me on my first project. Jason, Desheng and Jing, thank you for your hard work on a very demanding collaborative project. Padma from Dr. Maria Castro's lab, thank you for always helping me when I have glioblastoma questions and for conducting our animal experiments. Corrine, thanks for spending the last few months with me, I have really enjoyed working with you and know you will do great in your future. Rose, thank you for all your help throughout the past 5 years. I am forever grateful for your help on my projects and teaching me so much, but I am easily more grateful to have gotten to know you as a friend. Karl, thank you for all of your help and friendship, you are always quick to lend a hand to everyone in our lab and make our lives easier, I hope to see you in Indy in the future! To my cubicle space past and present, Jason, Minzhi, Justin, Alex, Jay, Sang, Emily, Maria for many fun and knowledgeable chat sessions filled with sports, politics, and mostly cute pictures of animals. Nianqiu, thanks for making me laugh and always telling me how important it is to enjoy life. Alex, thanks for putting up with me and brining in snacks for the past 5 years. We survived sitting next to each other and I am happy to call you my friend. To Jay, thank you so much for being the kindest person I know and always there to support me and tell me you loved me, meeting you was one of the best things to come from my time at Michigan. I could speak to each and every one of the Schwendeman lab members that I got to work with: Jie, Greg, Ash, Yayuan,

Ling, Lisha, Hong Liang, Jason, Richard, Justin, Minzhi, Alex, Jay, Maria, Sang, Emily, Avital, Tina, Jia, Nianqiu, Jing, Desheng, Cameron, Jill, Troy, Kristen, Corrine, Tao, Lindsay, Morgan, Rae, Karthik, Max. Having a positive environment full of great people has meant so much to me, I will miss you all.

Table of Contents

Dedication ii

Acknowledgements iii

List of Tables ix

List of Figures xi

Abstract xvii

Chapter 1: Introduction 1

1.1 Background and significance 3
1.1.1 Controlled drug release from polymers 3
1.1.2 PLGA 6
1.1.3 Protein stability in PLGA 11
1.1.4 Microencapsulation 14
1.1.5 Release kinetics and mechanism 16
1.1.6 PLGA coating of implants for improved release kinetics 19
1.1.7 Antibody therapeutics 21
1.1.8 Toll-like receptor 9 agonist, CpG 29
1.1.9 Docetaxel 31
1.1.10 Glioblastoma 32
1.2 Thesis scope 41
1.3 Thesis overview 42

Chapter 2: PLGA Implants for Local Controlled Release of Monoclonal Antibodies 44

2.1 Abstract 44
2.2 Introduction 45
2.3 Materials and methods 48

2.3.1 Materials 48
2.3.2 Methods 49
2.4 Results 55
2.4.1 Immune checkpoint inhibitor implant *in vitro* release and stability characterization 55
2.4.2 Immune checkpoint inhibitor implant *in vivo* efficacy 56
2.4.3 Reduced diameter implants 57
2.4.4 PLGA-glucose STAR coated implants 57
2.5 Discussion 58
2.6 Conclusion 60
Chapter 3: Controlled Release of CpG ODN and Docetaxel 69
3.1 Abstract 69
3.2 Introduction 70
3.3 Materials and methods 71
3.3.1 Materials 71
3.3.2 Methods 72
3.4 Results 77
3.4.1 CpG implants 77
3.4.2 Docetaxel implants 79
3.5 Discussion 80
3.6 Conclusion 82
Chapter 4: In Vitro Degradation and Erosion Behavior of Commercial PLGAs Used for Controlled Drug Delivery 90
4.1 Abstract 90
4.2 Introduction 92
4.3 Materials and methods 95
4.3.1 Materials 95
4.3.2 Methods 95
4.4 Results and discussion 101
4.4.1 Effect of polymer molecular weight 101
4.4.2 Effect of polymer end-capping 103
4.4.3 Effect of formulation geometry 104
4.4.4 Effect of polymer manufacturer 105
4.5 Conclusion 113

Chapter 5: Conclusions, Significance, and Future Outlook 121

References 126

List of Tables

Table 2-1. Literature analysis of key criteria for development of long-term biodegradable dosage forms for controlled release of stabilized mAbs. Red text indicates the desired criteria was not met. The first, blue, row in each table indicates the current study. Grey rows are used to highlight most interesting results. PLGA= poly(lactic-co-glycolic acid); FLR= fluorescence; PK= pharmacokinetic; NR=not reported; HAMC= hyaluronan and methyl cellulose; SEC= size exclusion chromatography; ELISA= enzyme-linked immunosorbent assay; FTIR= fourier-transform infrared spectroscopy; CD= circular dichroism; HEMA= hydroxyethyl methacrylate; PCM= polycaprolactone dimethacrylate; pLHMGA=poly(d,l lactic-co-hydroxymethylglycolic acid); PEG= polyethylene glycol; PBT=polybutylphthalate. 62

Table 2-2. Loading of twice coated, 10% theoretical mAb core implants. 64

Table 2-3. Extracted loading of STAR coated BVZ implants. Values represent mean ± SE, n=3. 66

Table 3-1. CpG loading and encapsulation efficiency. Data represents mean ± SE, n=3-5..... 84

Table 3-2. BSA loading and encapsulation efficiency from initial implant formulation. Data represents mean± SE, n=3. 85

Table 3-3. Optimized CpG implant formulation loading and encapsulation efficiency. Data represents mean± SE, n=3 or [a]n=2. 87

Table 3-4. Solubility of Docetaxel in PBST with various amounts of ethanol. 88

Table 3-5. Docetaxel loading and encapsulation efficiency. Data represents mean± SE, n=3. 88

Table 4-1. List of polymers used and their properties. L/G ratio and end-capping as listed by the manufacturer, molecular weight as reported by the manufacturer (determined by gel permeation chromatography), inherent viscosity as reported by the manufacturer, dry glass transition temperature (T_g) as determined by differential scanning calorimetry (n = 2), and the lot number for each polymer used. Similar polymers are shown grouped together. [a]Resomer® inherent viscosity (i.v.): 0.1% in chloroform at 25°C. Expansorb® i.v.: 0.5% chloroform, 25°C. Purasorb® PDLG 5004A i.v.: 0.5 g/dL in chloroform at 25°C. Purasorb® PDLG 7502A, and Purasorb® PDL 02A i.v.: 1 g/dL in chloroform at 25°C. Lactel® i.v.: 0.5 g/dL in chloroform at 30°C. Wako® i.v. method not reported. 114

Table 4-2. Formulation vehicle starting molecular weights, apparent first order degradation rate constants and molecular weight half-lives for polymer formulations. Data represents the mean (standard error), n=3. Statistics represent unpaired t-test; * $p<0.05$. 115

Table 4-3. Apparent erosion rates and onsets for polymer formulations. Data represents average (standard error), n=3. Statistics represent unpaired t-test, *$p<0.05$. NA = Not applicable, erosion not significant enough to analyze kinetics. 116

List of Figures

Figure 1-1. Structure of lactic and glycolic acid and PLGA after direct condensation. Adapted from ref [37]. 10

Figure 1-2. Structure of lactide and glycolide used to synthesize PLGA through ring opening polymerization. Adapted from reference [37]. 11

Figure 1-3. Random and sequenced polymer examples and relative rates of hydrolysis. Adapted from reference [54]. 12

Figure 1-4. Events and mechanisms of release from PLGA. Adapted from ref [64]. 19

Figure 1-5. Typical release profiles. Phase 1 indicates the initial burst phase. Phase 2 indicates a period of slower release or lag phase where drug may be slowly diffusing out of the polymer matrix. Phase 3 indicates a period of faster release where significant mass loss may be occurring. Adapted from [64]. 20

Figure 2-1. Schematic overview of PLGA mAb implant formulation. 64

Figure 2-2. In vitro characterization of the twice coated implants. (a) Release kinetics and (b) monomer content of twice coated mAb implants from murine anti-PD-1 (●), murine anti-CTLA-4 (∇), human anti-PD-1 (■), and human anti-CTLA-4 (◇), and release kinetics for once coated implants of human anti-PD-1 (▲) and human anti-CTLA-4 (⬡). Symbols represent mean ± SE, n=2 for murine and mean ± SE, n=3 for human mAb samples. (c) Immunoreactivity by ELISA of human anti-PD-1 (■) and human anti-CTLA-4 (◇). Symbols represent mean ± SE, n=4-6. (d,e) CD spectra of (d) human anti-CTLA-4 and (e) human anti-PD-1 from extract and release

media compared to 1.5:1 (trehalose:mAb, w/w) powder formulation and control antibody (anti-PD-1 day 1 release concentration was too low for analysis). 64
Figure 2-3. In vitro bioactivity and immunoreactivity of anti-PD-1 and anti-CTLA-4. Cell-based bioactivity (bioassay) and immunoreactivity (ELISA) assays were performed for human anti-PD-1 and human anti-CLTA-4 antibodies on days 1 and 28 post in vitro release in PBST. Symbols represent mean ± SE, n=2-3. 65
Figure 2-4. Intratumoral PD-1 and CTLA-4 neutralization treatment in combination with radiation enhances survival of GBM-bearing mice. (a) Mice with GL26 tumors were implanted with blank, anti-PD-1 implant or anti-CTLA-4 implant on day 7 and administered 2 Gy/day for 10 days. (b) Kaplan-Meier survival analysis of GL26 tumor-bearing animals treated with IR in combination with blank, anti-PD-1 or anti-CTLA-4 implants. Long-term survivors from checkpoint blockade and radiation treatment strongly inhibit intracranial tumor re-challenge. (a) GL26 tumors were implanted stereotactically into the contralateral hemisphere of the long-term survivors from the anti-PD-1 + IR and anti-CTLA-4 + IR treatment groups. (c) Kaplan-Meier survival plot for re-challenged long-term survivors from the anti-PD-1 + IR and anti-CTLA-4 + IR treatment groups. Data were analyzed using the log-rank (Mantel-Cox) test. **$p < 0.01$; ****$p < 0.0001$. MS indicates median survival. 65
Figure 2-5. In vitro characterization of reduced diameter PLGA implants containing bevacizumab. a) In vitro release kinetics and b) monomer content of BVZ from reduced diameter PLGA implants with various amounts of coating. Symbols represent mean ± SE, n=2-3..... 66
Figure 2-6. Schematic overview of PLGA STAR coated, linear PLGA core implants. 66
Figure 2-7. In vitro characterization of STAR coated, linear PLGA core implants containing bevacizumab (BVZ). a) Cumulative BVZ release and b) monomer content from uncoated, 1X

STAR coated, and 2X STAR coated implants. Red dotted line represents optimized BVZ loaded PLGA implants coated with linear PLGA. Symbols represent mean ± SE, n=3. 67
Figure 2-8. Confocal images of PLGA implants. Cross sectional images of Cy-5 labelled coatings of a) 1X linear PLGA, b) 2X linear PLGA, c) 1X STAR-PLGA, and d) 2X STAR PLGA. Scale bars represent 100μm. 67
Figure 2-9. Circular Dichroism spectra of bevacizumab before and after release from linear and STAR PLGA coated implants. 68
Figure 2-10. Water uptake of linear and STAR PLGA coated implants during incubation in PBST. Water uptake of BVZ implants were determined after 1, 2, and 4 weeks of incubation. Symbols represent mean ± SE, n=3.....68
Figure 3-1. Schematic overview of initial CpG implant formulation and analyses. 84
Figure 3-2. In vitro release of CpG from PLGA implants. Cumulative release of CpG from PLGA implants made by cryomilling CpG with BSA before mixing, or mixing without cryomilling. Implants were incubated in PBST or PBSTE. CpG determined in release media by SEC-HPLC. Data represent mean± SE, n=3. 84
Figure 3-3. In vitro release of BSA from PLGA implants. Cumulative release of BSA from implants made by cryomiling BSA with CpG before mixing or by mixing without cryomilling. Implants were incubated in PBST or PBSTE and release media was monitored by SEC-HPLC. Data represents mean± SE, n=3.....85
Figure 3-4. CpG TLR9 binding activity. Reactivity of released CpG determined by incubation with TLR-9 expressing HEK293 cells using SEAP detection. Data represents mean± SE, n=3..86
Figure 3-5. 5-PL standard curves used for CpG bioactivity determination. Absorbance at 260 nm vs concentration of CpG standards incubated with TLR-9 expressing HEK293 cells after SEAP

detection. Data graphed with Prism using a 4PL sigmoidal fitting, dashed lines represent a 95% confidence interval. 86
Figure 3-6. Schematic overview of optimized CpG PLGA implant formulation. 87
Figure 3-7. In vitro characterization of optimized CpG formulation. a) Cumulative release percent b) main peak percent and c) μg released of CpG from PLGA implants incubated in PBST. CpG-1,2 and 3 formulations are described in Table 3-3. Data represents mean± SE, n=3. 87
Figure 3-8. Schematic overview of docetaxel PLGA implant formulation. 88
Figure 3-9. In vitro release of docetaxel. Total cumulative release % and total cumulative μg DTX released from PLGA implants accounting for all peaks (a,b, respectively) and accounting only for the main DTX peak only (c,d, respectively). Release samples were analyzed by RP-C18 UPLC. Data represents mean± SE, n=2. 89
Figure 3-10. In vitro characterization of released docetaxel. a) %Main peak of docetaxel released from PLGA implants, determined by RP-C18 UPLC. b) pH of release media during incubation. Data represents mean± SE, n=2. 89
Figure 4-1. Effect of molecular weight on erosion behavior in 50/50 acid-terminated PLGA films. Kinetics of water content, molecular weight (MW) loss as determined by gel permeation chromatography, and mass loss are represented for Expansorb® (a-c) and Resomer® (d-f) films, respectively. Data represents mean ± standard error (SE), n=3. 117
Figure 4-2. Effect of end-capping on erosion behavior in 50/50 PLGA films. Kinetics of water content, molecular weight (MW) loss as determined by gel permeation chromatography, and mass loss are represented for Expansorb® (a-c) and Resomer® (d-f) PLGA films, respectively.

Data for Expansorb® DLG 50-2A and Resomer® RG 502H were reproduced from Figure 4-1. Data represents mean ± standard error (SE), n=3.....117
Figure 4-3. Effect of formulation size and geometry on erosion behavior and lactic content, in acid-terminated 75/25 PLGA implants and microspheres. Kinetics of water content (a-d), molecular weight (MW) loss as determined by gel permeation chromatography (e-h), and mass loss (i-l) were determined for Expansorb® (a,e,i), Purasorb® (b,f,j), Resomer® (c,g,k) and Wako® (d,h,l) PLGA formulations, respectively. The remaining lactic content was determined for microspheres (j) and implants (k) by ^{1}HNMR. Data represents mean ± standard error (SE), n=3. 118
Figure 4-4. Effect of manufacturer on the erosion behavior and lactic content of 50/50 acid-terminated PLGA films. Kinetics of water content (a, e), molecular weight (MW) loss as determined by gel permeation chromatography (b, f, j), mass loss (c, g), and lactic content (d, h) are shown for two sets of comparable Expansorb® and Resomer® polymers in a-d and e-h, respectively, and for Purasorb (i-l). Data for Expansorb® DLG 50-2A, Expansorb® DLG 50-5A, Resomer® RG 502H, and Resomer® RG 504H were reproduced from Figure 4-1. The remaining lactic content was determined by ^{1}HNMR and actual differences relative to their raw polymer starting %lactic content were used for statistical analyses. Data represents mean ± standard error (SE), n=3. Statistics represent unpaired t-test; * $p \leq 0.05$. 119
Figure 4-5. Effect of manufacturer on the erosion behavior and lactic content of 75/25 ester-terminated PLGA films. Kinetics of water content (a), molecular weight (MW) loss as determined by gel permeation chromatography (b), mass loss (c), and lactic content (d) are shown. The remaining lactic content was determined by ^{1}HNMR and actual differences relative

to their raw polymer starting %lactic content were used for statistical analyses. Data represents mean ± standard error (SE), n=3. Statistics represent unpaired t-test; * $p<0.05$. 119
Figure 4-6. Effect of manufacturer on the erosion behavior of acid-terminated PLA implants. Kinetics of water content (a), molecular weight (MW) loss as determined by gel permeation chromatography (b), and mass loss (c) were determined for Expansorb®, Resomer®, and Purasorb® implants. Data represents mean ± standard error (SE), n=3. Representative confocal images of microspheres after 21 days of incubation (d-f) and effective BODIPY diffusion coefficients and are shown (g). Data represents mean ± standard error (SE), n=4. Statistics represent unpaired t-test; *$p<0.05$. 120
Figure 4-7. Lactic content remaining in 50/50 acid- and ester-terminated PLGA films as a function of incubation time. The remaining lactic content was determined by ^{1}HNMR and actual differences relative to their raw polymer starting %lactic content were used for statistical analyses. Data represents mean ± standard error (SE), n=3. Day 21 was used in place of day 28 for Resomer® RG 502H and Expansorb® DLG 50-2A due to significant film mass loss. Statistics represent unpaired t-test, *$p<0.05$..... 120

Abstract

Poly(lactic-co-glycolic acid) (PLGA) is the most commonly investigated biodegradable polymer for long-acting release (LAR) applications and has been used in 19 FDA-approved products. Despite this success, there has been a slow increase in PLGA-based commercial products since the first approval in the 1980s. There are no existing options for controlled release of large molecules which are far more complicated than small molecules and can undergo stability issues during or after encapsulation in PLGA.

Glioblastoma is a devastating disease with a median survival of 12-14 months and a high rate of recurrence, complicated by an immunosuppressive tumor environment with few treatment options due to the blood brain/blood tumor barriers without systemic toxicity, and thus a local sustained release option could be beneficial. To approach the immunosuppressive, heterogenic, and abnormal solid stress tumor environment of GBM we have formulated immune checkpoint inhibitors, anti-PD-1 and anti-CTLA-4, immune-stimulatory agent, CpG, and penetration-enhancer, docetaxel, into PLGA LAR implants. Coated PLGA implants achieved high loading (6-8% w/w) of anti-PD-1 and anti-CTLA-4 and released *in vitro* over 60 days with minimal monomer content, secondary structure and immunoreactivity losses. CpG implants (loading ~6% w/w) released continuously *in vitro* over 40 days with >95% cumulative release and showed retained TLR-9 binding activity. Docetaxel implants (loading ~50% w/w) released over 110 days with >80% total cumulative release. Anti-PD-1 and anti-CTLA-4 implants combined with radiation resulted in enhanced median survivals of 71 days and 74 days, respectively, relative to

controls. Two long-term survivors from each mAb group were resistant to tumor cell re-challenge, indicating the generation of an immunological memory response.

To bridge the gap between slow development of FDA-approved controlled release products using PLGA, including those for delivery of large molecules, we investigated 17 different PLGAs from five different manufacturers and compared their *in vitro* degradation and erosion behaviors as drug-free films, microspheres, and implants as a function of L/G ratio, MW, end-capping, manufacturer, and formulation geometry. We found that comparable PLGAs from different manufacturers could vary in their *in vitro* performance due to differences in their microstructural properties and possibly their manufacturing conditions. Higher glycolic sequence blockiness or block lengths, led to increased initial degradation due to the increased hydrolysis rate of glycolic-glycolic linkages. We found that the increased auto-catalysis preferentially increased the loss of glycolic units over lactic units in 75/25 PLGA implants compared to microspheres, with implants becoming ~97% lactic acid within two weeks, while microspheres only gradually lost glycolic units faster than lactic units, indicating differences in their hydrolytic mechanisms. Better knowledge and control of relevant macro/micro-properties of the polymer may help bridge the gap between the effects of raw materials and the product performance, allowing for better polymer selection and potentially increase the number of approved PLGA-based LAR products.

This thesis develops PLGA LAR implants for monoclonal antibodies, which are injectable through a small gauge needle. The implants are applied to five different drugs, and exhibit high drug loading, ideal slow and continuous release over months, maintained stability, efficacy in a glioblastoma model and investigates formulations for intraocular delivery. To address the disproportion of LAR products available on the market, and especially lack thereof

for large molecules, this work investigates the effects of PLGA raw material on performance behavior and establishes key differences between manufacturers and effects of macro/micro-properties of PLGA on degradation and erosion.

Chapter 1: Introduction

Glioblastoma (GBM) is the highest occurring primary brain tumor with a median survival of 12-14 months and a high rate of recurrence[1,2]. GBM tumors are highly heterogeneous and have immune suppressive properties that hinder therapy[3]. The blood brain barrier (BBB) and the blood tumor barrier (BTB) are both significant obstacles for current systemic therapies. Systemic treatments do not easily reach the brain, and thus, therapeutics must be given in high concentrations which can pose toxic side effects. Numerous methods have been studied to disrupt the BBB to improve the systemic delivery of drugs to the brain, but are impractical, unsafe, or suffer from inadequate drug accumulation at the tumor site[4–6]. The effective treatment of GBM is also hindered by the glioma tumor's ability to evade the immune system by the overexpression of immune checkpoint inhibitors such as CTLA-4 and PD-1[7]. It has been demonstrated that the ligands for PD-1 and CTLA-4, i.e., PD-L1 and CD80, are expressed by tumor cells, myeloid derived suppressor cells, and other various immune cells, and that PD-1 expression on T cells is a marker of T cell exhaustion leading to dysfunctional T cells[8,9]. These effects lead to immunosuppression that, if blocked, can enhance long-term survival in glioblastoma animal models when administered systemically[8]. PD-1 and CTLA-4 blockade monoclonal antibodies (mAbs) are the two most commercially developed products. Yervoy® (ipilimumab, anti-CTLA-4) and Opdivo® (nivolumab, anti-PD-1), both approved for various cancer treatments, are currently undergoing clinical trials for the treatment of GBM, and have demonstrated success in animals as well as tolerability in humans with high-grade gliomas.

Although there is promise for immune checkpoint blockade therapy, there are issues with toxicity due to the selectivity of the blood brain barrier, creating potential difficulties balancing therapeutic levels in the brain with the systemic induced toxicities. Systemic delivery of immune checkpoint inhibitors alone, and more so in combination with each other, lead to immune related adverse events that often require termination of treatment or the addition of medications to combat side-effects[3,10]. For this reason, controlled release is an advantageous option, offering local and long-term delivery of therapeutic levels while avoiding the systemic toxicity. Polymeric delivery systems are successfully used to deliver proteins and peptides that would benefit from controlled release[11–14]. Poly(lactic-co-glycolic acid) (PLGA) is a biodegradable polymer that is used for long-term controlled release delivery of proteins and approved in many long-acting release drug products[11,14–16]. Our approach to improve therapeutic outcomes for GBM, involves locally delivering immune checkpoint inhibitors to block immune suppressive signals and improve their delivery and efficacy with the aid of tumor penetrating enhancing agent, docetaxel, and immune stimulatory agent, CpG. The combination of these therapies will be further improved through local delivery using PLGA controlled release implants as a platform. PLGA is not easily formulated to encapsulate high levels of mAbs for slow release while avoiding significant loss of protein activity. However, we have previously optimized the delivery of complicated molecules with judicious formulation adjustments[11,17–24]. Herein, we have developed injectable implants that efficiently encapsulates ~7% w/w mAbs and slowly release stable drug for > 6 weeks. These formulations overcome difficulties to stabilize protein during encapsulation and release by protecting the mAb from harsh organic solvent/water interfaces, the addition of a poorly soluble base to avoid an acidic microclimate, the addition of stabilizing disaccharide to inhibit mAb unfolding/aggregation and protect during

cryomicronization, and apply a PLGA coating around the drug-loaded core to obviate osmotic pressure caused by the critical trehalose stabilizer and reduce the high initial burst release. Our approach will allow for local sustained release of anti-PD-1, anti-CTLA-4, CpG, and docetaxel in order to improve the drug exposure at the tumor site while avoiding systemic toxicities.

PLGA is the most commonly used biodegradable polymer for controlled release, yet, there are only ~19 FDA approved products using PLGA and no available generic options for any of these medications despite many patent expirations. The complexity of manufacturing variables and influence of raw materials contributes to the overall slow approval of PLGA-based products[15]. It is not well-understood how and why polymers differ between manufacturers or across different batches and to what extent this can affect product performance. Better knowledge and control of the relevant properties of the polymer may help bridge the gap between the effects of raw materials and the product performance and could potentially increase the number of approved PLGA drug products. In this thesis we approached this knowledge-gap by investigating 17 different PLGAs from five manufacturers and investigated differences in their water uptake, degradation, and erosion behaviors during incubation as a function of L/G ratio, molecular weight, end-capping, and formulation geometry and have also evaluated the differences in a lesser-investigated property, sequence distribution of glycolide/glycolic acid, for these polymers and how this can affect *in vitro* performance and ultimately, how these variables could potentially influence drug release.

1.1 Background and significance

1.1.1 Controlled drug release from polymers

Over the past few decades, controlled release delivery has been of interest across multiple engineering and pharmaceutically based fields due to its great potential in improving the

effectiveness of therapies. Controlled release can improve the effectiveness of a therapy in multiple ways: by achieving targeted and local delivery of drugs that are difficult to administer or control their therapeutic levels, decreasing unwanted side effects, improving patient compliance and drug availability to communities by lowering the number of painful injections and hospital visits for treatment. Temporal controlled release is focused on delivering the drug over an extended period and is specifically beneficial for drugs that have a short circulation half-life. With temporally controlled release therapies, the drug releases slowly and stays within the therapeutic window longer, over a period that would normally require multiple administrations of the drug. Distribution controlled release focuses on delivering the drug to a specific site like the tissues, the systemic circulation, or a tumor cell, and can also be over extended periods of time. This type of release is beneficial in avoiding toxic side effects that occur when the drug accumulates in an unwanted area and can increase efficacy by distributing the drug preferentially to the site of action. Many controlled release systems are a combination of temporal and distribution controlled and can be manipulated to control the release rate or site of release of a drug by changing the type of polymer, using various signals such as pH or a magnetic field to trigger the release, or by implanting at the site of action.[25] Examples that focus on local/regional controlled-release include intravaginal rings releasing contraceptives and preventive drugs for sexually transmitted diseases[26,27], drug-eluting stents for the treatment of peripheral artery disease[28,29], and intra-articular extended release formulations for osteoarthritis knee pain.[30] To achieve controllable release of drugs, many different natural and synthetic polymers have been studied and considered for drug delivery systems.[31] Natural polymers such as bovine serum albumin, collagen, gelatin and hemoglobin are all biodegradable and have been used in various commercial products, but have drawbacks such as batch to batch variability, poor mechanical

properties, and limited processing abilities.[32] Synthetic biodegradable polymers, such as PLGA, offer a possible alternative to the natural polymers and avoid the difficulties that exist with natural polymers.[31] Biodegradable polymers are often chosen due to their potential for elimination after their degradation. Degradation is a chemical process that occurs through bond cleavage while erosion is a physical-chemical process resulting in loss of polymer mass. Erosion can be further classified as either surface or bulk erosion. . Surface erosion is where the polymer's surface erodes faster than the interior. One concept put forward is that surface erosion occurs because of the polymer erodes at a faster rate than the water permeation into the polymer, leading often times to a zero-order drug release.[25] Another possibility is that the polymer at the surface completely degrades to form insoluble monomers, which are slow to release owing to a pH gradient at the surface which suppresses dissolution of the diacids (often p-carboxyphenoxy propane and sebacic acid).[33] In bulk erosion, water permeates the polymer faster than the polymer erodes, leading to more complex release kinetics. In bulk erosion, water permeates the polymer faster than the polymer erodes, leading to more complex release kinetics. Most biodegradable polymers undergo bulk erosion.[25] Different types of polymers include: poly(esters), poly(ortho esters), poly(anhydrides), poly(amides), and phosphorous-containing polymers. Of these polymers, the most studied for drug release are the poly(esters). Poly(esters) undergo bulk erosion and include the well-known examples: poly(lactic acid) (PLA), poly(glycolic acid) (PGA), and the copolymer poly(lactic acid-co-glycolic acid) (PLGA). This family of poly(esters) also includes poly(ethylene glycol) (PEG), which is often used to increase circulation time since PEG is a hydrophilic compound and hydrogen bonds with water, decreasing the protein adsorption processes. Poly(ortho esters) are an important class because they release drug through hydrolysis and surface erosion allowing well controlled drug release.[34]

The poly(anhydrides) undergo surface erosion that creates a heterogeneous disappearance of the surface and system and has been thought to be desirable for the maximum control of release from these polymers.[35] Poly(amides) are a class of polymers that include the poly(amino acids), used for low molecular weight drug formulations that are expensive and difficult to make but were first investigated because they are completely natural monomeric building blocks for polymers that would have little to no toxicity in the body. The poly(amino acids) are limited because the use of three or more different amino acids can result in immunotoxicity and their materials are functionally poor for fabricating delivery devices.[35] The phosphorus-containing polymers degrade predominantly through the changes in their side chains as opposed to changes in the polymer backbone like other polymers, making them functionally different depending on what side chain is chosen.[25] Of the high number of choices for polymers, most do not reach clinical trials or FDA approval due to high cost, poor functionality, or toxicity risks.[14]

1.1.2 PLGA

1.1.2.1 Synthesis

Although PLGA itself is not FDA-approved, it is used in 19 FDA approved products, and has properties that can be easily manipulated for a range of degradation and erosion rates. [14,15,36] PLA, PGA, and PLGA are all poly(esters) of monomers, lactic and glycolic acid, that are biocompatible and biodegradable.[31] Lactic acid and glycolic acid are both present in nature to a certain extent and through direct condensation can be polymerized into PLGA (Figure 1-1). Lactide and glycolide, cyclic diesters, are often used in ring opening polymerization (ROP) to synthesize high molecular weight PLGA using various catalysts and initiator species (Figure 1-2). Direct condensation, or polycondensation, is a simple method of synthesizing PLGA by reacting the two acid monomers, with or without the need for a catalyst, in either the solid or

solution state. In the solid state, the polymerization reaction of the two acid monomers, lactic acid and glycolic acid, is in competition with the depolymerization into the dimers due to the generation of water in the reaction which requires high temperatures and vacuum to control. For this reason, direct condensation can typically only obtain lower molecular weight polymers and is used far less commercially.[37,38] ROP is the most commonly used method for commercial PLA/PLGA synthesis. ROP involves the reaction of lactide and glycolide dimers in the presence of a catalyst and initiator species at around 130-220 °C for 2-6h.[37,38] The most used and accepted catalyst is stannous octoate, which is used as a food additive, and co-initiators are typically various alcohols, or even lactic acid itself. The reaction most likely proceeds through a coordination-insertion mechanism with the following main steps: i) stannous-octoate reacts with an hydroxyl containing species, the co-initiator, to form the true initiator, tin alkoxide, ii) lactide or glycolide coordinates with the lewis-acid metal center, iii) lactide or glycolide inserts in the metal alkoxide bond via a nucleophilic attack, and iv) ring opening occurs via acyl-oxygen cleavage, this process continues for each monomer insertion.[37] The type of catalyst is important because it can be influential in the chain growth process. Metal catalysts can have more than one reactive site that could result in more than one chain growth and a clustering of the polymer and metal causing a broadening of the molecular weight, thus, single-site catalysts are often exploited in polymerization.[39] The increasing of the polymer average molecular weight is dependent upon the rate of chain propagation and chain initiation.[37,39,40] The peak molecular weight is achieved through a balance of the reaction time, temperature, and amount of catalyst present. The conversion of monomers into the growing polymerization is in competition with depolymerization at longer reaction times and higher temperatures, thus, a peak conversion exists at optimal reaction times and temperatures where increasing either will result in lower molecular

weights.[41] Similarly, as you increase the amount of catalyst the conversion of monomer to polymer chain increases, but past an optimal catalyst amount, more initiator species are formed which lowers the overall molecular weight and broadens the chain dispersity.[41] The polymer chain termination can be unmodified, acid-terminated, or modified, typically ester-terminated. The type of chain termination is typically determined by the initiator species used or the chain transfer molecule used at the end of the reaction. Alcohols or water are used to terminate in a carboxylic acid, and varying alkyl esters, such as lauryl esters, are used to create an ester-terminated polymer.[42–44] A capped or modified PLA/PLGA has an alkyl ester at its chain terminus that is more hydrophobic than an uncapped, carboxylic acid end group. The presence of residual monomer in the polymer increases the number of terminal carboxylic acids that can initiate auto-catalyzed hydrolysis, and acts as a plasticizer, increasing polymer chain mobility and lowering the glass transition temperature, all of which can increase the hydrolysis and degradation rates.[45,46] After reaction completion, the catalyst is removed or deactivated, and the product is purified by reprecipitation and drying under vacuum which can remove residual monomers.[47]

1.1.2.2 Monomer sequence

Lactide has two stereocenters that results in three different conformation possibilities for starting materials, stereopure (D,D or L,L) racemic (50% mixture of D,D and L,L), and meso (D,L dimer) that have drastic effects on the polymer physical properties such as glass transition and melting temperature.[48] Typically, in drug delivery, the racemic form of lactide is used to avoid crystallization. PLA can therefore have different enantiomer sequence distributions, or tacticities, such as isotactic, syndiotactic and atactic resulting from differences in the selectivity of isomer addition to the growing polymer chain.[49,50] The stereoselectivity of addition to the

polymer chain is thought to be controlled by two mechanisms, i) chain end control where the last unit of the chain controls the next addition and ii) enantiomorphic control where the chirality of the catalyst controls the next addition.[39,50] PLA synthesis using stannous octoate has been shown to result in both atactic (random pattern of enantiomers) and also to have degrees of syndiotactic, or alternating, sequences.[47,51] The effect of the tacticities on polymer degradation and erosion is not as well known, but would be expected to affect the polymer physical properties which could lead to differences in behavior. During polymerization, glycolide/glycolic acid monomers are more reactive and add to the growing polymer chain easier than lactic monomers, which often leads to larger blocks of glycolic linkages than lactic linkgages.[37,52] This is described as the monomer sequence distribution and can influence the degradation rate of PLGA because of increased reactivity of glycolic linkages to hydrolysis (Figure 1-3).[49,53,54] Previously, Vey et al. determined that the glycolic unit consistently hydrolyzes 1.3 times faster than the lactic unit across different L/G ratio polymer films submerged in phosphate buffer.[55] It has been shown that random polymers, polymers with 'blocks' of lactic and glycolic units, have increased swelling and faster erosion compared to 'sequenced' polymers that have a controlled sequence of monomers.[53] These properties can ultimately translate to drug release, Li et al. showed that microspheres of sequenced PLGA released rhodamine-B, a low molecular weight hydrophilic dye, more gradually and consistently compared to microspheres made from random PLGA.[53] The sequenced-controlled polymers are more tedious to synthesize and high molecular weights are more difficult to obtain, and thus, have not been adopted into commercial production.

1.1.2.3 PLGA attributes

Lactic acid is more hydrophobic than glycolic acid, so when a copolymer of has a higher content of lactic acid, the more hydrophobic the copolymer is. The hydrophobic properties make the copolymer less able to absorb water and hence they degrade slower[31], although the additional methyl group is also expected to create steric hinderance for nucleophilic attack of the carbonyl carbon of the ester bond in the polymer. PLGA containing 50% or less of glycolic acid is soluble in many organic solvents, while PGA (100% glycolic acid polymer) is not soluble in many common organic solvents.[37] The mechanical strength of the polymer is a main contributor to its ability to be formulated into a drug delivery system. The system needs to be able to withstand the physical stress inside and outside of the body during formulation and degradation of the drug delivery device. The mechanical strength of PLGA is affected by its chain structure, molecular weight, composition (lactide/glycolide ratio), and its crystallinity[31]. The glass transition temperature (T_g) of PLGA is above 37°C, physiological temperature. However, the T_g can decrease once the polymer phase has rapidly equilibrated with plasticizing agents or water molecules either in formulation processes or the interstitial fluid once administered *in vivo*.

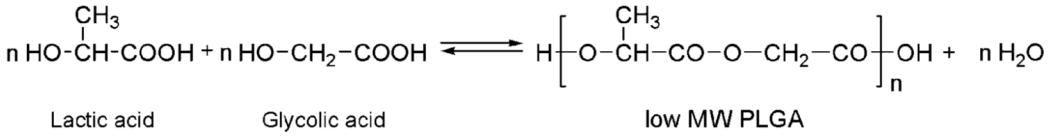

Figure 1-1. Structure of lactic and glycolic acid and PLGA after direct condensation. *Adapted from ref [37].*

Degradation of PLGA occurs once in contact with an aqueous environment causing swelling. Then, through hydrolytic chain scissions resulting in an increase in the number of carboxylic acid groups present, the process of biodegradation continues and the produced carboxylic acids autocatalyze degradation of the polymer[31]. Once the polymer starts to degrade, the lactic acid products released by in the body get converted to carbon dioxide and water by the tricarboxylic

acid cycle and are eliminated as such. Glycolic acid can either be excreted by the kidney as glycolic acid or can enter the tricarboxylic acid cycle and be eliminated as carbon dioxide and water, similar to lactic acid[31]. PLGA 50/50 is the fastest degrading of the copolymer and increasing either the lactic or glycolic content will result in slower degradation, although PGA is not commonly used for drug delivery because ultimately the increase in crystallinity leads to decreased in vivo degradation.[37] PLGA can be sterilized by γ- or β- radiation, but may result in a decrease in its molecular weight and mechanical strength and affect its general degradation properties.[56] Ethylene oxide has also been used to sterilize PLGA with little or no adverse effects.[37] PLGA has been of the most interest due to its tunable properties for release from months to 2 years, its biocompatibility and common use in pharmaceutical long-acting release depots, and the ability to stabilize PLGA encapsulated proteins when appropriate pH-control measures are taken.

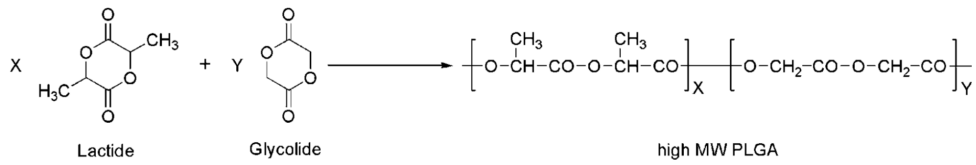

Figure 1-2. Structure of lactide and glycolide used to synthesize PLGA through ring opening polymerization. *Adapted from reference [37].*

1.1.3 Protein stability in PLGA

Despite numerous FDA-approved products using PLGA, there are no long acting release products for proteins or larger molecules due to their complexity and potential for degradation. It

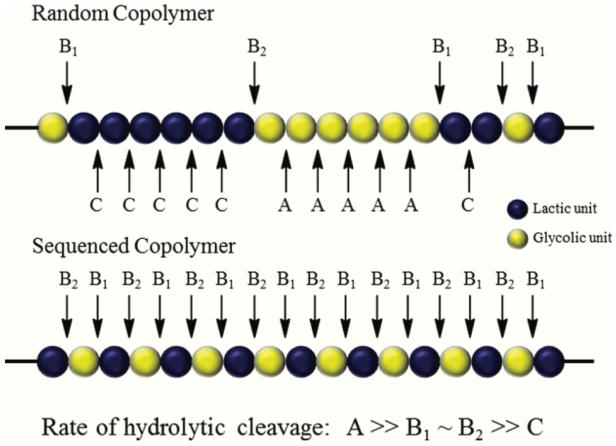

Figure 1-3. Random and sequenced polymer examples and relative rates of hydrolysis. *Adapted from reference [54].*

is important in protein therapeutics and formulation that the protein retain its native structure, which can be very complex. Protein instability can result from many different factors and at many stages of protein development including, the formulation and manufacturing process, administration to the patient, and the exposure to the biological system. During manufacturing and formulation, proteins are exposed to high stress conditions that can damage their structure, such as contact with mixtures of aqueous and organic solvents, temperature extremes, agitation, and other excipients. Once a protein is administered, it is immediately exposed to biological conditions that include an increase in temperature as well as exposure to moisture within the polymer matrix, both of which can destroy a protein and affect its funtion.[57] Once inside the body, the polymer system delivering the protein begins to degrade and can cause a change in the microenvironment leading to protein degradation[58]. To stability, the underlying mechanism of instability needs to be determined. For example, is the polymer breakdown causing a pH drop, which is contributing to the degradation of the protein? Next, there are a couple options in dealing with the instability and stress: namely, either to minimize the stress, or to directly inhibit the underlying mechanism.

Stability issues arise during the encapsulation, storage and release of protein in PLGA formulations. Encapsulation of a protein in PLGA often includes contact with water, which can make the protein more mobile and more susceptible to denaturation than when in the immobilized solid state. This process also requires dispersion of the protein into a microparticulate or an emulsion, which can involve large hydrophobic surface areas leading to protein unfolding. The protein is also exposed to different organic solvents and added excipients as well as a drying step at the end to remove water or solvents, all potential sources of instability. During *in vitro* release, there are numerous factors that can contribute to instability of the protein including: moisture, temperature, pH, buffer, container interface. As water enters the polymer matrix, it causes the PLGA to swell from between 20 to over 100 percent of its initial weight. This water uptake causes mobility of the protein that can increase the likelihood of instability pathways to occur. Another important issue in this topic is the pH in the microclimate of the PLGA and protein matrix. The pH is known to decrease in the pores of the PLGA due to the breakdown of the PLGA into its acidic components, lactic and glycolic acid. This drop in pH can induce instability of proteins unless prevented by the addition of basic excipients. Another issue that could be occurring is the protein adsorbing to the polymer surface and undergoing a conformational change in a reversible or irreversible fashion[57].

To properly address potential protein instability, it is important to know the stress responsible as well as the mechanism, this can be elucidated through experimenting with a model protein that would narrow down an instability pathway to just the one or more operative mechanisms. Another way to begin working out the mechanism of instability is to simulate the stresses that could be occurring or to monitor the protein interaction with the polymer through noninvasive techniques such as FTIR spectroscopy so not to damage the protein by trying to

remove it from the polymer. In certain polymer matrices such as microspheres, the matrix is extremely small, making analysis and characterization difficult. In this case, it is often useful to use an alternative polymer matrix to better investigate the instability issues. The pathways and mechanism of instability can change when moving from one matrix to another, so it is also important to verify the findings in the actual polymer matrix of interest[57].

1.1.4 Microencapsulation

Drug delivery by PLGA is the most studied of any other polymer and thus multiple different platforms of PLGA drug delivery have been developed. These deliver platforms include microparticles, nanoparticles, in situ forming devices, and implants[31]. The focus for this discussion will be on microspheres and implants and their formulation techniques. For this purpose, the formulation of these two techniques can be broken up into two categories: encapsulation with and without the presence of water. Encapsulating proteins into microspheres often occurs by dissolving the protein in an aqueous solution and mixing this with PLGA dissolved in organic solvent. This process can be achieved by a few different techniques: solvent evaporation (single and double emulsions), phase separation (coacervation), and spray drying. One disadvantage of the common microparticle system is the contact with organic solvents and the water/oil interface, providing multiple deleterious avenues to proteins and peptides[57]. PLGA implants have many advantages over microspheres in their preparation, high encapsulation efficiencies, stabilizing abilities, and in vivo delivery and removal options. Implant preparation is anhydrous and does not involve water/oil interfaces that can cause protein degradation. Implants are typically 0.5-1.5 mm in diameter and can vary in length and the duration of release[12]. Implants can also be implanted at their site of action, are retrievable after implantation, and are appealing for local delivery, especially in the brain or eye where it may be difficult for other

therapies to be efficacious. Two types of cylindrical polymer implant products have been FDA approved, Ozurdex®, an intravitreal implant containing dexamethasone, and Rolodex®, an implant releasing a gonadotropin releasing hormone agonist (GnRH), goserelin[59,60]. The formulation of implants is also simple and encapsulation efficiency is typically very high, >80%. Preparation can be achieved by methods such as hot melt extrusion, solvent extrusion, and compression molding[31,61]. Our lab has optimized a solvent extrusion method which involves dissolving the polymer in acetone and mixing the solid drug and any excipients until fully homogenous. Then, the mixture is extruded through silicone tubing with various diameters to form the implant shape, and then dried at elevated temperature and pressure to remove the solvent. The drug is never in contact with water during the preparation and does not need to be dried under freeze-drying conditions, both of which cause protein damage[12,62]. The extrusion process is also appealing for commercialization since it can be a continuous process and the implants can easily be reproduced in size, shape and content[36]. In our lab, we have further improved the implants by developing a technique of coating them with PLGA so that they can achieve optimal controlled release. Previously, we have shown that the controlled release of the monoclonal antibody therapeutic, bevacizumab, can be achieved when coated with a layer of polymer at an optimal concentration[16]. This technique has previously been done by Zhang et al., where they showed the inner core of their coated implants degrades much faster than the outer core under release conditions[63]. The drug release is dependent on the implant size, drug loading, and drug particle size. Increasing the length of the implant resulted in a slower release rate. As the drug loading increases, the extent of release also increases. Finally, by increasing the particle size, the implants reach their full release quicker than a smaller particle size[63]. These properties,

the ease of preparation, and the high efficiency of making implants an ideal polymer delivery device.

1.1.5 Release kinetics and mechanism

The process of drug release and polymer erosion from PLGA matrices begins with water diffusing into the polymer matrix inducing hydrolysis of the ester bonds. As ester hydrolysis continues, this creates more and more acid end groups which can also catalyze ester hydrolysis. This ultimately leads to a reduction of molecular weight and once the molecular weight gets low enough to produce water soluble oligomers and monomers (~1 kDa), these can diffuse out of the polymer, leading to mass loss.[64,65] The extent and time course of these events can be altered by changing the polymer properties and/or the formulation device properties, such as the polymer L/G ratio, the molecular weight, and the end capping, the most commonly manipulated variables when selecting a polymer for drug delivery. Properties such as the glass transition temperature (T_g), monomer sequence distribution, tacticity, type of end cap or residual monomer are not typically used to select polymers for drug delivery but can also affect the polymer mobility and hydrolysis rate which will ultimately affect drug release.[42,47,49–51,53,54,66,67]

Drug release from PLGA typically occurs through a combination of mechanisms such as: diffusion through water-filled pores, diffusion through the polymer, osmotic pumping, and erosion (Figure 1-4).[64] Diffusion through water-filled pores is a likely dominating mechanism for peptides or proteins that are water soluble and too hydrophilic to be transported through the polymer phase. Drug molecules can be transported through the water-filled pores and channels by diffusion driven by random movements and a concentration gradient, or by osmotic pressure created by an influx of water without swelling of the polymer system. Typically, PLGAs have mobile polymer chains that allow for rearrangement and swelling of the device upon hydration.

Drug can also be released without transport because of polymer erosion. Erosion can also help to increase drug transport by creating more pores within the polymer device.[64] These mechanisms can all be happening to result in drug release, with one or more dominant mechanism possible. Controlled drug release over time profiles generally have three phases (Figure 1-5), an initial burst phase, a lag phase, and an active erosion phase. These phases can all be distinctly present, overlapping, or not present at all. The initial burst phase can occur over one to several days and is generally the release of the drug that is not encapsulated or is present at the surface of the polymer matrix and can easily diffuse out of the matrix. During the lag phase, barely any drug release is seen due to the lack of polymer degradation or erosion and there is very little diffusion of protein through the pores of the matrix. In the last phase, polymer is actively degrading and eroding and drug is being released continuously through transport or from erosion. The release kinetics are governed by a combination of competing rates. The first is the rate at which water can enter and hydrate the polymer matrix and thus create pores and increase the chain mobility of the polymer. Once the polymer is hydrated, drug can more easily diffuse out if it is readily soluble. The second competing rate is the process of the pore network in the matrix connecting and forming cracks or opening and making pathways for drug to diffuse out of the polymer. The third competing rate follows with the ability for the drug to diffuse out of the polymer through the formed pore network. The last competing rate is the pore closing or healing of the polymer, preventing or inhibiting drug transport. Specifically, for cylindrical implants, there are three common release mechanisms controlled by: diffusion, osmotic pressure, and degradation[68]. The drug particles should be uniformly mixed and distributed throughout the implant. Upon hydration, these particles can either form a water pore around itself and be isolated, or multiple pores can become connected to form water channels that can create a pathway out of the polymer

implant. If the drug particle resides in a water pore but it is not connected to any other water pore or channel, then it is not releasable through diffusion by the water pathway. If multiple water pores connect and form pathways to each other and to the polymer surface, the dissolved drug can be released through the interconnected pores that have formed to the surface of the implant. This release is controlled by a percolation threshold where increasing the drug loading achieves a higher threshold that eventually will lead to a higher fraction able to release by diffusion. In osmotic pressure control, water enters the polymer matrix and increases the osmotic pressure and force, helping to pump drug out of the device through any openings that are available. If there are no pathways available for the drug to be released and no swelling occurs in the polymer device, the osmotic pressure will continue to increase and form cracks and rupture the implant. Drug release in this case will depend on the osmotic pressure and the strength and thickness of the polymer wall. When the polymer starts to degrade at low molecular weights, the drug can be released through degradation pathways[68]. Since PLGA degrades through bulk erosion[25], the drug release in implants is not expected to be governed solely by degradation for highly water-soluble drugs. At first, the polymer begins to degrade immediately as water enters the polymer and causes swelling and new pore formation which allows for an initial burst of drug release. Gradually, the molecular weight of the polymer decreases and the polymer begins to erode[64,68]. To achieve sustained and gradual release, the implant release should not depend only on diffusion through water channels, it should involve osmotic pressure, which may only occur at the beginning of hydration before the polymer chains become more mobile and allow for significant swelling. To do this, the loading of the implants should be below the percolation threshold so that osmotic pressure can induce diffusion through the water channels which

requires more time[63]. This manipulation of the release kinetics of implants requires optimization for each case, but overall, the release properties of implants is quite adjustable.

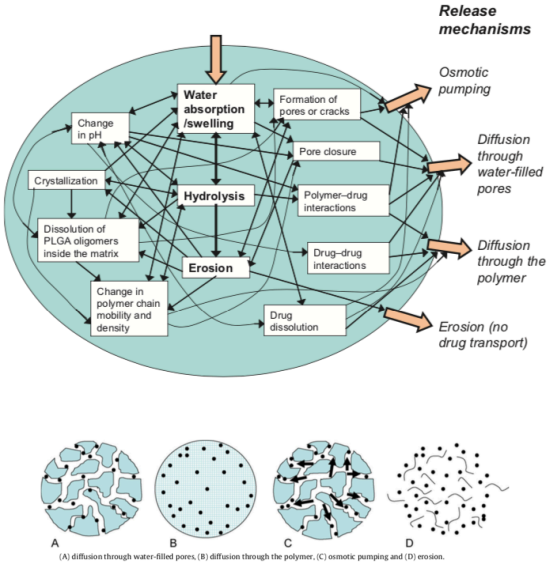

Figure 1-4. Events and mechanisms of release from PLGA. *Adapted from ref [64].*

1.1.6 PLGA coating of implants for improved release kinetics

PLGA has been widely used to coat various materials and devices to help sustain and control drug release. Kim et al used a PLGA coating to sustain the release of paclitaxel from expanded polytetrafluoroethylene (ePTFE) grafts. They showed that by increasing the concentration of the PLGA in the coating, the release was slowed down[69]. Drug eluting stents (DES) have often used biodurable polymers for coating and for prolonged and local release of drugs. However, unwanted side effects can occur, such as partial drug release or intact polymer coating remaining after drug release, causing adverse reactions such as hypersensitivity and thrombosis. Zhu et al discussed the complex nature of polymer coating degradation and how PLGA properties such as polymer molecular weight, porosity, and diffusivity can be manipulated

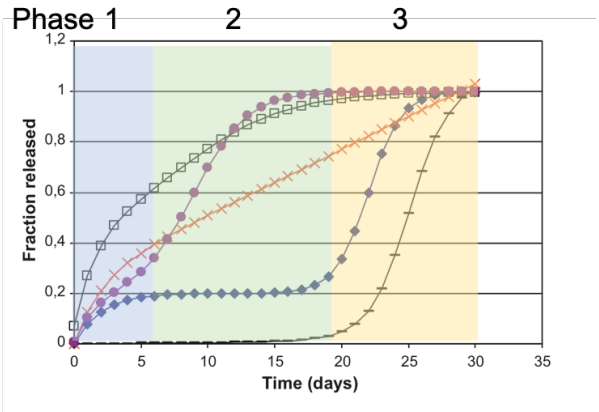

Figure 1-5. Typical release profiles. *Phase 1 indicates the initial burst phase. Phase 2 indicates a period of slower release or lag phase where drug may be slowly diffusing out of the polymer matrix. Phase 3 indicates a period of faster release where significant mass loss may be occurring. Adapted from [64].*

to control the stent coating and can also be applied for related PLGA encapsulated systems[70]. Wang et al, also showed how PLGA can be used to control the release of drug, particularly by using multi-layer PLGA coatings that differ in content. They showed that a tri-layer PLGA coating consisting of a base layer of PLLA, a drug loaded PLGA 53/47 layer, and finally a PLGA 50/50 layer slowed release of sirolimus due to inhibition of water diffusion into the drug-containing layer[71]. Our lab has developed and performed coating of implants containing high levels of bevacizumab and stabilizing excipients using ester terminated PLGA 50/50 of moderate molecular weight (0.64 inherent viscosity) for both the drug-loaded core of the implant and for the outer, drug-free PLGA coating.[62] Results from this show that implants coated with PLGA showed a lower initial burst release and slower, more continuous, zero-order release. By coating the PLGA core implants with a solution of 10%, 30%, and 50% PLGA in acetone, Chang was able to optimize the coating of the bevacizumab core implants to achieve slow and continuous release with optimal coating being 30% PLGA[62]. We have found that PLGA coating is useful to control the release of large molecules, such as monoclonal antibodies, that require a high level of excipients in order to keep them stabile. The high level of excipients required to stabilize antibodies are above the percolation threshold of the implant and increases the osmotic pressure,

typically resulting in a high initial burst and fast overall release, but the extra layer of PLGA coating around the drug-loaded core has allowed us to optimize the level of excipients and lower the initial burst for a slow and continuous release of stabile monoclonal antibody[62].

1.1.7 Antibody therapeutics

1.1.7.1 Antibody structure

An antibody is composed of two major components, the fragment of antigen binding (Fab) and fraction crystallizable (Fc)[72]. An antibody consists of two Fab domains and one Fc domain. The two Fab domains are identical and each consists of two light chains and two heavy chains. The Fc domain contains the C-terminal constant region of the heavy chains. A hinge region connects the Fab and Fc domains; this region varies in disulfide bonds between the different classes and isotypes[73]. The variable and constant regions form globular structures consisting of a bilayer of hydrogen-bonded beta-strands, connected by disulfide bonds. These beta strands give rise to the main secondary structure of antibodies, with some alpha helices found throughout the bends[73]. The variable regions of the light and heavy chains associate closely with one another in the Fab domain, as do the constant regions of the heavy and light chains of the Fab. The variable and constant regions are connected by a polypeptide chain known as the switch. The variable region has two degrees of variability, the hypervariable or complementarity-determining regions (CDRs), and the non-hypervariable, also referred to as framework regions. The CDRs make up loops near the N-terminus of the Fab region and their variability in the amino acid sequence and size creates a highly variable surface. This surface variability creates pockets or protrusions that are involved in antigen binding. The framework regions are mainly conserved in amino acid sequence and similar in their three-dimensional structures. The framework and the CDR residues interact with each other to form connections

between the heavy and light chains of the variable regions. These interactions between the CDR and the framework regions highly impact the variation in the conformation of the CDR and are important in the overall surface morphology. The interaction between the constant heavy (C_{H1}) and the constant light (C_L) of the Fab contributes to the proper structural interaction between the variable regions and provides better flexibility of the molecule. Between the variable and constant residues, the interaction is weak and variable, forming an Fab bend which can vary in degree of bending. The hinge region between the Fab and the Fc gives the molecule flexibility between its segments, giving the antibody the ability to rotate, wag, or flex. There are three parts to the hinge, the upper and lower flexible regions, and the middle rigid section. The rigid section of the hinge region is defined by the inter-heavy chain disulfide bonding and the multiple proline residues. The sizes of these three sections can vary between the antibody classes[73].

The core function of an antibody is to bind to an antigen[73]. This binding can occur at varying specificity depending on the complementarity of the antibody binding site and the antigen determinant, or epitope. The complementarity of the antibody and antigen is due to the shape and the physical and chemical properties between the two. The interactions between them include hydrogen bonding, van der Waals', and ion pairing[73]. The CDRs are the main contributor to the antigen binding specificity which is determined by the CDRs' sequence and structural variability[72,73]. CDRs contain sections that are more variable than others and are expected to contribute more to the antigen binding specificity and diversity.

1.1.7.2 Antibody function

There are five classes of antibodies, IgM, IgD, IgG, IgE and IgA, all differentiated by the sequencing of their heavy chains and constant regions[74]. Of the classes of antibodies, IgG is the most used and studied due to its high specificity, relatively small size compared to the other

types, reasonable stability and solubility, manufacturing ease and success in humanization[75]. Both ipilimumab and nivolumab are IgG monoclonal antibodies[76,77]. There are four general effector functions of an antibody, antibody-dependent cellular cytotoxicity (ADCC), complement-dependent cytotoxicity (CDC), phagocytosis, and half-life circulation, each one corresponding with a structural feature of the antibody. The Fc fragment is responsible for binding to effector cells and initiating the complement-dependent cytotoxicity (CDC) as well as binding to Fcγ receptors (FcγRs) for ADCC activity and phagocytosis, and neonatal FcR (FcRn) binding for clearance[72,75]. In ADCC, antibodies bind to antigens that are present on tumor cells and then also bind with the Fc receptors that are on the surface of immune effector cells such as natural killer (NK) cells. There are many identified FcRs, FcγRIIIa has been the most clinically relevant receptor, as it is the one that is expressed on human NK cells[74,78]. Importantly, this mechanism has not only been proven in vitro, but has clinical significance[74]. It has been shown that patients who have the higher affinity allele of the FcγRIII show a higher response to rituximab, an anti-CD2- mAb, than patients who were heterozygous or homozygous for the lower affinity allele[74]. In a human tumor xenograft mouse model, grown in wild-type or murine FcγRII/III knockout mice, anti-tumor activity was depleted in the FCγRII/III knockout mice. These cases suggest that the FCγRIII interaction does lead to anti-tumor efficacy and may be an underlying mechanism of action[78]. CDC is another pathway that mAbs use to induce tumor cell death. IgM is the most effective at this, but is rarely used in clinical practice, IgG1 and IgG3 are both effective at eliciting the CDC response. The CDC pathway starts with the antibody binding to an antigen and forming a complex that reveal C1q binding sites on the C_{H2} domain. This binding leads to a cascade of events with other proteins and the release of effector-cell chemotactic/ activating agents, C3a and C5a, and finally the formation of the membrane attack

complex leading to cell lysis[78]. These mechanisms of immune response can act alone but most of the time they interact with each other to create a complex anti-tumor activity that is still being studied[74].

1.1.7.3 Antibody stability

Antibodies are large, ~150kDa, complicated molecules compared to peptides or small molecules, and are typically dosed at high concentrations, both of which can lead to stability issues. Although antibodies are generally similar in structure and mostly differ in their variable, Fv segments, they can still have large differences in their surfaces that can cause differences in stability and formulation requirements to maintain stability. The major and most detrimental irreversible stability issues that can occur are oxidation, deamidation, aggregation, and fragmentation. Oxidation mainly occurs with methionine and cysteine residues, but can also occur in histidine, tyrosine, tryptophan, and phenylalanine residues[79]. Methionine is the most commonly oxidized of the amino acids in IgG and leads to the formation of methionine sulfoxide and an overall change in the ionizability of nearby amino acids[79,80]. The change in charge can alter the overall surface charge of the protein. Methionine oxidation can also affect the structure and function of an antibody, for example, changes in Fab-antigen specificity, secondary and tertiary structures, and Fc-binding protein interactions. FcγR functions are generally not changed by oxidation, but FcRn binding is affected and can suggest a reduced half-life in oxidized forms of IgG. These changes depend on where the oxidation occurs on the antibody, the CDR surface versus the constant regions, and should be monitored during production[80]. Deamidation occurs mostly with glutamine and asparagine residues on both heavy and light chains with more prevalence in asparagine, leading to a more acidic protein[79,80]. Deamidation occurs slowly in IgG when in native state and is accelerated when unfolding of the antibody begins[79,80]. The

deamidation of asparagine is also more likely to occur when the asparagine is next to a glycine or in a flexible region of the protein, again suggesting that the conformation of the antibody is reflected in deamidation rates. Effects of deamidation have been shown to be minimal since the most common sites of reactivity are far from any FcRn or FcγR binding sites. It is still a minorly controlled parameter in the case that the negative charge introduction by deamidation affects the biological function, especially when occurring in the binding region of an antibody[79,80].

Aggregation is an important parameter of antibody formulations. Antibodies are typically formulated as high concentration liquids, which can lead to increased aggregation. Proteins are arranged or folded so that their hydrophobic surfaces are internalized, and the hydrophilic surfaces are facing the aqueous environment, as this is a more stable and thermodynamically favorable conformation. When proteins start to unfold and undergo molecular motion, they can rearrange themselves to a more energetically favorable state where the hydrophobic surfaces that may have been surface-exposed are now protected from the outside environment. This stabilization of contact between proteins is the beginning of dimerization, trimerization, and eventually aggregation. Aggregation events increase with increasing temperature and protein concentration because these conditions lead to more favorable energy states for the protein. At decreased temperatures, aggregation can occur in some antibodies and create reversible associations called cryoimmunoglobulins. There have been several additives identified to help reduce aggregation including small agents that can better interact in grooves or channels and prevent conformations that are more aggregation prone, and large agents that can interact with the larger surfaces of the protein which would reduce surface contacts that can lead to aggregation[81]. Protective agents include additives such as urea, guanidinium chloride, amino acids, sugars, polyalcohols, polymers, and surfactants, and the chosen agent depends on the

antibody formulation. Another important parameter to consider in antibody formulations is the fragmentation. Since antibodies can have many flexible sites in their structures, such as the segment between the Fc and Fv domain, fragmentation at these places is common. Fragmented forms of antibodies may not have a huge effect on their efficacy, but can make the antibody more susceptible to degradation, proteases, or clearance. In general, any type of stability issue could lead to immunogenicity, inactivity, or differences in the biodistribution, so monitoring these instability pathways, whether they are major or minor, is a top priority for formulation and manufacturing[79].

1.1.7.4 Immune checkpoint inhibitors

Cancer immune therapy can be classified into two categories: adoptive immunotherapy and active immunotherapy. Adoptive immunotherapy uses molecules that can directly attack the tumor cells, like cytokines or antibodies. Active immunotherapy involves treatments that indirectly attack the tumor cells and activate the immune system specific to tumor antigens[82]. Immune checkpoint inhibitors fall into the active immunotherapy, as they indirectly work to combat tumor cells, not directly targeting the tumor cells[82,83]. The immune checkpoint molecules are a part of the regulatory immunity, which is a system that must be overcome in order to eradicate tumor cells[82]. The goal of the immune checkpoint inhibitory therapy is to block the inhibitory pathways that are not allowing the immune system to be activated and create an anti-tumor response[44]. The immune system consists of an important class of molecules, the T cells. T cells have receptors, CD28, that engage with antigens on the major histocompatibility complex (MHC) class I molecules. When this connection is made along with a costimulatory connection between CD28 and B7 ligands (CD80 and CD86) on the antigen presenting cells, this leads to tumor cell death[83–85]. T cell response is regulated by a combination of co-stimulatory and

inhibitory signals, or immune checkpoints. In a normal functioning state, immune checkpoints are useful in making sure that the immune system does not damage tissues, or cause autoimmunity that could be harmful. In tumors, there is often an imbalance in the immune checkpoint proteins that leads to the tumor cells evading the immune system[86]. The two most researched immune-checkpoint receptors for immunotherapy are the cytotoxic T-lymphocyte-associated antigen 4 (CTLA-4) and the programmed cell death protein 1 (PD-1). These receptors are both inhibitory receptors that, when blocked, work independent mechanisms to enhance antitumor activity. CTLA-4 has been referred to as the 'godfather' of checkpoints as it was the first immune-checkpoint receptor that was used for a target in immunotherapy. CTLA-4 works by counteracting the action of the co-stimulatory receptor, CD28, because it binds with higher affinity to the stimulatory ligands, CD80 and CD86 which normally bind to CD28. This binding causes CD28 to be less effective at amplifying the TCR signaling[86]. PD-1 is also a receptor in the CD28 family with two different ligands, PDL-1 and PDL-2[84]. In a normal cell environment, PD-1 acts by keeping the activity of T cells in check when they are responding to an inflammatory event, to prevent autoimmunity. In the tumor environment, this mechanism is used to evade the immune system. PD-1 binds to one of its ligands and then inhibits T cell activating kinases through the phosphatase, SHP2. It has also been found that PDL-1 and PDL-2 have binding interactions with co-stimulatory receptors on T cells, similar to the mechanism of CTLA-4. As the PD-1 receptor sequesters the ligands, they are not being used as immune-activating ligands[86]. PD-1 and CTLA-4 differ in that PD-1 mainly works by affecting the effector T cell activity, while CTLA-4 works earlier by inhibiting T cell activation[7,86]. Currently, there are three FDA approved immune checkpoint inhibitory drugs for anti-PD-1 and anti-CTLA-4: Yervoy® (ipilimumab, Bristol-Myers Squibb), Opdivo® (nivolumab, Bristol-Myers Squibb), and

Keytruda® (pembrolizumab, Merck). Keytruda® is an anti-PD-1antibody approved for melanoma, non-small cell lung cancer, small cell lung cancer, head and neck squamous cell cancer, classical Hodgkin lymphoma, primary mediastinal large B-cell lymphoma, urothelial carcinoma, gastric cancer, esophageal cancer, cervical cancer, Merkel cell carcinoma, renal cell carcinoma, and endometrial carcinoma[87]. Keytruda® is typically administered at 200 mg every three weeks by intravenous infusion[87]. Keytruda® is a humanized IgG4 kappa antibody, ~149 kDa produced by CHO cells. It is formulated as a lyophilized powder of 50 mg pembrolizumab (anti-PD-1), 3.1 mg L-histidine, 0.4 mg polysorbate 80, and 140 mg sucrose at pH 5.5[87]. Opdivo®, from Bristol Myers Squibb, is also an anti-PD-1 antibody and was first approved in 2014, shortly after Keytruda, for advanced melanoma. It is now also approved for renal cell carcinoma, lung cancer and advanced lung cancer, classical Hodgkin lymphoma, squamous cell carcinoma of the head, urothelial carcinoma, and hepatocellular carcinoma[76]. Opdivo® is administered at 240 mg every two weeks by intravenous infusion[76]. Opdivo® is an IgG4 kappa immunoglobulin, ~146 kDa, made by CHO cells. It is formulated into a liquid containing 10 mg nivolumab (anti-PD-1), 30 mg mannitol, 0.008 mg pentetic acid, 0.2 mg polysorbate 80, 2.92 mg sodium chloride, and 5.88 mg sodium citrate dihydrate, per mL at pH 6[76]. Yervoy®, also sold by Bristol Myers Squibb, is an anti-CTLA-4 antibody and was first approved in 2011 for late-stage melanoma and is now also approved for renal cell carcinoma, colorectal cancer, hepatocellular carcinoma, and metastatic non-small cell lung cancer[77]. Yervoy® is administered at 1-3 mg/kg by intravenous infusion[77]. Yervoy® is an IgG1 kappa immunoglobulin, ~148 kDa, made by CHO cells. It is formulated as a liquid containing (per mL), 5 mg ipilimumab (anti-CTLA-4), 0.04 mg diethylene triamine pentaacetic acid (DTPA), 10 mg mannitol, 0.1 mg polysorbate 80 (vegetable origin), 5.85 mg sodium chloride, 3.15 mg tris hydrochloride, at a pH of 7[77]. Opdivo® and

Yervoy® have approvals in combination with each other as well, including, BRAF V600 wild-type melanoma and unresectable or metastatic melanoma across BRAF status, renal cell carcinoma, colorectal cancer, hepatocellular carcinoma, and metastatic non-small cell lung cancer[77].

1.1.8 Toll-like receptor 9 agonist, CpG

CpG oligodeoxynucleotide (ODN) is a toll-like receptor 9 (TLR-9) agonist composed of unmethylated, single stranded DNA molecules containing cytosine connected to guanine (CpG) motifs. The backbone of CpG is partially or completely made of phosphorothioated bonds as opposed to phosphodiester, which makes it resistant to nuclease digestion and increase the in vivo half-lives to ~30-60 min. TLR-9 is an integral membrane glycoprotein, located in the endoplasmic reticulum/endolysosomal compartment of cells, thus CpG must be internalized to interact with TLR-9[88]. Upon interaction of TLR-9 and its ligand, the TLR dimerizes and recruits downstream signaling molecules, triggering the immune response. Molecules involved in this signaling include: myeloid differentiation primary-response protein 88 (MyD88), IL-1R-associated kinases (IRAKs), transforming growth factor-β (TGF-β)-activated kinase (TAK1), TAK1-binding protein (TAB1), TAB2, and tumor-necrosis factor (TNF)-receptor associated factor 6 (TRAF6)[89]. This signaling cascade involves both the innate and adaptive immune activation. The elicited innate response involves production of proinflammatory cytokines, chemokines, type I interferons (IFNs), and antimicrobial peptides. The adaptive immune response triggered by TLR9 activation involves the expansion of Ag-specific T and B cells that help create a lasting immune memory response[88]. CpG ODNs can be organized into different classes that have different structures and triggered immunological responses, class K (or Class B), class D (or class A), class C, and class P. Class K can have one or multiple CpG motifs and

typically have a phosphorothioate backbone; they trigger pDC differentiation and production of TNF-α and stimulate B cell proliferation and IgM secretion. D or A type ODNs have a single CpG motif surrounded by palindromic sequences and have a phosphodiester core with terminal phosphorothioate nucleotides. Class D triggers pDC maturation and IFN-α secretion but they do not affect B cells. C type ODNs also contain palindromic CpG motifs but have full phosphorothioate backbones. C type ODNs activate B cells and pDC to secrete IL-6 and IFN-α. P-class ODNs have double palindromes and form hairpin structures that illicit the strongest type I IFN response[88]. CpG ODNs are of particular interest for vaccine adjuvants as well as standalone and combination therapies. The first FDA approved oligonucleotide therapy was a 21-mer phosphorothioate CpG, fomivirsen, from Isis Pharmaceuticals and Novartis Ophthalmic, approved for treatment of cytomegalovirus (CMV) retinitis in 1998. This drug is no longer marketed due to a decreased need after the development of high-activity, anti-retroviral therapy for CMV. Since then, there has been one other approved drug, Heplisav-B, a hepatitis B vaccine which uses CpG as an adjuvant[90]. CpG ODNs are investigated in many clinical trials, some in combination with radiation, antibodies, and chemotherapy, and in general are well tolerated[88]. Nucleic acid derived drugs can undergo both chemical and physical instability. The main chemical instabilities that can occur are hydrolysis and oxidation, while physical instability can include denaturation, adsorption to surfaces, aggregation, or precipitation. Hydrolysis of the sugar-phosphate backbone can be acid or base catalyzed either by intermolecular or intramolecular nucleophilic attack. In acidic conditions, isomerization (intramolecular transesterification) and the cleavage of the N-glycosidic bond. The substitution of the sulfur for one of the oxygens to make the phosphorothioate bond is helpful to protect against nuclease degradation, but it can also undergo desulfurization in the presence of metals[91]. CpG has

previously encapsulated in PLGA, mostly in micro or nanospheres[91–101]. Due to the inclination of the cleavage of the N-glycosidic bond, it would be important to include an antacid to avoid PLGA acidic byproducts from inducing hydrolysis.

1.1.9 Docetaxel

Docetaxel is a molecule from the taxane family and is a semi-synthetic analog of 10-deacetylbaccatin III, naturally occurring and isolated from the *taxus baccata* plant. Docetaxel is a small molecule, similar to paclitaxel, a BCS class IV drug, poorly soluble and low permeability in the gastrointestinal tract, the MW~ 861 g/mol and the logP=4.1[102]. Taxotere® (Sanofi-Aventis) is a commercially available docetaxel product formulated at 40 mg/ml with polysorbate 80 and ethanol for enhanced solubility. Docetaxel differs from paclitaxel by a hydroxyl group at the C-10 position and a tertbutoxy moiety in the C-13 ester side chain and has about a 25% enhanced solubility. Degradation of docetaxel can occur in both basic and acidic medium but is slower or to a lesser extent in acidic medium[103]. Docetaxel is approved for the treatment of solid tumors such as non-small cell lung cancer and breast cancer, metastatic prostate cancer, and advanced squamous cell carcinoma of the head and neck and is typically dosed at 60-100 mg/m^2 by i.v. infusion every three weeks[104]. Docetaxel is a microtubule-stabilizing agent, or a microtubule inhibitor (MTI). Microtubule function is critical during mitosis and the formation of the mitotic spindle and is an important target for anti-cancer drugs[105,106]. During the G2/M phase, microtubules are going through a 'treadmilling' of constant addition and loss of tubulin at their ends[67]. MTIs disrupt this microtubule function and cause cell cycle arrest in the G_2/M phase, resulting in cell death. Docetaxel binds to the β–subunit of tubulin in a 1:1 stoichiometry, and when used at low concentrations, results in stabilization of the microtubule, suppression of its dynamics, and finally, apoptosis[67]. Resistance to MTIs such as paclitaxel or docetaxel is a

current issue that is not completely understood or solved. It is believed that an overexpression of ABC-transporters, such as P-glycoprotein, occurs and decreases the intracellular drug levels leading to cross resistance to drugs of different chemical structures[106]. Docetaxel binds to the tubulin site 1.9 times greater than paclitaxel and has higher microtubule inhibitory activity[103]. Docetaxel and paclitaxel have been previously formulated in PLGA matrices[107], such as microspheres, films and discs, but typically suffers from low loading, high initial burst, and/or incomplete release[108–111]. For example, Ong et al. formulated a 5-10% w/w paclitaxel loaded PLGA disc that resulted in incomplete release (8-30%) over 35 days[108]. Musumeci et al. formulated 0.5 w/w% docetaxel loaded PLA nanospheres that released most of the drug in the first day, and completion of release was around 14 days[112]. Fonseca et al. prepared 1% w/w loaded paclitaxel in PLGA nanoparticles and this dosage form released almost all of the drug in the first day, and release completion to ~80% after 10 days[110]. Our lab has successfully formulated highly hydrophobic anti-cancer agents that show poor or slow release and found that they may benefit from using a lower molecular weight polymer with a carboxylic end group which we have considered for docetaxel encapsulation[13,113].

1.1.10 Glioblastoma

1.1.10.1 Background

Glioblastoma is a devastating disease with a poor prognosis. It is classified as a World Health Organization (WHO) grade IV tumor, accounting for 82% of all malignant gliomas[114]. Gliomas are the most commonly occurring primary brain tumor in the EU and US and the median survival 12-14 months, and a two-year survival rate of 10%[1,2]. Gliomas are further divided into a grading system by the WHO that have features correlating with natural disease course. The presence of the IDH1 or IDH2 mutations and the presence or absence of 1p or 19q

chromosomal deletions further classify gliomas into three main groups: IDH-mutant, 1p/19q co-deleted with a favorable prognosis, IDH-mutant with an intermediate prognosis, non-1p/19q-co-deleted tumors, and IDH-wild-type tumors that are mostly glioblastomas WHO grade IV with a gain of chromosome 7 and a loss of chromosome 10, and have the worst prognosis[115]. The mechanism behind the development of glioblastoma is still being studied, but there are three pathways that are confirmed by the Cancer Genome Atlas (TCGA) as commonly disrupted in glioblastoma. These pathways include the receptor tyrosine kinase (RTK)/Ras/PI3K, p53, and Rb signaling pathways[1]. The RTK/Ras/PI3K pathway alterations occur in 88% of glioblastomas including multiple mutations, amplifications, or both. An example of these are the EGFR, HER2, PDGFRA, and the MET pathway alterations, leading to constitutive activity of their downstream effectors and ultimately a decrease in tumor responsiveness[1]. The p53 and Rb signaling pathways both affect the cell cycle. In the p53 pathway, the TP53 gene encodes for the p53 protein which is responsible for cell-cycle arrest and apoptosis in the presence of DNA damage. Loss of the p53 function is common in glioblastoma and is caused by mutations or deletions in the TP53 gene or in amplification of MDM2. Rb signaling also regulates the cell cycle progression, and with deletion or mutation of the Rb1 protein or with CDK4 amplification, the cell cycle is no longer regulated, leading to abnormal cell growth[1]. These pathways are potential targets for future therapies. It had been previously reported that the central nervous system (CNS) was immune privileged until 2015 when recent data showed that the CNS actually has an active immunosurveillance and immune response.[115] It was found that a unique route of lymphatic drainage exists from the brain, along the sinuses, to the deep cervical lymph nodes where antigen presenting cells can prime T and B lymphocytes.[115] Thus, the brain possesses a unique and not

entirely understood immune surveillance, although not absent, as was previously thought leaving the potential for more therapeutic options.

1.1.10.2 Current therapy

The current standard of care for glioblastoma is maximal safe surgical resection of the tumor, chemotherapy, and radiation[114]. It has been shown that gross surgical resection is an important aspect of survival and that below 70% resection survival is reduced, but above 70% resection, survival becomes proportional to the amount resected[3]. Radiation therapy, 60 Gy administered in 30 fractions to the tumor region as well as a small margin of non-tumor areas, was added to therapy and doubled the survival[115]. Patients with a poor prognosis or an unfavorable Karnofsky performance status (KPS) have benefited from hypofractioned radiotherapy, 40 Gy administered in 15 fractions. The addition of chemotherapy, temozolomide, was established in 2005 after it showed improvement in the 2-year survival of 10.4% to 26.5%.[115] Temozolomide (TMZ), an oral DNA alkylating agent, in combination with radiotherapy is the established treatment around the world[2,114]. TMZ has a better outcome for tumors with methylation of the 6-O-methylguaninine DNA methyl-transferase (MGMT) gene, because this decreased the expression of MGMT which is a DNA-repair protein resulting in decreased activity of TMZ.[115] For most patients, tumor reoccurrence happens after first-line treatment within 7-10 months. Recurrence is typically treated with salvage therapies such as surgical resection, bevacizumab (anti-VEGF), temozolomide rechallenge, nitrosoureas (carmustine and lomustine), and carboplatin, but many patients choose not to receive second-line therapoes.[115] Salvage therapies have not shown significant improval in overall survival, and likely, the recurrent tumors have been exposed to genotoxic stress from previous therapy and are expected to have a higher mutational load and immunogenicity, causing more difficulties in

response to more treatment.[115] After recurrence and salvage therapy, the typical survival is 3-4 months, with most of the treatments having toxic side effects such as hematotoxicity as well as patient discomfort, nausea and vomiting[77].

1.1.10.3 Local delivery to the brain: overcoming barriers

Glioblastoma therapies fail to improve the poor prognosis because they must cross the blood brain barrier to reach the tumor site, which is difficult for a systemically delivered drug because it requires a high concentration to reach therapeutic levels in the brain, leading to toxicity. The blood brain barrier (BBB) is not only a physical barrier consisting of tight junctions and capillaries, but is also a pharmacological barrier that limits the molecules that can be delivered to the brain. The BBB allows for a small percentage of small, neutral, lipophilic molecules to cross, it does not allow large, charged, hydrophilic molecules to pass which includes some chemotherapeutics and antibodies[4]. Due to the high doses needed to reach therapeutic levels in the brain, systemic toxicity often occurs, and can lead to termination of treatment. There have been many attempts to overcome the challenges of GBM therapy, yet median survival has only increased 12 months over the last 80 years[3]. Local delivery for the treatment of GBM is further motivated by the fact that 80% of gliomas recur within just 2 cm of the original tumor[116,117]. There have been many efforts to improve local delivery[118,119]. One way to improve the delivery of chemotherapeutic agents to the brain is to tailor their properties to be able to cross the BBB by making them more lipophilic. Two examples of this are lomustine (CCNU) and semustine (methyl-CCNU), which are lipophilic versions of the chemotherapeutic, carmustine (BCNU), used to treat malignant brain tumors[4]. Another way to enhance the delivery of drugs to the brain is to disrupt the BBB. This can be done multiple ways, for example, hyperosmolar disruption, solvent and adjuvant mediated disruption, or ultrasound[4–6].

Hyperosmolar disruption involves administering a solution, typically mannitol, into the arteries causing an increase in their permeability, followed by the intra-arterial administration of the drug[6]. This may also increase the delivery to the tumor through the blood tumor barrier (BTB), but can also lead to toxicity due to the non-selective opening of the barriers leading to increased brain fluid[4,6,120]. Solvents and adjuvants such as DMSO, detergents, or Freund's adjuvant destabilize the membranes of the BBB and allow the systemic delivery of otherwise undeliverable agents to the brain. Ultrasound techniques have been of interest to disrupt the blood brain barrier, often in combination with a high dose of air bubbles[121]. For example, Liu et al. used a focused ultrasound to treat glioblastoma in rats with the chemotherapeutic agent, BCNU. The results showed significantly better treatment with the focused ultrasound in comparison to the BCNU alone, but the disruption of the BBB varied depending on the location[5]. While these techniques may improve the delivery of drugs to the brain, they often cannot guarantee an improved delivery to the actual tumor, and still risk toxic systemic exposure. In order to avoid systemic exposure, delivering directly to the tumor by implanting a device can help to control the spatial and local delivery of drug[4]. Local delivery for the treatment of glioblastoma is necessary since 80% of gliomas recur within just 2 cm of the original tumor[116,117]. There have been many efforts to improve local delivery[118], but only one FDA approved local delivery exists. Gliadel® was first approved in 1996 and is indicated for the treatment of newly diagnosed, high-grade malignant glioma in adjunct to surgery and radiation and for recurrent glioblastoma multiforme as an adjunct to surgery[122]. Gliadel® is a wafer made of a polyanhydride copolymer of poly [bis(p-carboxyphenoxy)] propane and sebacic acid in a 20:80 molar ratio, containing the chemotherapeutic agent, carmustine (BCNU). The recommended dose of 8 wafers (61.6 mg BCNU) are implanted in the tumor area at the time of

resection and degrade over 3 weeks[122,123]. Gliadel® has shown an increase in survival of 2.4 months compared to placebo when used as initial therapy and has no significant perioperative adverse events[116,123]. The Gliadel® implants showed BCNU tissue concentrations 2 cm from the implanted wafer for up to 30 days. This successful implantation efficacy and safety is significant because most recurrence occurs with a 2 cm region of the original tumor[84]. The promising potential of local implantation during surgical resection and delivery of drug to the tumor site has been shown by the use of Gliadel® [4,116,118], yet there is still more to accomplish because the Gliadel® wafers have not been adopted as the first line therapy and have not significantly improved survival more than several weeks. Recurrence after implantation still occurs at the site of implantation and at farther distances. The lack of significant improvement in survival using Gliadel® could possibly be due to poor tumor penetration and BCNU resistance[124,125]. Besides the BBB, the tumor microenvironment still presents a challenge even for drugs that can get across the BBB. The tumor microenvironment is acidic, hypoxic, and have "solid stress" causing intratumor vessel compression, and abnormal vasculature which leads to leaky vessels and poor drug penetration[126]. Anti-angiogenesis agents, such as anti-VEGF, have been used to improve drug delivery by normalizing the vasculature, but use of anti-VEGF in GBM has conflicting results although it is an approved therapy for tumor recurrence[127,128]. Another way to alleviate the solid stress and improve tumor penetration is use of apoptosis-inducing agents such as docetaxel. The abnormal environment of gliomas creates a blood-tumor-barrier (BTB) that is similar to the BBB, limiting the passage of therapeutics into the tumor environment[120]. The BTB is comprised of brain tumor capillaries that may have overexpression of drug-transporting ligands to help target improved drug delivery, but can also have overexpression of ABC transporters that lead to chemoresistance[120]. Use of receptor-mediated transport and blocking of

the drug-efflux transporters is under investigation for GBM treatment[120]. Direct injection into the tumor, infusion by catheters or pumps, has been investigated in the past in clinical trials, but this has not been easily adopted in practice due to insufficient drug delivery, neurotoxicity, limited capacity and catheter obstruction[120,124]. Furthermore, direct tumoral injection of BCNU did not show improved survival advantage over the polymeric implantation and release of BCNU in a rat gliosarcoma model[129]. Convection enhanced delivery (CED) can be used to overcome the BBB and the BTB using a motor-driven pumping of the drug after stereotactically placing a catheter. There is still a far way to come in CED due to complications with catheter use and placement that has limited the advancement of clinical use[130].

1.1.10.4 Immunotherapy for glioblastoma

Immunotherapy has been a growing interest in the treatment of glioblastoma as with many other cancers, due to their highly immunosuppressive microenvironment[131,132]. It is known that glioma tumors overexpress immune inhibitory molecules helping them to evade the immune system[133]. Normal tissue contains the transcript for PD-L1, but express little or no PD-L1 protein, whereas PD-L1 protein is highly expressed in many solid tumors such as gliomas, which use this expression to evade the immune system[134]. It is known that the ligands for PD-1 and CTLA-4, PD-L1 and CD80, are expressed on tumor cells and myeloid derived suppressor cells and that PD-1 expression on T cells is a marker of T cell exhaustion leading to dysfunctional T cells[8,9]. Berghoff *et al.*, found that tumor samples from patients with newly diagnosed and recurrent glioblastoma have prominent expression levels of PD-L1 and PD1+ tumor infiltrating lymphocytes (TILs). Nduom *et al.* similarly show higher expression of PD-L1 is correlated with a worse outcome after therapy and therefore there is a potential for using PD-L1 expression as a biomarker in immunotherapy. The overexpression of PD-L1 is thought to be caused by the loss

of PTEN which is a common mutation in glioblastoma[1,135]. Parsa *et al.*, show that glioma cells that have a deletion of PTEN result in higher expression levels of PD-L1[134] Glioblastoma is known to have an increase of infiltration by regulatory T cells (Tregs), which are shown to have an increased expression of CTLA-4 in malignant brain tumor samples, contributing to the suppression of anti-tumor response[136,137]. The PD-1 and CTLA-4 mechanisms are distinct from each other, spatially and temporally, thus they are often investigated as combination therapies. The CTLA-4 mechanism occurs more upstream, in the lymph nodes during T-cell activation, while the PD-1/PD-L1 mechanism occurs more downstream on the effector sites during T-cell activation[138]. There have been numerous animal studies that showed promise for the use of immune checkpoint inhibitors, likely leading to their clinical investigation[8,139–143]. Ipilimumab (anti-CTLA-4), Nivolumab (anti-PD-1), and pembrolizumab (anti-PD-1), are all undergoing clinical trials for the treatment of glioblastoma in many different combinations, some with the current therapies temozolomide and bevacizumab. As of March 2020, there are 39 Phase I/II clinical trials for glioblastoma testing different combination of immune checkpoint inhibitors[138]. Systemic delivery of ICIs alone and more so in combination with each other lead to immune related adverse events (irAEs) that often require termination of treatment or the addition of medications to combat the side-effects[3,10]. Other immunotherapeutic approaches include tumor associated antigens/peptide vaccines, dendritic cell vaccines, oncolytic vaccines, gene therapy, CAR T-cells, and various nanotechnologies, all are reviewed by Garcia-Fabiani *et al.*[138].

1.1.10.5 CpG for treatment of glioblastoma

TLR9 is expressed differently among species, in humans, TLR9 is expressed in pDCs, B cells, microglial cells, and has been detected in human resected GBM tumors, although it is suspected that the tumor TLR9 levels are mainly due to infiltrating cells[144]. It is important to

consider the expression of TLR9 on tumor cells because this could actually promote metastasis and has been shown to positively correlated with higher glioma grade and worse prognosis, and thus, CpG therapy, especially direct tumoral injection, is controversial[145–147]. CpG is expected to activate and mature DCs and increase inflammation. It may be more beneficial to administer multiple smaller doses as opposed to a single, high dose[145]. In a completed phase II clinical trial (NCT00190424) for recurrent GBM, intracerebral administration of CpG was well tolerated and improved the progression free survival compared to controls[148]. CpG administered via retro orbital injection to mice with GL261 intracranial tumors improved survival (MS=40d) compared to untreated controls (MS=28d)[149]. CpG therapy is expected to be synergistic with other therapies, such as radiation. Radiation therapy can induce apoptosis and release tumor specific antigens, reduce the tumor mass, and promote local inflammation in order to increase the efficacy CpG[150]. Meng et al. showed improved survival in a flank GBM rat tumor model by combining local CpG administration with radiation therapy, both when CpG was given before and after radiation[150]. CpG therapy has also shown improved survival alone and in combination with anti-CTLA-4 and anti-PD-1 in GBM and bladder cancer[151,152]. Scheetz et al. have tested the combination of HDL nanodiscs containing CpG and tumor specific neoantigens with anti-PDL1 therapy in an intracranial GL261 GBM murine model and showed improved survival and immunological memory[141]. These results are promising for future investigation into combined immunotherapies for glioblastoma.

1.1.10.6 Docetaxel for treatment of glioblastoma

Docetaxel is not only a commonly used chemotherapeutic and apoptosis inducing agent, it has also been shown to be a tumor penetration enhancing agent for solid tumors such as gliomas[126]. The GBM tumor environment is characterized by abnormal vasculature resulting in

longer distances for drugs to travel from blood vessels to reach tumor cells, and high intratumoral pressure, or solid stress, that is unfavorable for drug delivery and drug penetration[126]. Jessie L-S. Au and colleagues have done extensive research using paclitaxel, another member of the taxane family, to increase tumor penetration[126,153–159]. They showed that paclitaxel enhances its penetration 24h after administration, at which point apoptosis has occurred and tumor cell mass has decreased[160]. With a high enough dose of paclitaxel ~48h before administration of doxorubicin loaded liposomes, doxorubicin penetration was selectively enhanced into tumors compared to controls, even when switching the order of the administration to liposomes then paclitaxel, confirming the importance of the priming from the induced apoptosis[158]. They also found that the penetration enhancement is more effective giving two smaller doses around 16-24h apart as opposed to one single dose to allow for apoptosis and tumor cell reduction[154]. Furthermore, Kadiyala et al, showed very successful results combining docetaxel and CpG treating glioblastoma. They also found that docetaxel was more potent than paclitaxel at inducing cell-death in glioma tumor cells. Intratumoral administration of HDL-nanodiscs loaded with DTX and CpG combined with radiation resulted in increased survival and long term memory upon tumor cell rechallenge in intracranial GBM murine tumor models[161]. These results are excellent evidence for our future studies for combined local administration of CpG and docetaxel and our further improvement by reducing the need for multiple intratumoral injections by providing sustained local delivery from PLGA implants.

1.2 Thesis scope

The introduction of this thesis has presented background information on PLGA controlled release, protein/monoclonal antibody therapeutics and their potential instabilities in polymer matrices, and glioblastoma and its treatment with immune checkpoint inhibitors, CpG, and

docetaxel. Glioblastoma treatment has not greatly improved in decades and is complicated by the blood brain barrier which prevents many therapeutics, including the aforementioned, from reaching the site of action after systemic administration. This work will focus on a viable PLGA implant formulation to locally deliver stable and therapeutically active monoclonal antibodies, CpG and docetaxel for the treatment of glioblastoma and on a reduced diameter implant formulation to deliver monoclonal antibodies for intraocular administration. An extensive analysis of PLGA raw polymer in vitro behavior and considerations of manufacturer differences and microstructural properties will be presented as it relates to the successful development of PLGA use in FDA-approved products.

1.3 Thesis overview

The goal of this thesis is to further develop controlled release of monoclonal antibodies as local treatment options for glioblastoma which would benefit from long-term local treatment due to its biological barriers that prevent many desirable therapeutics, such as monoclonal antibodies, from being effectively and safely administered, systemically. An additional goal is to understand basic aspects of polymer selection that contribute to eventual PLGA performance should the controlled release systems described be translated.

Chapter 2 investigates the formulation of immune checkpoint inhibitors, anti-PD-1 and anti-CTLA-4 into PLGA implants to treat GBM as well as the potential of a reduced diameter implant for intraocular applications.

Chapter 3 investigates the formulation if immune stimulatory agent, CpG ODN, and tumor-penetrating enhancer, docetaxel, into PLGA implants for treatment of GBM.

Chapter 4 investigates the effects of PLGA properties and variables, such as L/G ratio, MW, end-capping, manufacturer, and formulation geometry on in vitro degradation and erosion

behaviors for a better understanding of how manufacturer changes or source changes in commercial polymers could affect specific and reproducible performance.

The conclusions, significance, and future directions of this work are discussed in Chapter 5.

Chapter 2: PLGA Implants for Local Controlled Release of Monoclonal Antibodies

2.1 Abstract

Currently available drug treatments for diseases of the brain and eye are complicated by the need for frequent intravitreal injections and severe systemic toxicity. One established approach to overcome these issues is local and sustained exposure of the therapeutic agent at the target site, which can be achieved with polymer controlled-release implants. Monoclonal antibody (mAb) therapeutics are a growing drug class with applications in the treatment of and glioblastoma multiforme (GBM) and neovascular age-related macular degeneration (wet AMD). However, there are no FDA-approved products for local long-term controlled release of mAbs. Herein, we demonstrate injectable biodegradable poly(lactic-co-glycolic acid) (PLGA) implants delivering mAbs, anti-PD-1 and anti-CTLA-4 for brain disease treatment, and bevacizumab for the potential of intraocular treatment of wet AMD. We show that PLGA coated implant formulations slowly and continuously release stable and immunoreactive mAbs for >6 weeks *in vitro* and are efficacious in animal models for GBM after single local implantations. We show some reduction of the implant size for an improved intraocular mAb implant. The injectable PLGA platform can be utilized for locally delivering mAbs and other cofactors, offering an improved therapeutic option for treating diseases amenable to antibody therapy.

2.2 Introduction

Monoclonal antibody (mAb) therapeutics have become a powerful drug class occupying five out of ten spots on the current US drug sales list.[162] Unlike many biologics, mAbs typically have longer circulating plasma half-lives owing to the neonatal Fc receptor-mediated recycling mechanism.[163] MAbs encompass diverse pharmacologic targets and have been successfully administered systemically. Certain organs such as the brain and the eye are difficult to reach for mAbs, as well as other drugs, thus limiting the ability to achieve optimal dosage without inducing significant off-target side effects.[164,165] The brain and the eye possess protective endothelial barriers and surrounding blood vessels comprising the blood-brain and blood-retinal barriers, respectively. These barriers preclude optimal and effective treatment for a multitude of diseases such as glioblastoma (GBM) and neovascular age-related macular degeneration (also referred to as wet AMD). GBM is one of the most deadly cancers with a high rate of recurrence and a poor median survival (14-20 months), which has not greatly improved over the past several decades.[2,3,166] Due to the immunosuppressive nature of GBM, immune checkpoint inhibitor immunotherapies such as anti-PD-1 and anti-CTLA-4 blockade are currently being investigated as a treatment option. However, systemic administration of these antibodies showed adverse side effects.[3,10,115,167,168] Local controlled release of immune checkpoint inhibitors for GBM offers the potential of superior local drug exposure while avoiding systemic toxicity and mitigating systemic immunosuppression.[168] Wet AMD is one of the most common causes of blindness[169–172] and may be treated with monthly intravitreal injections of an anti-vascular endothelial growth factor (VEGF) mAb such as Avastin (bevacizumab, Genentech), Lucentis (ranibizumab, Genentech) or the VEGF trap Eylea (aflibercept, Regeneron).[169,173,174] Despite the inherently long intravitreal half-life of bevacizumab, the monthly injections are problematic, posing risks of

infection, inflammation and hemorrhage.[175] Additionally, monthly injections are a real burden on patients leading to compliance issues.[176] An injection frequency of at least 3-months between doses is a highly desired clinical goal.[177–179]

An approach to overcome such biological barriers to drug delivery is the application of biodegradable polymer implants capable of releasing the drug from weeks to months after local delivery. Intravitreal injections in the physician's office[180] or implantation after tumor resection[123] are common applications of this strategy. Other examples that focus on local/regional controlled-release include intravaginal rings releasing contraceptives and preventive drugs for sexually transmitted diseases,[26,27] drug-eluting stents for the treatment of peripheral artery disease,[28,29] and intra-articular extended release formulations for osteoarthritis knee pain.[30] Collectively, these diseases demonstrate an unmet need and significant opportunity to develop generalizable approaches for sustained, local release of mAbs. However, mAbs as proteins are often unstable when encapsulated and slowly released from polymers.[181] General strategies for slow and continuous release of mAbs from poly(lactic-co-glycolic acid) (PLGA), the most common polymer used in FDA-approved long-acting release (LAR) products, have not been achieved. Most mAb LAR formulations previously reported are deficient in one or more of these important categories: high and efficient loading of mAb[182–185], low initial burst release (<20%)[184,186], >80% total mAb release[182–184,186–190], >2 month of release[182,184–186,191–193], extensive analyses of mAb structural stability and activity during formulation and during release[182–185,187,188,190–193], a lack of polymer build-up after drug release[194], and evaluation of mAb tolerability and efficacy in vivo[182–184,186–196]. In Table 2-1, we have provided an analysis of current literature for controlled release mAb formulations and their relevant performance. Many of these formulations are satisfactory in one or more of these aspects but are lacking in an overall successful formulation and have only been

applied to 1-2 antibodies, and thus are not optimal candidates. To address this challenge we previously selected bevacizumab contained in Avastin® [197,198] as a model mAb, and developed a LAR formulation approach based on injectable pencil-lead sized, sub millimeter-scale rods[62]. The formulation was built on multiple protein-stabilizing features previously developed for other PLGA-encapsulated albumin and growth factors.[11,12] Trehalose is known to stabilize proteins in the solid state by multiple mechanisms including, vitrification, water-replacement, and preferential exclusion.[199,200] Here, found the necessity to include a high amount of trehalose (15% w/w) in order to stabilize the mAbs during cryomicronization and encapsulation. We also included a poorly water soluble base, $MgCO_3$ to effectively control the drop in microclimate pH from PLGA degradation products.[11] To account for the high loading of water-soluble excipients, we applied a drug-free PLGA coating to better control the high initial burst and fast release. Using this approach, we demonstrated the generality of this strategy for delivery of four additional mAbs, murine and human anti-PD-1 and anti-CTLA-4. Our optimized implants delivering bevacizumab have a diameter of ~0.88 mm. Ideally, an intraocular implant would be <0.46mm, the diameter of the approved intraocular implant, Ozurdex®[60], to avoid increased intraocular pressure or patient discomfort. Thus, in this chapter, we have investigated using our optimized formulation and adjusting the tubing inner diameter to reduce our implant size and using a PLGA-glucose-STAR, which is used in commercial product Sandostatin® LAR, for a more efficient coating of the core implant. PLGA-glucose STAR is a referred to as a STAR shaped polymer because it is a glucose molecule with potentially 5 branches of PLGA coming off of it[201]. This PLGA has shown to have rapid pore closing, polymer healing properties that may be beneficial in creating a coating around our linear PLGA core implants[202].

Here we present our unique mAb encapsulation technique (Figure 1), implant composition, *in vitro* performance and *in vivo* efficacy for GBM and potential future formulations for reduced diameter implants to treat intraocular disease such as wetAMD. Our previously optimized implants delivering bevacizumab have a diameter of ~0.88 mm. Ideally, an intraocular implant would be <0.46mm, the diameter of the approved intraocular implant, Ozurdex®[60], to avoid increased intraocular pressure or patient discomfort. Thus, in this chapter, we will investigate using our optimized formulation and adjusting the tubing inner diameter and PLGA coating in order to reduce our implant diameter and more efficiently coat the implant.

2.3 Materials and methods

2.3.1 Materials

Avastin®, commercial solution of bevacizumab was purchased from the pharmacy and used within its shelf-life period. PLGA 50:50 (inherent viscosity=0.64 dL/g and M_w=54.3 kDa, ester terminated) was purchased from LACTEL Absorbable Polymers (Birmingham, AL). PLGA (Resomer® 5545 DLG 5GLU) was purchased from Evonik Corp. (Birmingham, AL). Trehalose dihydrate (trehalose), $MgCO_3$ basic, guanidine hydrochloride, DL-dithiothreitol (DTT), ethylenediamine-tetraacetic acid (EDTA), Na_2HPO_4, NaH_2PO_4, anti-human IgG-alkaline phosphatase antibody produced in goat and p-nitrophenyl phosphate liquid substrate system (pNPP) were purchased from Sigma-Aldrich Chemicals (St. Louis, MO). Tween 80 (10%), acetone, KH_2PO_4, K_2HPO_4, KCl, phosphate buffered saline (PBS), Amicon Ultra-15 Centrifugal Filter Units (10,000 MWCO), and coomassie plus reagent assay kit were purchased from Fisher Scientific (Hanover Park, IL). Platinum-cured silicone rubber tubing (0.8 mm i.d., 2.4 mm o.d.) was purchased from Cole Parmer (95802-01,Vernon Hills, IL). Murine and human anti-PD-1 and anti-CTLA-4 were a generous gift from Bristol-Myers Squibb.

2.3.2 Methods

2.3.2.1 Preparation of mAb powder

The buffer of the antibody solutions (human anti-PD-1 and anti-CTLA-4, murine anti-PD-1 and anti-CTLA-4, bevacizumab (Avastin®)) containing antibody and excipients was exchanged into 51 mM sodium phosphate buffer (pH 6.2) by using Amicon Centrifugal Filter Units (10,000 MWCO) to remove trehalose. Then, trehalose (100 mg/ml in 51mM sodium phosphate buffer) was added at a 1.5:1 weight ratio of trehalose:antibody, and the solution was diluted with 51 mM sodium phosphate buffer (pH 6.2) for the final antibody concentration of 25 mg/mL and lyophilized for 3 days. The solid was then ground by CryoMill (Retsch, Germany) at 30Hz for 30 min and sieved through 90-μm screen (Newark Wire Wearing, Newark, NJ).

2.3.2.2 Preparation of mAb implants

Preparation of 0.8 mm diameter implants:

The resulting mAb powder was suspended into 50% (w/w) PLGA solution in acetone with 3% (w/w) $MgCO_3$ in a 2 mL centrifuge tube, then mixed and transferred into a 3 mL syringe. The suspension was extruded into silicone rubber tubing (i.d.=0.8 mm) and sealed at the ends with paperclips, then dried at room temperature for 48 h followed by vacuum drying at 40 °C and 23 in. Hg vacuum for an additional 48 h. The final dried implants were obtained by removal of silicone tubing and were cut into 0.5 cm long segments for future use. For coated implants, the core implants were put back into silicone tubing and pure PLGA solution at various concentrations (10%, 30%, 50%) in acetone within a 3 mL syringe was extruded over the core implants to coat the surface, and the tubing was sealed at both ends before drying in vacuum oven at room temperature for 48 h and at 40 °C for an additional 48 h. Then, silicone tubing was

removed and the final coated implants were cut to 0.5 cm for the following experiments. For anti-PD-1 and anti-CTLA-4 implants, coating was repeated after drying for a total of two, 30% PLGA in acetone coatings, before silicone tubing removal.

Preparation of smaller diameter implants:

Bevacizumab implants were prepared the same as described above in "Preparation of mAb implants" section with the following adjustments. A smaller tubing (0.5 mm i.d., Cole Parmer, product no. 95802-00) was used and the 30% PLGA coating process was repeated for 1-4 coatings.

Preparation of STAR coated implants:

Uncoated bevacizumab implants were prepared as described above "Preparation of mAb implants" using 0.8 mm i.d. tubing. The coating of the core implant was obtained using a PLGA Glucose-STAR polymer (STAR). The STAR PLGA was dissolved in acetone at 30% w/w and extruded over the core implant and dried at room temperature under vacuum for 2 days, and at 40 °C under vacuum for 2 days. Finally, the implants were annealed at 50 °C under vacuum for 24 h. The coating process was completed for 1 or 2 coatings.

2.3.2.3 Measurement of mAb loading in implants

Implants (3-5 mg) were dissolved in 1 mL of acetone for 1 h and centrifuged to precipitate mAb. PLGA dissolved in supernatant was removed and the mAb pellet was washed with acetone and centrifuged three times more to remove residual PLGA. The pellet was then air dried, reconstituted in 1 mL of PBST (phosphate buffered saline with 0.02 % Tween-80, pH 7.4) at 37 °C overnight and analyzed by size-exclusion high-performance liquid chromatography (SE-HPLC) or size-exclusion ultra-performance liquid chromatography (SE-UPLC). The condition of SE-HPLC using a TSKgel G3000SWXL, 7.8mm ID x 30 cm, 5µm column (TOSOSH

Biosciences, LLC, Japan) to quantify monomer and soluble aggregates was followed as previously described[203] with slight modifications, which included the injection volume of 50 µL and filtration of all samples through 0.45 µm filter. Similarly, loading was determined for anti-PD-1 and anti-CTLA-4 after polymer removal by SE-UPLC with an injection volume of 10 µL, a flow rate of 0.4 mL/min through a BEH SEC 450Å, 2.5 µm column (Waters, Milford, MA) over 6 min, and elution was monitored at UV absorption of 280 nm. For both SE-HPLC and SE-UPLC, an isocratic elution of mobile phase (0.182 M KH_2PO_4, 0.018 M K_2HPO_4, and 0.25 M KCl , pH 6.2). Extracted loading and loading efficiency were calculated by the following equations (1) and (2).

$$(1)\ \text{Extracted loading}\ (\%) = \frac{\text{Weight of extracted bevacizumab}}{\text{Weight of total implant}} \times 100\%$$

$$(2)\ \text{Loading efficiency}\ (\%) = \frac{\text{Extracted loading}}{\text{Theoretical loading}} \times 100\%$$

2.3.2.4 In vitro release of mAb from implants

Implants (0.5 cm long, unless otherwise indicated) were added in 1.5 mL centrifuge tubes with 1 mL of PBST and incubated at 37 °C without agitation, as agitation was found to cause insoluble aggregation of the antibody in the release media. The release medium was replaced with fresh medium at each time point. The amount of released mAb at each time point was measured by SE-HPLC/UPLC as described above and calculated as percentage of the released amount out of the extracted loading of soluble mAb. In certain instances, the release media was also analyzed for protein structure and immunoreactivity, as described below.

2.3.2.5 Determination of water uptake

Water uptake of implants (W (t)) at time, t, was determined during the incubation period by Equation (3) below:

$$(3)\ W(t) = \frac{W_{wet}^{t} - W_{dry}^{t}}{W_{initial}^{t}}$$

Where W_{wet}^{t} and W_{dry}^{t} are the wet and dry formulation weights, respectively, after incubation and drying under vacuum (23 in Hg) at room temperature for 3 days.

2.3.2.6 Confocal microscopy

The distribution of the STAR PLGA coating over the bevacizumab core implants was visualized using confocal microscopy. The implant core was formulated without any dye and as described above. To visualize and distinguish the PLGA coating, Cyanine5 carboxylic acid dyes (Cy5, Lumiprobe, Hallandale Beach, FL) was dissolved at 10 μg/mL in STAR PLGA/acetone solution, and the core implants were coated with the Cy5/PLGA solution as previously described. The dried implants were cut for cross-sectional images and placed on a clean glass slide in immersion oil. A clean glass cover slide was placed over the implant slices. Samples were imaged using a confocal microscope (Nikon A1 Spectral Confocal Microscope) with excitation/emission wavelengths of 640/700 nm for the Cy5 STAR PLGA coating.

2.3.2.7 Measurement of monomer content

Monomer contents for the antibodies were determined from the peak areas determined by SEC and calculated by the following equation (4)

$$(4)\ \text{Monomer content}\ (\%) = \frac{\text{AUC of a monomer peak}}{\text{AUC of total peaks}} \times 100\%$$

2.3.2.8 Enzyme linked immunosorbent assay (ELISA) and cell-based bioassay

Immunoreactivity for anti-PD-1 and anti-CTLA-4 were performed using commercial ELISA kits from AcroBiosystems (Newark, DE, EPH-V1 and ECH-V1, respectively), or with a cell-based assay from Promega (Madison, WI, J1250 and JA3001, respectively) with slight modifications. Briefly, the competitive ELISAs used human PD-1 and human CTLA-4 as the coating ligands, then an equal parts mixture of release samples (n=3 for each time point, triplicated on the plate, diluted to ~1 ug/ml) and biotin labelled anti-PD-1 or anti-CTLA-4 were added to the coated plates and were detected by UV absorption at 450 nm after HRP conjugation using TMB substrate.

For the anti-PD-1 cell-based bioassay, human PD-L1 expressing aAPC/CHO-K1 cells were cultured overnight (37 °C, 5% CO_2) on a 96-well plate. The next day, standards and release samples were added to the cells followed by the addition of PD-1 effector cells (Jurkate T cells expressing human PD-1 and a luciferase reporter, NFAT response element) and incubate for 6h (37 °C, 5% CO_2). For the anti-CTLA-4 bioassay, CTLA-4 effector cells (Jurkate T cells expressing human CTLA-4 and a luciferase reporter), standards and release samples, and aAPC/Raji cells expressing CD80 and CD86 ligands were plated on a 96-well plate and incubated for 6h (37 °C, 5% CO_2). Standards were prepared using the same solutions of mAbs, provided by Bristol-Myers Squibb, that were used to make the mAb implants. Release samples were run in triplicate and concentration of reactive mAb was calculated based on the standard curve. Both bioassays were detected using the Bio-Glo Luciferase assay system (Promega, Madison, WI) using a 0.5s integration time, and standards were graphed using a 4-parameter

logistic curve for interpolating the release sample concentrations. For each release time point, n=3, each replicate was triplicated on the plate.

Immunoreactivity and bioactivity of all mAbs were calculated by the following equation (5):

$$(5)\ \text{Immunoreactivity/bioactivity}\ (\%) = \frac{\text{Concentration from ELISA/bioactivity}}{\text{Concentration from SE} - \text{HPLC/UPLC}} \times 100\%$$

2.3.2.9 Circular dichroism (CD)

CD was performed with Jasco J-815 CD spectrometer equipped with Jasco temperature controller (CDF-426S/15) and Peltier cell at 25 °C. The samples were diluted or buffer-exchanged into 51 mM sodium phosphate buffer (pH 6.2) and concentrated by using Amicon Centrifugal Filter Units (10,000 MWCO), so the final concentration ranged from 0.05 to 0.5 mg/mL for far UV measurements (200-250 nm). The samples were measured in quartz cuvettes (Hellma) with a path length of 1 mm. The spectra were collected in continuous mode at a speed of 50 nm/min, bandwidth of 1 nm and a DIT of 1 sec and were the averages of 5-10 scans. The spectrum of blank 51 mM sodium phosphate buffer (pH 6.2) was subtracted from each spectrum by using the Jasco spectra manager software (Version 2.1). The raw data was converted to mean residue ellipticity (MRE, $\theta_{mrw,\lambda}$) using the following equation (6):

$$(6)\quad [\theta]_{mrw,\lambda} = MRW \times \frac{\theta_\lambda}{10 \times d \times c}$$

Where is the θ_λ observed ellipticity in degree at wavelength λ, d is the path length in cm, c is the concentration in g/mL, and mean residue weight (MRW), calculated as the molecular weight of the mAb divided by the number of amino acids -1, in g/mol is 113 for bevacizumab, 112 for anti-CTLA-4, and 110 for anti-PD-1. Concentration of the total protein measured by SE-HPLC/SE-

UPLC was used to normalize all data. Data smoothing was performed using SigmaPlot software (Version 12.0, Systat Software, Inc.).

2.3.2.10 Determining therapeutic efficacy in a syngeneic GBM model

Intracranial GBM tumors were established in 6-8-week old C57BL/6 mice by stereotactically injecting 3.0 x 10^4 GL26 cells into the right striatum using the following coordinates: 1.00 mm anterior, 2.5 mm lateral, and 3.00 mm deep from the bregma[204]. At 7 days post-tumor implantation, when the tumor was well established, mice were assigned to 4 treatment groups: Group 1: Blank implants (trehalose, sodium phosphate, $MgCO_3$, PLGA); Group 2: Irradiation (IR); an overall dose of 20 Gy IR was administered (2 Gy/d for 10d on days 7-11 and 14-18), Group 3: anti-PD1 implant + IR, and Group 4: anti-CTLA-4 implant + IR (dose of 300 μg antibody/implant, same IR dose and administration as IR group 2). Implants were implanted intratumorally. Mice were perfused with paraformaldehyde (PFA) when they become symptomatic due to tumor burden. A long-term survival rechallenge study was performed by injecting 3.0 x 10^4 GL26 cells into the contralateral hemisphere of the two long-term surviving mice from each antibody implant group as well as 3 treatment-naïve mice, using the same coordinates as previously mentioned. Mice were monitored for tumor burden and survival.

2.4 Results

2.4.1 Immune checkpoint inhibitor implant *in vitro* release and stability characterization

We encapsulated four key immune checkpoint inhibitor mAbs, murine and human anti-PD-1 and anti-CTLA-4, using the same formulation (albeit with a second PLGA coating to improve uniformity, Figure 2-1), and investigated their controlled release and stability properties. The two human mAbs are FDA-approved and administered systemically to treat a variety of

cancers including melanoma, non-small-cell lung cancer, renal-cell carcinoma, and squamous-cell carcinoma of the head and neck.[205–207] In addition to challenges in reaching the brain, systemic immune checkpoint mAbs suffer unwanted side effects mainly in the gastrointestinal tract, endocrine glands, skin, and liver.[207]

As seen in Figure 2-2, both murine and human forms of anti-PD-1 and anti-CTLA-4 could be encapsulated (6-8% loading, Table 2-2) and released continuously for ~60 days, similar to that observed with bevacizumab. The immune checkpoint mAbs were released in a monomeric form in each case until the very end of the release period when small levels of soluble aggregates (<0.66-5.18% of total) were observed in anti-PD-1 implants (Figure 2-2b). The structure and immunoreactivity of released mAbs were also well preserved, as indicated by far UV CD and ELISA (Figures 2-2c-e). Some loss of immunoreactivity was noted during release for both mAbs, which is reasonable considering the excipients applied from the bevacizumab formulation were not optimized for these antibodies. The immunoreactivity results were in-line with cell-based bioactivity evaluations for days 1 and 28 (Figure 2-3).

2.4.2 Immune checkpoint inhibitor implant *in vivo* efficacy

To determine whether the long-acting mAb polymers could locally treat brain cancer, we inserted murine immune checkpoint mAb implants via intratumoral injection through a 1.5 mm diameter burr hole in a syngeneic GBM bearing mouse. Since radiation therapy (IR) is the standard of care for GBM patients[3,115], we combined controlled release mAb implant therapy with IR. The murine forms of the mAbs were used in place of the human forms to offset interspecies immunogenicity to the mAbs. Immunocompetent C57BL/6 mice implanted with GL26-wt tumors in the striatum were treated with blank implants, anti-PD implants + IR, and anti-CTLA-4 implants + IR, as indicated in Figure 2-4.

We observed an ~1.6 fold ($p<0.0023$) increase in median survival (MS) of mice in the anti-PD1 implant + IR (MS: 71 dpi) compared to the IR (MS: 44 dpi) and blank implant (MS: 28 dpi) groups; the highest survival advantage of ~3.0 fold ($p<0.0017$) was achieved in the anti-CTLA-4 implant + IR (MS: 75 dpi) treated group compared to all other treatment groups. Long-term survivors in each mAb implant/radiation group also went into remission (survival >120 days). To determine if the mAb implant/radiation treatment could protect against tumor recurrence, GL26 cells were injected at the same level into the contralateral side of the brain of each surviving animal at 120 days post original tumor inoculation. These animals survived two-fold longer (anti-PD-1 implant + IR MS: 56, anti-CTLA-4 implant + IR MS: 61 DPI) than control tumor bearing animals (MS: 28 DPI) providing a clear indication of the enhanced immunological memory of the animals receiving controlled-release mAb/radiation therapy.

2.4.3 Reduced diameter implants

Figure 2-5 shows the release kinetics (a) and the monomer content (b) from reduced diameter implants. The 1-2 coatings that sufficed for the larger diameter coatings resulted in a large initial burst and fast release overall due to the shorter distance required for antibody release. Thus, 3 and 4 coatings were necessary to reduce the initial burst and control release for ~50 days, while also maintaining monomer content. The 4X coated implants had an average diameter of 0.65±0.01 (avg±SE, n=3) and a total BVZ loading of 6.77 w/w%.

2.4.4 PLGA-glucose STAR coated implants

PLGA-glucose STAR (STAR) was used to coat the linear PLGA core implants containing bevacizumab and the release kinetics, monomer content, water uptake and level of coating were monitored. These implants were made similarly to our linear PLGA coated implants with some modifications during drying in order to anneal the STAR polymer (Figure 2-

6). Bevacizumab mAb loading in single and double coated implants ranged from 8.0 – 8.5% from the theoretical loading of 10% for core implants (Table 2-3). Implants coated once slowly and continuously released to completion over 56 days and showed stable monomer content up to day 41, with a notable loss of monomer occurring thereafter (Figure 2-7). Implants coated twice slowly and continuously released to around 70% cumulative mAb over 50 days and showed stable monomer content up to day 21 before displaying significant soluble aggregation (Figure 2-7). Confocal imaging in Figure 2-8 shows that the single coating of both linear PLGA and STAR PLGA is incomplete and the second coatings are both more complete around the core implant, the twice coated STAR implants appearing to be slightly thicker and more evenly distributed. Figure 2-9 shows the water uptake over 4 weeks; the twice coated implants of both types of PLGA showed higher water uptake than the once coated. The twice coated STAR implants showed much higher water uptake after 4 weeks than all other formulations. The circular dichroism (Figure 2-10) analyses of bevacizumab before and during release did not show drastic differences except for the STAR twice coated day 36 release which did not show the same profile, which may be related to altered secondary structure.

2.5 Discussion

The current standard-of-care treatment for GBM (resection, radiation, chemotherapy) results in a 14-20 month survival rate with only 5% of patients surviving approximately 5 years, making GBM one of the most common and deadly primary tumors.[114] GBM evades the immune system through upregulation of immune checkpoint inhibitors (i.e. PD-1/PD-L1) and has a high rate of recurrence within the tumor environment.[114,3] Anti-PD-1 and anti-CTLA-4 are both in ongoing clinical trials for GBM, but suffer from systemic-related toxicity that can result in cessation of treatment.[10] Locally delivering immune checkpoint inhibitors through controlled

release implants would greatly benefit GBM treatment by avoiding systemic toxicity and extending antibody exposure at the tumor site.[168]

Adapting the optimized implant formulation of bevacizumab[62] by adding a second PLGA coating over the core implant reduced the initial burst and sustained release of human and murine Anti-PD-1 and anti-CTLA-4 continuously over 6 weeks with maintained secondary structure and minor loss of monomeric content and immunoreactivity/bioactivity. Implants were evaluated in combination with radiation therapy in a GBM murine model and were effective at mitigating disease progression and increasing immunological memory. We have successfully shown the potential of our controlled release implants for the treatment of GBM with anti-PD-1 and anti-CTLA-4 in combination with radiation. The injectable sub-millimeter rod system is adaptable[13] to additional bioactive agents such as immune stimulators (e.g., CpG)[208,209] and tumor penetration-enhancing cytotoxic agents (e.g., docetaxel) which will be discussed in Chapter 3.[210,211] Combination therapies offer increased survival in GBM over single arm therapies and both CpG and docetaxel are actively pursued options for GBM.[7,149,152,161,210] Formulating PLGA implants into long-term release, and combining them with immune checkpoint inhibitor implants, we expect to increase the effective immune response through the TLR9-agonist, CpG, and induce apoptosis and tumor penetration with docetaxel.[151,152,154,160] In the coated PLGA system described here, the original cylinders releasing anti-PD-1 and anti-CTLA-4 are currently slightly larger than the desired diameter (e.g., 0.46 mm of Ozurdex® implant[212]) for intravitreal delivery and may require attention to PLGA-induced inflammation (e.g., addition of anti-inflammatory controlled release segments[13,213] or further lactic/glycolic acid neutralization by antacid excipients[11]). To address this issue, we investigated whether we could reduce the diameter and maintain our controlled release by simply using a smaller diameter silicone tubing

to make the drug-loaded core implants. The typical 1-2 PLGA coatings on the reduced diameter core implant resulted in fast release likely because the bevacizumab can be released through the lateral surface of the implant[62] and the smaller diameter would result in a shorter distance to traverse before escaping the PLGA matrix. By applying a total of 3-4 coatings, the bevacizumab initial burst was reduced and slowly and continuously released over ~50 days. The diameter of these implants was still larger than desired even when using a 0.5 mm inner diameter silicone tubing, likely because the tubing can expand during formulation. Next, we investigated whether we could improve the effectiveness of our drug-free PLGA coating and therefore reduce the level needed by using a PLGA-glucose STAR which has rapid healing properties and may offer a more efficient barrier to the high initial osmotic pressure induce release[202]. The PLGA-glucose STAR coating did not result in an optimal release profile. One iteration of the STAR coating still had a high initial burst release and a faster overall release, and the addition of a second STAR coating resulted in incomplete release and mAb aggregation, pointing to the likelihood of an acidic microclimate pH effect owing to thickness and completeness of coating affecting the mass transfer of water-soluble acids of the polymer matrix.

2.6 Conclusion

More research is necessary to realize the potential of this approach including: (a) further reduction in implant diameter to <0.5 mm to decrease intravitreal needle size for improved patient acceptability and reduced risk of adverse effects;[214] further evaluation and management of mild PLGA-induced inflammation in sensitive tissues such as the eye and joint;[215] the extent and necessity of tissue penetration[216–218] of immune checkpoint mAbs in brain tissues for GBM and other brain tumor therapies; the selection of appropriate adjunct therapies (e.g., radiation[139], adjuvants[208,209], neoantigens[219], chemotherapy[210,211]) for optimization of the local immune

checkpoint effect; and further optimization of the polymer formulation to maximize activity and reduce residual protein aggregation at the end of the release period for certain mAbs. With such initiatives, the application of local controlled-release strategies for mAbs, such as presented here, could become available in the foreseeable future.

Encapsulated moiety	Formulation type	mAb Loading	Encapsulation efficiency	Initial burst	Total cumulative release	Duration of release/exposure	ref
	Desired outcomes →	***High, therapeutically relevant loading desirable; varies by formulation***	***>70%***	***<20% w/w***	***>80%***	***>2 months***	
Anti-VEGF (bevacizumab), human anti-PD-1 and anti-CTLA-4, murine anti-PD-1 and anti-CTLA-4	PLGA implants	6.2-8.3% w/w	>90%	<10%	>89%	2 m in vitro	
Nogo R-66 pIgG	Hyaluronic acid hydrogel	13.5% w/w	NR	10%	80%	16 d in vitro	[191]
Trastuzumab	PLGA microspheres	4.9% w/w	NR	18.9%	25.9%	70 d in vitro	[187]
Anti-VEGF (bevacizumab)	PLGA nanoparticles	13% w/w	96.4%	~8.42%	64%	90 d in vitro	[188]
Anti-VEGF (bevacizumab)	Nano mesoporous SiO_2 film	23.6% w/w	NR	<5%	94%	30 d in vitro	[192]
IgG	HAMC Hydrogel with dispersed PLGA particles	15% w/w (in particles)	56%	<20%	60-70%	28 d in vitro	[182]
Anti-NogoA	PLGA nanoparticle in HAMC hydrogel	3% w/w (in particles)	43%	<20%	70%	54 d in vitro	[183]
hu IgG1	Alginate hydrogels	30 mg/ml	NR	<20%	90-100%	15 d in vitro	[193]
hIgG	PLGA microspheres	26% w/w	12.5%	30%	40%	25 d in vitro	[184]
hIgG	Peptide hydrogel	5µM, depends on antibody solubility in water, gel is 99.5% water	100%	1-27% in 2h, 20-50% 1d	25-80%	100 d in vitro (most released in first 10-40 days)	[186]
Anti-VEGF (bevacizumab)	In situ forming gel, HEMA/PCM	~1.25% (1.25mg/100µL)	NR	21%	96%	120 d in vitro, 60 d in vivo	[195]
Anti-CD40, anti-CTLA-4	pLHMGA microspheres	.4-1.1% w/w	>85%	20%	80%	30 d in vitro	[185]
Anti-VEGF dimeric, dual antibody	PolyActive™ microparticles: PEG-PBT hydrogel co-polymer microparticles	>15.3% w/w	71-90%	<20%	>80%	6-12 m in vitro, 6 m in vivo	[194]
Anti-VEGF (ranizumab)	Nanoporous PCL thin film disc, 10 mm diameter	6.8% w/w	NR	<10%	60%	16 w in vitro, 12 w in vivo	[189]
BSA	Hot melt extruded PLGA implants, 1mm diam	15% w/w	NR	3.75%	11.1%	12 w in vitro	[190]
Anti-VEGF (bevacizumab)	Poloxamine Hydrogel	6.25 mg/ml	NR	<6%	>90%	21 or 115 d in vitro	[196]

Table 2-1. Literature analysis of key criteria for development of long-term biodegradable dosage forms for controlled release of stabilized mAbs. *Red text indicates the desired criteria was not met. The first, blue, row in each table indicates the current study. Grey rows are used to highlight most interesting results. PLGA= poly(lactic-co-glycolic acid); FLR= fluorescence; PK= pharmacokinetic; NR=not reported; HAMC= hyaluronan and methyl cellulose; SEC= size exclusion chromatography; ELISA= enzyme-linked immunosorbent assay; FTIR= fourier-transform infrared spectroscopy; CD= circular dichroism; HEMA= hydroxyethyl methacrylate; PCM= polycaprolactone dimethacrylate; pLHMGA=poly(d,l lactic-co-hydroxymethylglycolic acid); PEG= polyethylene glycol; PBT=polybutylphthalate.*

Table 2-1 continued.

Encapsulated moiety	In vitro structural retention	In vitro binding retention	In vivo efficacy	Needle size	Tolerability/build up	Comments	ref
Desired outcomes →	***Maintained secondary and tertiary structure for duration of release***	***Maintained binding to relevant target for duration of release/exposure***	***Significant improval compared to controls***	***Smaller than or equal to 22G for intraocular***	***Nontoxic materials with no build-up after drug release***		
Anti-VEGF (bevacizumab), human anti-PD-1 and anti-CTLA-4, murine anti-PD-1 and anti-CTLA-4	SEC maintained in all mAbs during majority of release. <5% soluble aggregation in anti-PD-1 relative to total mAb after 60d. CD no significant differences for any mAb.	Anti-PD-1 and anti-CTLA-4 showed 40-80% immunoreactivity over 28d.	Anti-CTLA-4 and anti-PD-1 with radiation both significantly improved survival and immune memory in intracranial GBM model.	19G	PLGA well tolerated.	Coated PLGA implant system has been successfully applied to 5 mAbs.	
Nogo R-66 pIgG	NR	Qualitative receptor binding assay FLR	NR	NR	NR: although HA expected to be well-tolerated	Release was pH dependent, much faster release at pH 5, 6	[191]
Trastuzumab	NR	NR	NR	NR	Well-tolerated in rabbits	In vivo release similar to in vitro	[187]
Anti-VEGF (bevacizumab)	NR	NR	NR	NR	NR: although PLGA expected to be well-tolerated		[188]
Anti-VEGF (bevacizumab)	NR	ELISA used for release	NR	NR	NR: authors' previous work shows tolerability in rabbit vitreous		[192]
IgG	NR	NR	NR	30G	NR: authors' previous work shows HAMC tolerability in rats, and PLGA expected to be well-tolerated		[182]
Anti-NogoA	NR	<10% bioactive by day 14	NR	NR	NR: although HAMC and PLGA expected to be well-tolerated		[183]
hu IgG1	SEC: monomer content >94% up to Day 10 tested only	Cell based luciferase assay: >80% (Day 10 tested only)	NR	NR	NR: alginate is a natural polymer but is not as established as PLGA for drug delivery	Release is pH dependent, lower pH=lower release rate	[193]
hIgG	SEC: fragmentation after initial burst, FTIR: unaltered	ELISA: 37% active in initial burst	NR	NR	NR: although PLGA expected to be well-tolerated		[184]
hIgG	CD, FLR No detectable differences at initial and 2mo	PC-BSA antigen binding assay showed retained activity	NR	NR	NR: Although peptide hydrogel is expected to be biocompatible, non-toxic		[186]
Anti-VEGF (bevacizumab)	SEC :>95% monomer CD-maintained structure	ELISA used for release	NR	34G	Some cell death observed from use of photoinitiator/un-crosslinked polymer. No toxicity observed in rat eyes. PCM/HEMA used in FDA approved products.	100 µL injection volume needed for 1.25 mg dose of bevacizumab, 50 µL is the clinical injection volume.	[195]
Anti-CD40, anti-CTLA-4	Intrinsic FLR used for release. No analysis of aggregation/fragmentation	NR	In vivo efficacy evaluated in MC-38 murine flank tumor. Significant improval (40-50% survival rate) compared to untreated.	NR	pLHMGA similar to PLGA but with potentially less acidic products. Particles were fully degraded in vivo by 60 d.		[185]
Anti-VEGF dimeric, dual antibody	Some cleavage occurred; activity maintained	VEGF binding immunoassay: 70-90% active during release	Effectively protected against CNV lesions over 6 m in primate model.	30G	In vivo inflammation, particle migration, and delayed/incomplete particle breakdown. PBT does not fully degrade and degradation products are not well understood.	Dual antibody not FDA approved. CNV model not as clinically relevant for wet AMD,	[194]
Anti-VEGF (ranizumab)	SEC: 75% stabile in vivo 1-12 w >100% stabile in vitro 16 w	NR	NR	Administered by surgical insertion	No inflammation detected, cataracts observed in treated rabbit eyes.		[189]
BSA	BSA conformational changes via Raman	NR	NR	NR	NR: although PLGA expected to be well-tolerated		[190]
Anti-VEGF (bevacizumab)	FLR used for release, no analysis of aggregation	VEGF ELISA: 87% binding at 30 d	NR	NR	Some cellular cytoxicity seen in 8-arm poloxamine-maleimide.	Triphasic release, binding not measured after 30d.	[196]

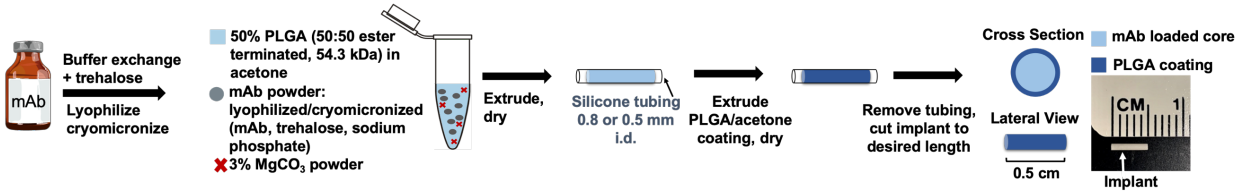

Figure 2-1. Schematic overview of PLGA mAb implant formulation.

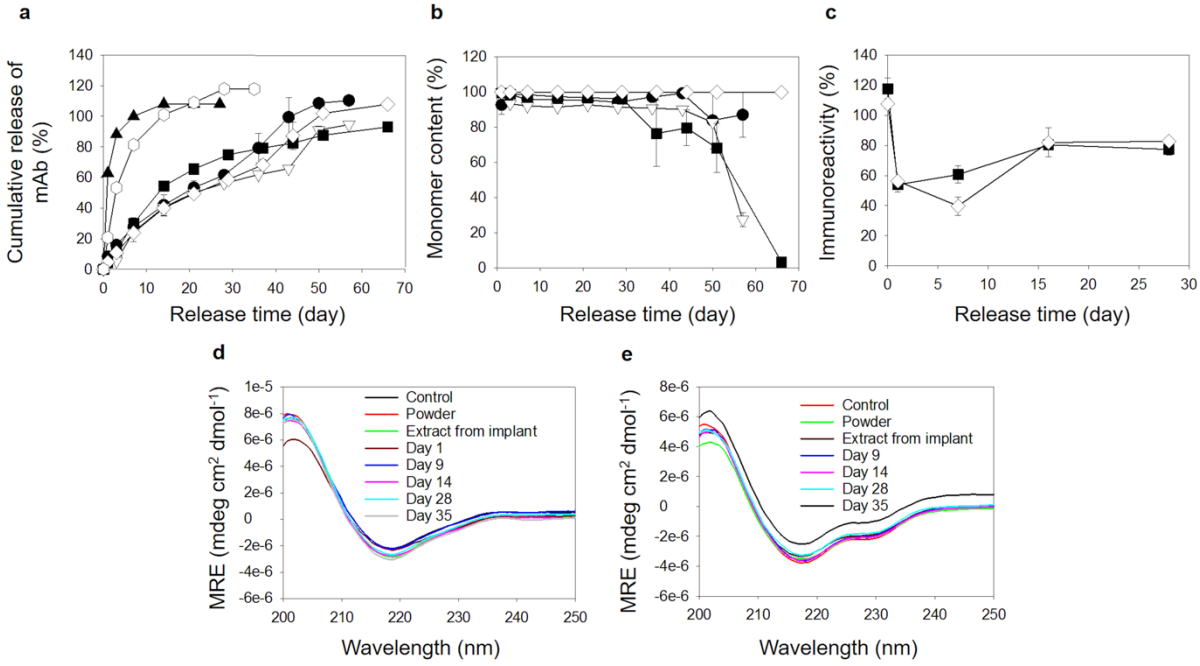

Figure 2-2. In vitro characterization of the twice coated implants. *(a) Release kinetics and (b) monomer content of twice coated mAb implants from murine anti-PD-1 (●), murine anti-CTLA-4 (▽), human anti-PD-1 (■), and human anti-CTLA-4 (◇), and release kinetics for once coated implants of human anti-PD-1 (▲) and human anti-CTLA-4 (○). Symbols represent mean ± SE, n=2 for murine and mean ± SE, n=3 for human mAb samples. (c) Immunoreactivity by ELISA of human anti-PD-1 (■) and human anti-CTLA-4 (◇). Symbols represent mean ± SE, n=4-6. (d,e) CD spectra of (d) human anti-CTLA-4 and (e) human anti-PD-1 from extract and release media compared to 1.5:1 (trehalose:mAb, w/w) powder formulation and control antibody (anti-PD-1 day 1 release concentration was too low for analysis).*

mAb	Extracted loading (%)
Murine Anti-PD-1	7.6 ± 0.2[a]
Murine Anti-CTLA-4	6.2 ± 0.1[a]
Human Anti-PD-1	8.3 ± 0.2[b]
Human Anti-CTLA-4	8.1 ± 0.4[b]

Data reported as mean ± SE, [a]n=2 or [b]n=3

Table 2-2. Loading of twice coated, 10% theoretical mAb core implants.

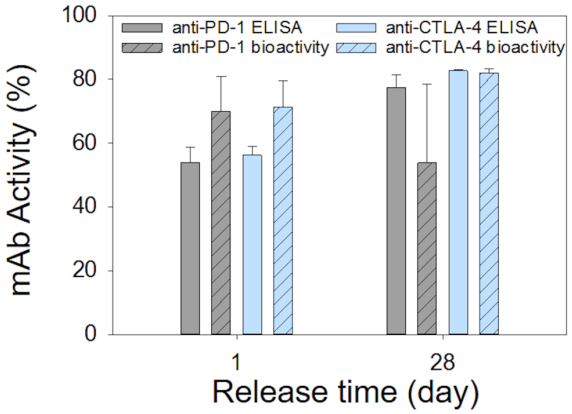

Figure 2-3. In vitro bioactivity and immunoreactivity of anti-PD-1 and anti-CTLA-4. *Cell-based bioactivity (bioassay) and immunoreactivity (ELISA) assays were performed for human anti-PD-1 and human anti-CLTA-4 antibodies on days 1 and 28 post in vitro release in PBST. Symbols represent mean ± SE, n=2-3.*

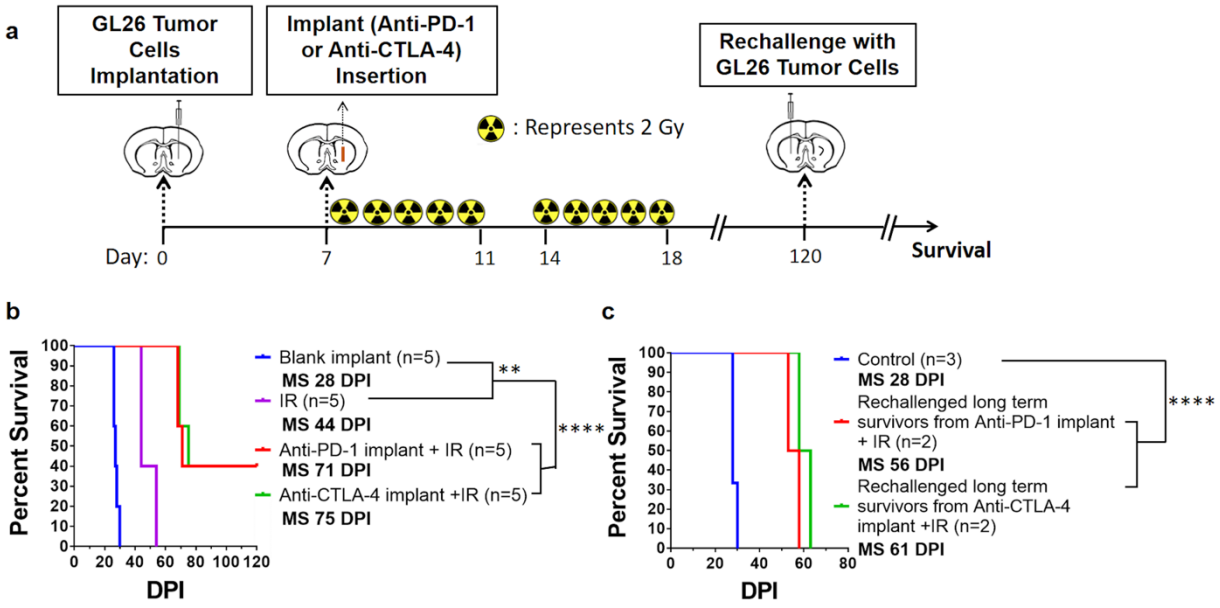

Figure 2-4. Intratumoral PD-1 and CTLA-4 neutralization treatment in combination with radiation enhances survival of GBM-bearing mice. *(a) Mice with GL26 tumors were implanted with blank, anti-PD-1 implant or anti-CTLA-4 implant on day 7 and administered 2 Gy/day for 10 days. (b) Kaplan-Meier survival analysis of GL26 tumor-bearing animals treated with IR in combination with blank, anti-PD-1 or anti-CTLA-4 implants. Long-term survivors from checkpoint blockade and radiation treatment strongly inhibit intracranial tumor re-challenge. (a) GL26 tumors were implanted stereotactically into the contralateral hemisphere of the long-term survivors from the anti-PD-1 + IR and anti-CTLA-4 + IR treatment groups. (c) Kaplan-Meier survival plot for re-challenged long-term survivors from the anti-PD-1 + IR and anti-CTLA-4 + IR treatment groups. Data were analyzed using the log-rank (Mantel-Cox) test. **p < 0.01; ****p < 0.0001. MS indicates median survival.*

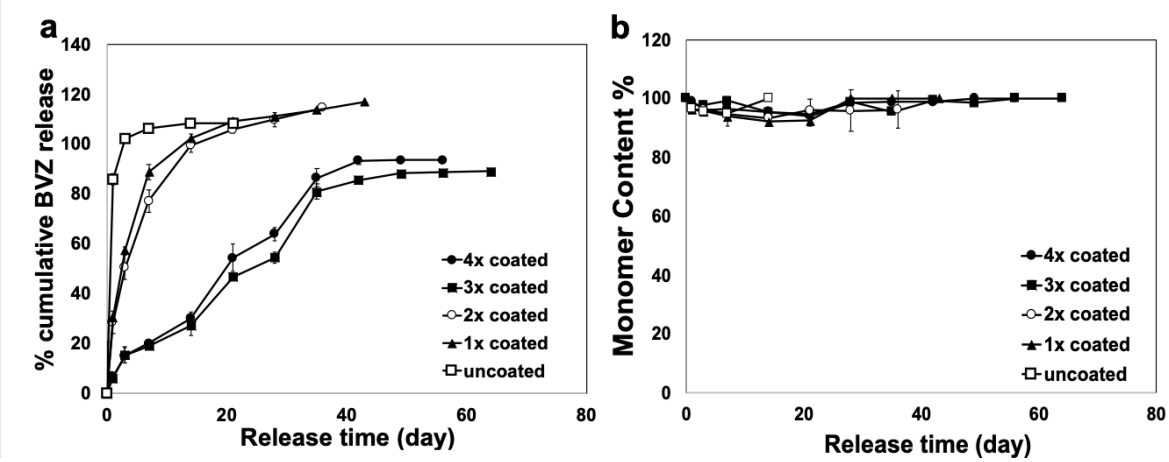

Figure 2-5. In vitro characterization of reduced diameter PLGA implants containing bevacizumab. *a) In vitro release kinetics and b) monomer content of BVZ from reduced diameter PLGA implants with various amounts of coating. Symbols represent mean ± SE, n=2-3.*

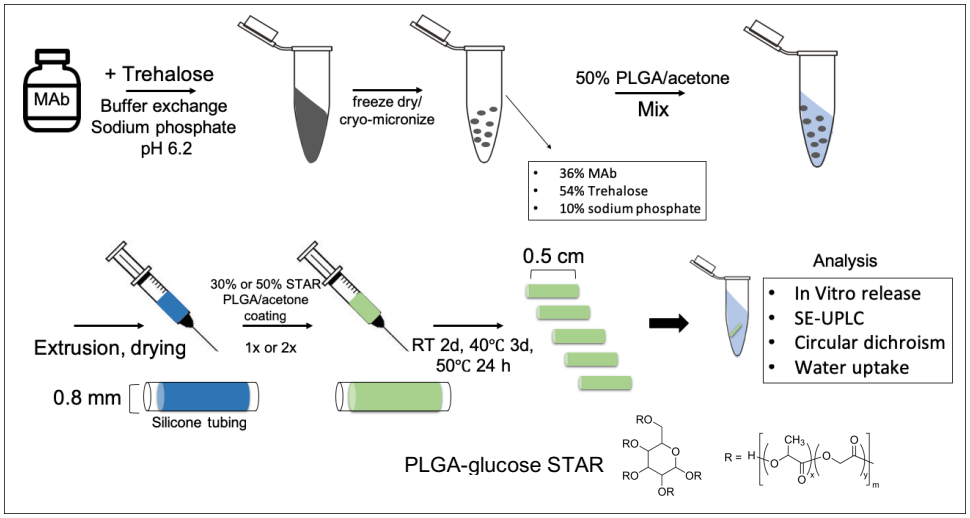

Figure 2-6. Schematic overview of PLGA STAR coated, linear PLGA core implants.

Implant Formulation	Extracted BVZ loading (%)
Uncoated	9.0 ± 0.1
STAR 1x coated	8.5 ± 0.4
STAR 2x coated	8.0 ± 0.7

Table 2-3. Extracted loading of STAR coated BVZ implants. *Values represent mean ± SE, n=3.*

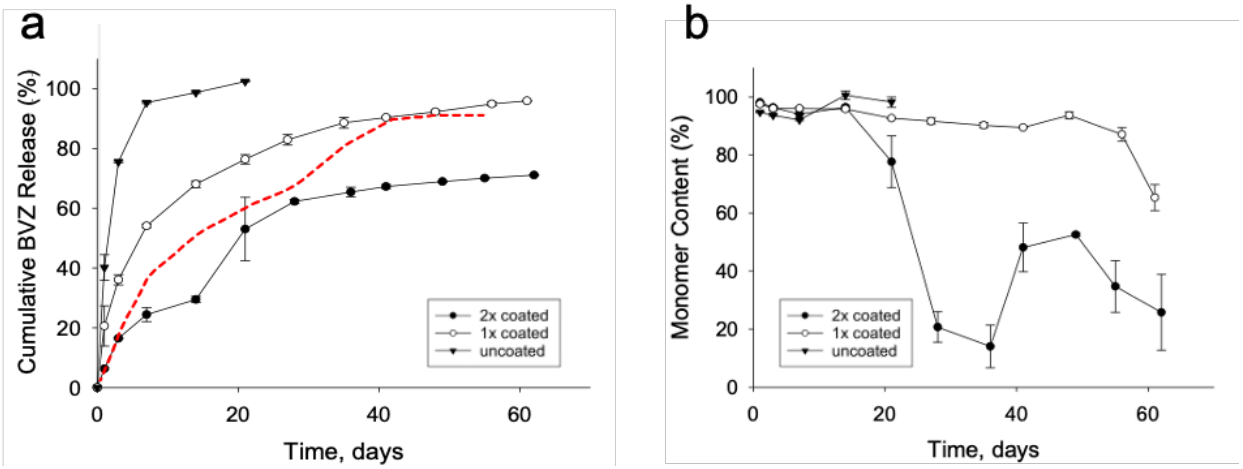

Figure 2-7. In vitro characterization of STAR coated, linear PLGA core implants containing bevacizumab (BVZ). *a) Cumulative BVZ release and b) monomer content from uncoated, 1X STAR coated, and 2X STAR coated implants. Red dotted line represents optimized BVZ loaded PLGA implants coated with linear PLGA. Symbols represent mean ± SE, n=3.*

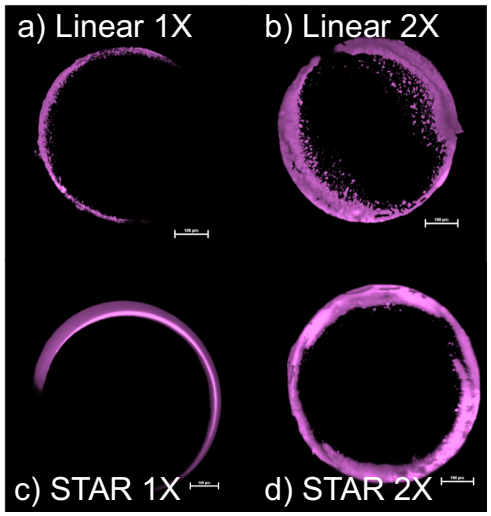

Figure 2-8. Confocal images of PLGA implants. *Cross sectional images of Cy-5 labelled coatings of a) 1X linear PLGA, b) 2X linear PLGA, c) 1X STAR-PLGA, and d) 2X STAR PLGA. Scale bars represent 100μm.*

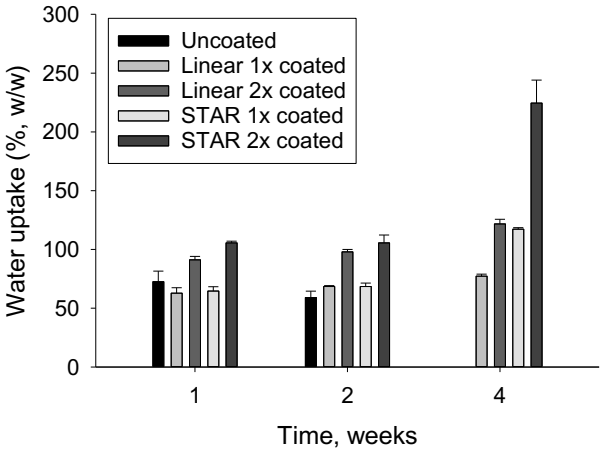

Figure 2-10. Water uptake of linear and STAR PLGA coated implants during incubation in PBST. *Water uptake of BVZ implants were determined after 1, 2, and 4 weeks of incubation. Symbols represent mean ± SE, n=3.*

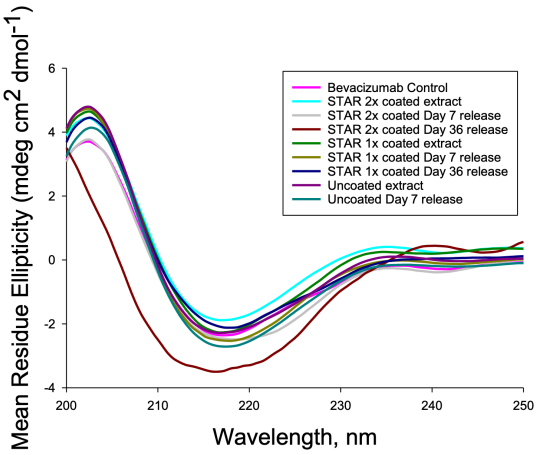

Figure 2-9. Circular Dichroism spectra of bevacizumab before and after release from linear and STAR PLGA coated implants.

Chapter 3: Controlled Release of CpG ODN and Docetaxel

3.1 Abstract

Glioblastoma has poor survival and a high rate of recurrence, owing to the difficulty to reach effective therapeutic levels at the tumor site due to the blood brain barrier and blood tumor barrier, the high heterogeneity of the tumor, and the immunosuppressive and abnormal tumor microenvironment. CpG is a toll like receptor-9 (TLR9)-agonist and can help to initiate an immune response. Docetaxel is not only an apoptosis inducing agent, but helps to reduce the solid tumor mass allowing for better penetration of itself and other agents into the glioma tumor. Both CpG and docetaxel do not readily cross the blood brain barrier and would benefit from a sustained local release option. Here, we have developed controlled release of CpG formulated with albumin and $MgCO_3$ from PLGA 50/50 implants that slowly released the oligonucleotide for >40 days and showed retained activity in binding to TLR9 receptors in vitro. Albumin and $MgCO_3$ were used to control microclimate pH and to provide continuous release. Docetaxel was formulated into PLGA 50/50 implants and sustained >80% total cumulative release for >100 days. Implants were formulated under anhydrous conditions by combining the drug and any excipients with a mild solvent, acetone, and extruding into silicone rubber tubing followed by drying to allow for solvent evaporation. In the future, these formulations will be combined with immune checkpoint inhibitors, anti-PD-1 and anti-CTLA-4, to locally treat glioblastoma after a single injection or implantation, allowing for a multi-faceted approach to treat the complicated aspects of glioblastoma.

3.2 Introduction

Glioblastoma (GBM) is the highest occurring primary brain tumor with a median survival of 12-14 months and a high rate of recurrence[1,2]. GBM tumors are highly heterogeneous and immune suppressive properties that obstruct therapy[3]. Treatment is typically administered by intravenous infusion and to reach the brain, therapeutics must be given in high concentrations, which can pose toxic side effects, especially for the administration of chemotherapeutic agents. The blood brain barrier (BBB) and the blood tumor barrier (BTB) are both significant obstacles for current systemic therapies. Numerous methods have been studied to disrupt the BBB to improve the systemic delivery of drugs to the brain, but are impractical, unsafe, or suffer from inadequate drug accumulation at the tumor site[4–6]. Glioblastoma is difficult to treat due to the heterogeneity of the tumor, thus, synergistic or combined therapies typically have better outcomes[7,140].

Docetaxel is a commonly used taxane similar to paclitaxel but has been shown to be more cytotoxic to GL26 cells *in vitro* (5-times lower IC_{50} value) than paclitaxel[161]. Taxanes are apoptosis inducing agents that have been shown to not only induce cell death but to decrease the tumor cell density, allowing for further drug penetration[154,160]. Kuh et al. showed that paclitaxel penetration into the solid tumor cells has a delayed effect, ~24 h, dependent on apoptosis and the reduction of the epithelial cell density before it penetrates deeper into the tumor[160]. Docetaxel has poor oral bioavailability and is a PgP substrate, causing poor brain distribution[220,221], thus, a local treatment option for brain cancer is necessary. Toll-like receptor-9 (TLR9), is expressed in human glioma tumors and CpG, a TLR9 agonist, has shown improved survival alone and in combination with anti-CTLA-4 and anti-PD-1 in GBM and bladder cancer[151,152]. CpG does not extensively distribute to the brain[222,223] and has been shown to be effective after multiple local,

intratumoral injections[161], and would benefit from a sustained local delivery. Combining these therapies is expected to overcome the immune suppressive nature of GBM tumors as well as initiate innate and adaptive immune responses.

3.3 Materials and methods

3.3.1 Materials

CpG ODN 1826 was custom made from Integrated DNA Technologies (IDT). $MgCO_3$ basic (part no. 63062) and BSA (part no. A7906) were purchased from Sigma Aldrich. Acuity UPLC® Oligonucleotide BEH C18 Column 130A, 1.7 µm, 2.1x100 mm column (part no. 186003950) and Acquity UPLC® BEH C18, 1.7 µm, 2.1x 100mm column (part no. 186002352) were purchased from Waters Corp. TSKgel G3000SWXL, 7.8mm ID x 30 cm, 5µm column (part no. 08541) was purchased from TOSOSH Biosciences, LLC, Japan. Docetaxel, 99% (part no. J60174), was purchased from Fisher Scientific. PLGA 50:50 (inherent viscosity=0.64 dL/g and M_w=54.3 kDa, ester terminated) was purchased from LACTEL Absorbable Polymers (Birmingham, AL). Platinum-cured silicone rubber tubing (0.8 mm i.d., 2.4 mm o.d.) was purchased from Cole Parmer (Vernon Hills, IL). Acetone, 99.8% extra dry AcroSeal® (part no. AC326801000) was purchased Fisher Scientific. Cryomill (part no. 20.749.0001) was purchased from Retsch GmBH (Germany). All chromatography reagents were at least HPLC grade and were purchased from Fisher Scientific.

3.3.2 Methods

3.3.2.1 Initial formulation of CpG implants: mixing vs cryomilling, PBST vs PBSTE release media

CpG ODN 1826 (IDT, Coralville, IA) was formulated similarly to the immune checkpoint inhibitors. We investigated the effects of cryomilling the CpG by formulating implants both with and without cryomicronization before mixing. CpG ODN 1826 is supplied as a lyophilized powder that is staticky and sometimes heterogenous and not always similar between batches. In the case of cryomilling, CpG (~6.25 mg) and BSA (~87.51 mg) was added to a 5 mL stainless steel cryomill jar with 3, 7mm steel balls. The sample was milled by a cryomill with an initial precooling cycle of 5Hz for 5 min followed by a 30 min cycle of 30Hz. The sample was brought to room temperature before opening the jar and sieving the powder to <90 μm. Powder was stored at -20 °C until use. For formulations without cryomilling, CpG was used as received. To formulate implants, CpG was weighed and combined with cryomilled BSA. The CpG (cryomilled with BSA, or not) and BSA (when not cryomilled with CpG) was mixed with a 50% PLGA in acetone solution. After mixing, the suspension containing (theoretically, 1% CpG, 14% BSA and 3% $MgCO_3$) was extruded into silicone tubing (0.8 mm i.d.) and dried at room temperature (23°C) for 2 days then at elevated temperature and under vacuum (40°C and 23 inHg) for 3 days for acetone removal. Implants were cut (0.25 cm) and placed in a 2 mL low binding Eppendorf tube for *in vitro* release in both phosphate buffered saline with 0.02% Tween80 (PBST), pH 7.4, and PBST with 1mM EDTA (PBSTE) and incubated at 37 °C with shaking at 240 rpm. Media was collected and replaced with the respective fresh media at 1,3, and 7 days, and weekly thereafter. Release samples were stored at 4 °C.

3.3.2.2 Optimized CpG formulation

CpG was used as received and was not cryomilled. We investigated encapsulation of CpG with BSA and another formulation with MSA after optimization with BSA in order to conduct future murine animal studies. To formulate implants, CpG was weighed and combined with weighed BSA or MSA, as a carrier protein and buffering agent, which was cryomilled and sieved <90um before use in all formulations. CpG and the BSA or MSA were mixed with a 50% PLGA in acetone solution. After mixing, the suspension containing CpG (6%), BSA (9, 11.5, 14%) or MSA (14%), and $MgCO_3$ (3%) was extruded into silicone tubing (0.8 mm i.d.) and dried at room temperature (23°C) for 2 days then at elevated temperature and under vacuum (40°C and 23 inHg) for 3 days for acetone removal. Implants were cut (0.25 cm) and placed in a 2mL low protein binding Eppendorf tube for *in vitro* release in only PBST and incubated at 37 °C with shaking (240 rpm). Media was collected and replaced with fresh media at 1,3,7 days and weekly thereafter.

3.3.2.3 Determination of loading of CpG and BSA

Implants (2-4 mg) were dissolved in 1 mL of acetone in a 2 mL Eppendorf tube for 30 min and centrifuged at 9000 rpm for 5 min to dissolve the PLGA and precipitate the CpG and BSA. PLGA dissolved in supernatant was removed and the pellet was washed with acetone and centrifuged three times more to remove residual PLGA. The pellet was then air dried, reconstituted in 1 mL of PBST or PBSTE at 37 °C with shaking at 240 rpm overnight and analyzed as described in '*Detection of CpG and BSA by HPLC/UPLC'* and calculated by equation (2) below. The encapsulation efficiency was calculated as described by equation (3) below.

$$(2)\ \text{Extracted loading}\ (\%) = \frac{\text{Weight of extracted CpG or BSA}}{\text{Weight of total implant}} \times 100\%$$

$$(3)\ \text{Encapsulation efficiency}\ (\%) = \frac{\text{Extracted loading}}{\text{Theoretical loading}} \times 100\%$$

3.3.2.4 Detection of CpG and BSA by HPLC/UPLC

The CpG and BSA release from the initial CpG formulation was determined by size exclusion chromatography using Waters Alliance HPLC system with a UV detector. Samples were run on a TSKgel G3000SWXL, 7.8 mm ID x 30 cm, 5µm size exclusion column with a flow rate of 0.5mL for 30 min with PBS as the eluent. Injection volume was 50 uL and detection was by UV absorption at 260 nm for CpG and 215 nm for BSA. The CpG from the optimized formulation was determined by RP-UPLC using a Waters Acquity® UPLC Oligonucleotide C_{18} column that separates oligonucleotides based on ion-pairing, reverse-phase chromatography. Eluent A is 100mM triethylammonium acetate pH 7 made by mixing equal molar ratio of triethyl amine (Millipore Sigma, 121-44-8) with glacial acetic acid in water. Eluent B is 20% acetonitrile, 80% of Eluent A. The running conditions starts at 70:30 of Eluent A:B ramped to 10:90 A:B over 20 min using "gradient curve 6" on the Waters Empower 3 software, which is a linear change of gradient. Then from minute 20 to 21, the conditions are similarly ramped back to 70:30 A:B and held there for 4 more minutes for a total 25 minute run. The flow rate was 2 ml/min, injection volume was 10 uL, and detection was by UV absorption at 260 nm for CpG. The peak areas were used to determine the concentrations by using a linear standard curve of the respective analyte in the same buffer as the sample.

3.3.2.5 Bioactivity of CpG after encapsulation and release

To assess CpG bioactivity, a TLR9 binding assay was used (Invivogen, San Diego, CA). The HEK 293, murine TLR9 expressing cell-based assay was used according to manufacturing protocol. Briefly, after culturing the cells, release samples and standard CpG were incubated with cells in SEAP detection medium in a 96-well plate for 24h at 37°C, 5% CO_2 and UV absorption was read at 620 nm. A standard curve using the same CpG as encapsulated in the implants dissolved in the same buffer as the release (PBST or PBSTE) was generated to determine the concentration of active CpG. A 5-PL curve fitting was used to determine the concentration of the samples (Figure 3-5). The percent reactivity is the ratio of the concentration determined by TLR9 assay to the concentration measured via SE-HPLC and is displayed in equation (1) below.

$$(1)\ \text{reactivity}(\%) = \frac{\text{Concentration from TLR9 assay}}{\text{Concentration from SE} - \text{HPLC}} \times 100\%$$

3.3.2.6 Docetaxel implant formation

Resomer 503H PLGA was dissolved in dry acetone at a 50:50 weight ratio of PLGA:acetone in a 2 mL Eppendorf tube. Docetaxel (sieved < 90 um) was added to the PLGA/acetone mixture at three different theoretical loadings, 40,50, and 60 w/w% relative to the total weight of docetaxel and PLGA, and mixed until it appears homogenous, ~1-2 min, using a straightened paperclip. After mixing, a hole was poked in the bottom of the tube using a 16G needle and the mixture was added to a 3mL syringe with a 18G blunt tip, ½" needle. The mixture was extruded into 0.8mm i.d. silicone tubing and capped at both ends with paperclips. The extrudates were dried at room temperature for 2 days followed by 3 days at 40 °C under 23 in Hg vacuum. After drying for solvent removal, the silicone tubing was removed by cutting with a

single blade razor. Implants were cut to 0.25 cm for subsequent release experiments and stored with desiccant at -20 °C until use.

3.3.2.7 Determination of docetaxel implant loading by extraction

To determine the docetaxel loading, implants were weighed (2-4 mg) into 2ml Eppendorf tubes. 1 mL of 60:40 ACN:water was added to the implants and shaken on a vortex on speed ~3 for 30 min. Implant samples were then centrifuged at 15000 rpm for 4 min and the supernatant was filtered through a PTFE syringe filter into a UPLC vial for analysis.

3.3.2.8 Determination of docetaxel concentration by UPLC

Samples from either release or extraction were run on a Waters UPLC system with a UV detector at 229 nm, a reverse phase C18 column, a flow of 0.3 mL of 60:40 ACN:water for 3 min**.** The samples were filtered through a PTFE filter for organic solvent (60:40 ACN:water) or PVDF filters for PBST + EtOH samples. Injection volume was 10 uL. Peaks were integrated using the Empower 3 software, using the Apex tracking processing method. Standards were prepared by dissolving docetaxel in 60:40 ACN:water and diluting for a concentration curve that would include your expected sample range.

3.3.2.9 Determination of docetaxel by RP-UPLC

Docetaxel implants were cut to 0.25 cm and submerged in 15 mL PBST pH 7.4, containing 15% ethanol (media is adjusted to pH 7.4 after ethanol addition). At each time point, 1,3, and 7 days, and weekly or bi-weekly thereafter, 1 mL of the supernatant was collected and stored for analysis at 4 °C the rest of the supernatant was discarded and a fresh 15 mL of media was replaced. The supernatant was analyzed by UPLC as described in the previous section.

3.3.2.10 Determination of solubility

Docetaxel was weighed (~1.5 mg) and added to 0.5 mL of either PBST, PBST +5% ethanol, or PBST + 15% ethanol. Samples were incubated overnight at 37 °C with shaking (240 rpm). After incubation, samples were centrifuges at 8000 rpm for 5 min and the supernatant was filtered through a 0.45 um PVDF filter for analysis by UPLC as described in "*Determination of docetaxel by RP-UPLC".*

3.3.2.11 Determination of release media pH

The pH of the release media of docetaxel was determined by a Fisher Scientific accumet® AE150 pH meter, calibrated with standards, pH 4,7, and 10 (Fischer Scientific).

3.4 Results

3.4.1 CpG implants

CpG implants were initially formulated with 1% theoretical loading of CpG and 14% BSA included as a porosigen and carrier, by cryomilling BSA and CpG together before mixing, or by mixing them without cryomilling (Figure 3-1), referred to as 'cryomilled' and 'mixed', respectively. To inhibit microclimate pH drops and hydrolysis of CpG, 3% $MgCO_3$ was also included. Table 3-1 shows the loading and encapsulation efficiency results from the cryomilled or mixed implants. The CpG yield after cryomilling was 66%, and the CpG encapsulation efficiency, after accounting for the loss in cryomilling, was 83%. The CpG encapsulation efficiency for the mixing formulation was 63%. CpG release was evaluated in both PBST and PBST with EDTA (PBSTE), as EDTA may improve stability of CpG after it is released. Release in PBSTE resulted in increased release compared to PBST in both the cryomilled and mixed conditions (Figure 3-2). In general, CpG release was faster and increased for the mixed

formulations compared to cryomilled (Figure 3-2). Mixed CpG had initial bursts (after 1 day of release) of 7.0% and 7.2% in PBST and PBSTE, respectively. Cryomilled CpG had initial bursts of 6.0% and 10.8% in PBST and PBSTE, respectively. Mixed CpG had total cumulative releases after 49 days of 56.7% and 68.2%, in PBST and PBSTE, respectively. Cryomilled CpG had total cumulative releases after 49 days of 33.8% and 40.8%, in PBST and PBSTE, respectively. The encapsulation efficiency of BSA was high, i.e., 98%, for both cryomilled and mixed formulations, resulting in 13.8%w/w loading of BSA (Table 3-2). Figure 3-3 shows the cumulative released BSA from the same formulations that CpG release was determined from. Mixed BSA initial bursts were 8.8% and 9.3%, for PBST and PBSTE, respectively. Cryomilled BSA initial burst was 12.6% and 14.0%, for PBST and PSTE, respectively. Mixed BSA cumulative release was 54.4% and 63.0% for PBST and PBSTE, respectively. Cryomilled BSA cumulative release was 41.6% and 44.8% for PBST and PBSTE, respectively. Next, we assessed the activity of the released CpG by determining binding with TLR9 using HEK 293, TLR9-expressing cells that allow for quantification of TLR9 binding via UV absorbance (Figure 3-4). The concentration of CpG binding to TLR9 was compared relative to the concentration determined via SEC to determine the reactivity using 5-PL standard curves (Figure 3-5) of CpG standards incubated under the same conditions as the released samples. All formulations and conditions showed high reactivity throughout release (Figure 3-4). CpG activity from the mixed formulation released in PBST showed 230%, 102%, 100%, and 67% reactivity for the extraction (day 0), day 1, 14 and 35, respectively. CpG activity from the cryomilled formulation in PBST showed 169%, 154%, 97%, and 84% reactivity for the extraction (day 0), day 1, 14 and 35, respectively. CpG activity from the mixed formulation released in PBSTE displayed 56%, 142%, and 129% reactivity for the day 1, 14 and 35, respectively. CpG activity from the cryomilled

formulation released in PBSTE similarly displayed 95%, 87%, and 70% reactivity for the day 1, 14 and 35, respectively.

In order to improve the CpG loading and encapsulation efficiency, we formulated a second, optimized set of implants with a higher theoretical CpG loading (6%w/w), three different levels of BSA (9,11.5, and 14% w/w), and $MgCO_3$ (3%w/w), referred to as 'optimized implants' (Table 3-3). For these formulations, we did not cryomill the CpG, it was mixed with the BSA and PLGA as supplied by the manufacturer (Figure 3-6). We monitored release in PBST not PBSTE. Release was monitored by RP-UPLC using a column specific for detecting oligonucleotides, instead of SEC-HPLC. All formulations resulted in enhanced encapsulation efficiencies (Table 3-3). The higher the BSA loading, the higher the initial burst of CpG, i.e., formulation CpG-1, 2, and 3 had initial bursts of 8.5, 10.7, and 17.7%, respectively (Figure3-7a). The overall release of formulation CpG-1 was lower compared to formulation CpG-3 which had a higher BSA loading (Figure 3-7a). Total cumulative CpG release was 72.9, 55.6, and 95.1% over 45 days for formulations 1,2, 3, respectively. The RP- UPLC detection method of CpG in the release media showed multiple peaks, represented in Figure 3-7b. These peaks were not due to BSA, and were likely shorter lengths of the nucleotide sequence. CpG standards also contained these peaks (<5%).

3.4.2 Docetaxel implants

As expected, docetaxel had a very low solubility in PBST release media, but with increasing amounts of ethanol, solubility was enhanced, especially with 15% ethanol, thus release was conducted in 15% ethanol PBST to allow for more efficient sink conditions as well as to correlate better with what can occur in vivo (Table 3-4**)**. Docetaxel was encapsulated in PLGA by simply mixing the sieved (<90 μm) docetaxel powder into the PLGA/acetone mixture

(Figure 3-8). Docetaxel was encapsulated with very high efficiencies for all formulations, i.e., 40, 50, and 60% w/w loading (Table 3-5). Docetaxel release was higher for the 40% and 50% formulations, and slowest for the 60% formulation (Figure 3-9). During release analysis by UPLC, more than one main peak appeared at a later retention time from the main peak. Thus, Figure 3-9 shows the calculated cumulative release and amount released based on both the sum of all apparent peaks (Figure 3-9 a,b) and on the main peak only (Figure 3-9 c,d), respectively. The portion of the main peak for each release sample is demonstrated in Figure 3-10a. To determine any possible cause of the appearance of potential degradation products, the pH of the release media was determined (Figure 3-10 b). The pH decreased after day 3 to ~6, and the most drastic decrease in the main peak occurred during the first 7 days for all formulations. Thus, the pH may be have caused instability such as precipitation[224], resulting in the incomplete release of the 60% formulation and the appearance of multiple degradation products.

3.5 Discussion

During our first formulations of CpG, we started with a theoretical loading of 1% CpG, 14% BSA, and 3% $MgCO_3$, two different formulation processes, termed mixing and cryomilling. And two different release conditions, PBST and PBSTE. For the cryomilled formulation, the CpG encapsulation efficiency after cryomilling CpG with BSA was low (~66%). This is likely due to the low amount of CpG used in the milling process, it may be lost to the sides of the container or during sieving. Both the cryomilling and mixed formulation processes resulted in low encapsulation efficiencies most likely due to the low amount of CpG present during this process. The CpG release from all conditions was incomplete. This is likely due to a low total water-soluble solid loading in the implants, ~15% including the BSA and CpG. Previous work from our lab on monoclonal antibody implants has shown that there is a percolation threshold

that allows for continuous and complete release through a water filled pore network, relying on a high enough level of water-soluble components to create this network that allows for drug release. Below this threshold you would expect incomplete release, the farther above this threshold, you would expect faster release[62,63,225]**.** To further investigate whether there was instability of CpG causing the incomplete release or if the low solids loading was indeed the main cause, we monitored the release of BSA from the same implants. BSA was encapsulated very efficiently but also released similar to CpG, incomplete over 49 days. This indicated that it was most likely the low total solids loading that led to the incomplete release. Therefore, we proceeded with an optimized formulation with a higher theoretical loading of CpG (6%w/w), 3% $MgCO_3$, and three different levels of BSA (9.5, 11, 14.5%) to test our theory of increased total water-soluble solids would increase release. We also simplified the method and did not cryomill the CpG to avoid loss and any possible damage that could be done during this process. We only tested the release in PBST because it is possible the EDTA is sequestering the $MgCO_3$ which resulted in the faster release compared to PBST before. With these optimized conditions and a simplified process, the CpG encapsulation efficiency was dramatically improved. The release of CpG was nearly compete with the highest BSA loading condition (14% BSA) compared to the two lower BSA loading conditions (9.5 and 11%). These two lower BSA loadings, and therefore lower total solids loadings, still resulted in incomplete release. Thus, the percolation threshold for these implants must be somewhere between 17% and 20% of total water-soluble solids. The cumulative % release of the 11% BSA loading formulation appears to be lower than the 14% BSA condition, but looking at the CpG release in terms of micrograms instead of relative to the loading (Figure 3-7c), the two formulations perform similarly, indicating there may just be an error in the CpG loading determined for the 11% BSA formulation.

Docetaxel is a hydrophobic, poorly water-soluble drug and we showed that increasing its loading in PLGA resulted in lower overall cumulative release. This could potentially be explained by precipitation of docetaxel which increases with increasing the mass of docetaxel per implant. Zlomke, et al. showed similar trends in PLGA implants loaded with nifedipine and nicardipine and further analysis by x-ray diffraction showed precipitated drug crystals.[224] Further analysis of the physical state of our docetaxel implants would be needed to support this hypothesis. Kumar et al., investigated the degradants of docetaxel and identified impurities that occur when docetaxel is in both acidic and base stressed conditions, with less degradation appearing in acidic conditions[226]. The peaks that are present in our release appear downfield from the main peak. In similar RP-C18 UPLC conditions, Kumar et al. identified the peaks appearing downfield of the main peak as 7-epi docetaxel and 7-epi 10-oxo docetaxel[226]. Both of these degradation products still contain the intact taxane ring and ester side chain, important structural features in the mechanism of action for docetaxel[221]. Thus, the acidic microclimate occurring in the PLGA implants due to the degradation of PLGA into lactic and glycolic acid may be inducing some instability, which could be improved by adding a poorly soluble base, such as $MgCO_3$ as we have done in our other formulations for delivery of acid-labile macromolecules.

3.6 Conclusion

In conclusion, CpG and docetaxel were both successfully formulated into PLGA implants with sustained and complete release over 40 and 100 days, respectively. CpG and Docetaxel would benefit from local delivery options since they do not readily cross the BBB[220–223]. Future work will focus on evaluating the combined therapy of immune checkpoint inhibitors, anti-PD-1 and anti-CTLA-4, with the CpG and docetaxel to locally treat glioblastoma. We expect the

combination of the immune checkpoint inhibitors to remove the immunosuppressive environment of GBM, the immune stimulatory effects of CpG, and the increased cell death and enhance solid tumor penetration of docetaxel to improve the poor prognosis and inevitable recurrence of glioma tumors.

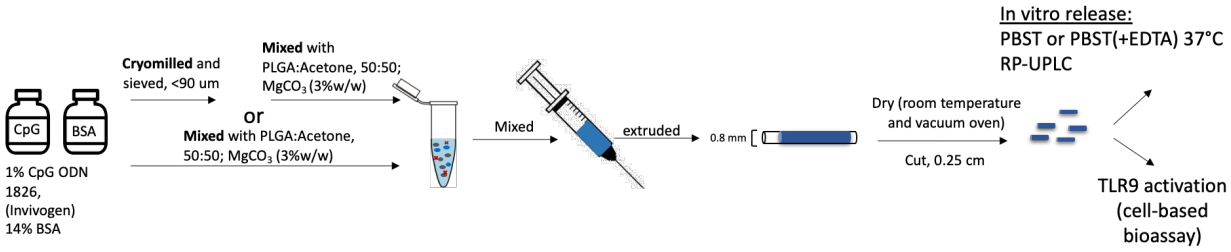

Figure 3-1. Schematic overview of initial CpG implant formulation and analyses.

Formulation	CpG Loading %	EE%	CpG dose / 1 mg of implant (0.25 cm)
Cryomilled	0.54 (0.01)	83% (66% yield from cryomilling)	~5.4 µg
Mixed	0.63 (0.02)	63%	~6.3 µg

Table 3-1. CpG loading and encapsulation efficiency. *Data represents mean ± SE, n=3-5.*

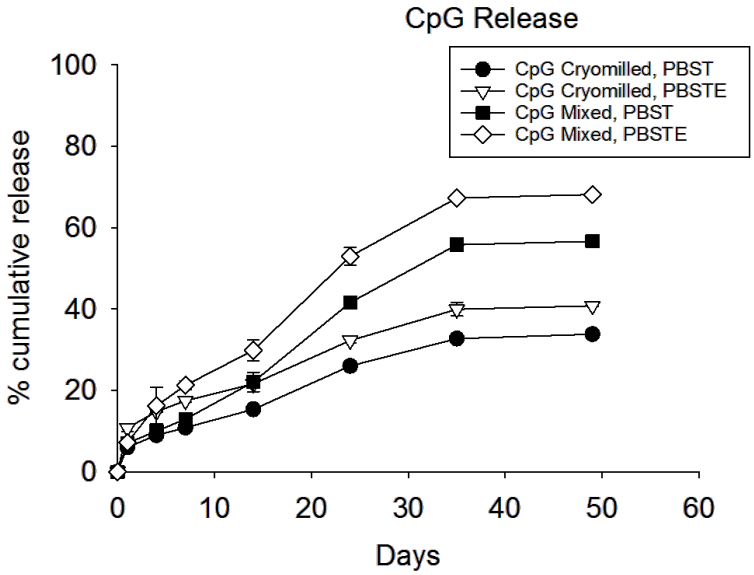

Figure 3-2. In vitro release of CpG from PLGA implants. *Cumulative release of CpG from PLGA implants made by cryomilling CpG with BSA before mixing, or mixing without cryomilling. Implants were incubated in PBST or PBSTE. CpG determined in release media by SEC-HPLC. Data represent mean± SE, n=3.*

Formulation	BSA Loading %	EE%
Cryomilled	13.8 (0.1)	98.5 (0.9)
Mixed	13.8 (0.3)	98.8 (2.0)

Table 3-2. BSA loading and encapsulation efficiency from initial implant formulation. *Data represents mean± SE, n=3.*

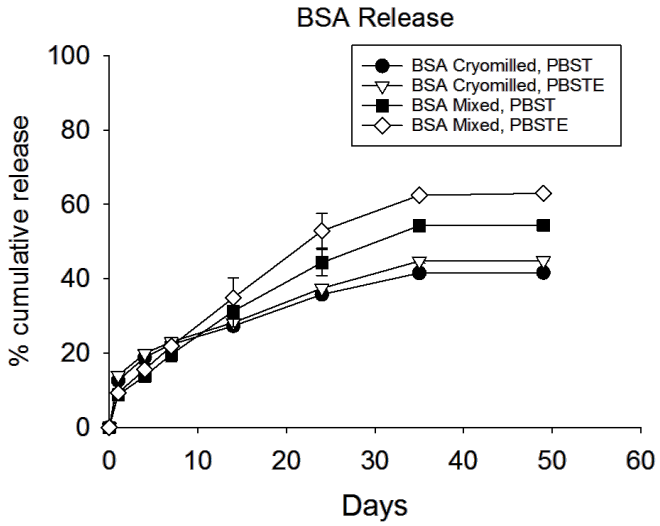

Figure 3-3. In vitro release of BSA from PLGA implants. *Cumulative release of BSA from implants made by cryomiling BSA with CpG before mixing or by mixing without cryomilling. Implants were incubated in PBST or PBSTE and release media was monitored by SEC-HPLC. Data represents mean± SE, n=3.*

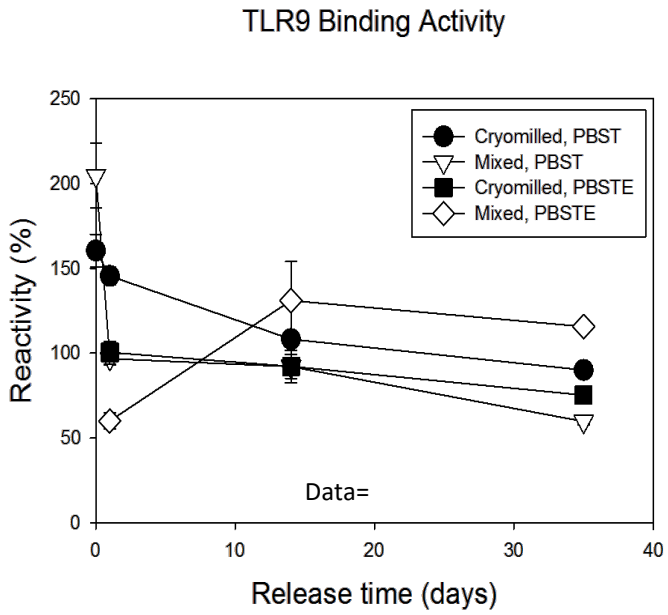

Figure 3-4. CpG TLR9 binding activity. *Reactivity of released CpG determined by incubation with TLR-9 expressing HEK293 cells using SEAP detection. Data represents mean± SE, n=3.*

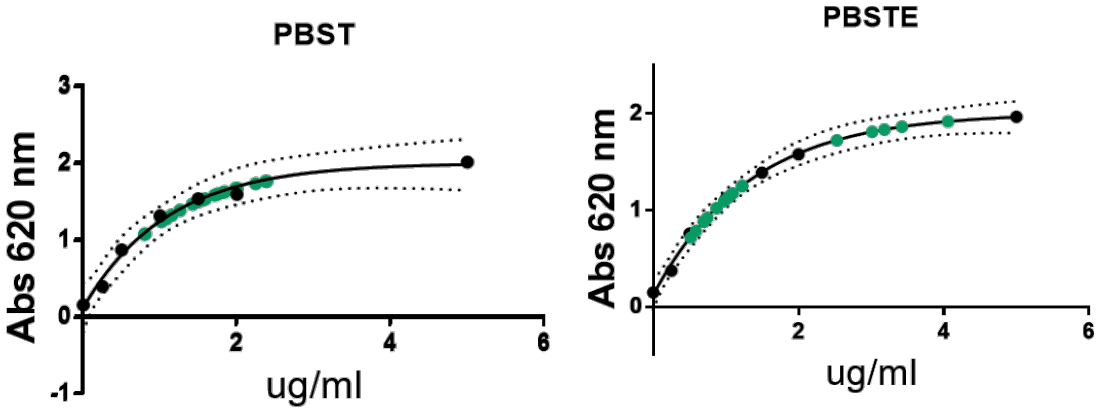

Figure 3-5. 5-PL standard curves used for CpG bioactivity determination. *Absorbance at 260 nm vs concentration of CpG standards incubated with TLR-9 expressing HEK293 cells after SEAP detection. Data graphed with Prism using a 4PL sigmoidal fitting, dashed lines represent a 95% confidence interval.*

Formulation name	Theoretical BSA loading (% w/w)	CpG Loading %	EE%
CpG-1	9	6.3 (0.02)	104.8 (0.4)
CpG-2	11.5	6.9 (0.7)[a]	115.3 (11.6)
CpG-3	14	5.8 (0.2)	96.7 (3.9)

Table 3-3. Optimized CpG implant formulation loading and encapsulation efficiency. *Data represents mean± SE, n=3 or [a]n=2.*

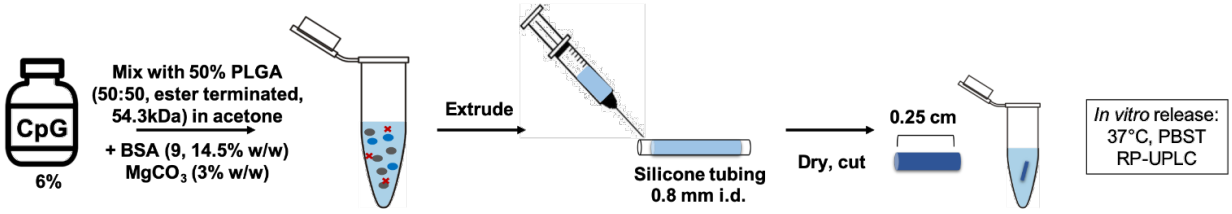

Figure 3-6. Schematic overview of optimized CpG PLGA implant formulation.

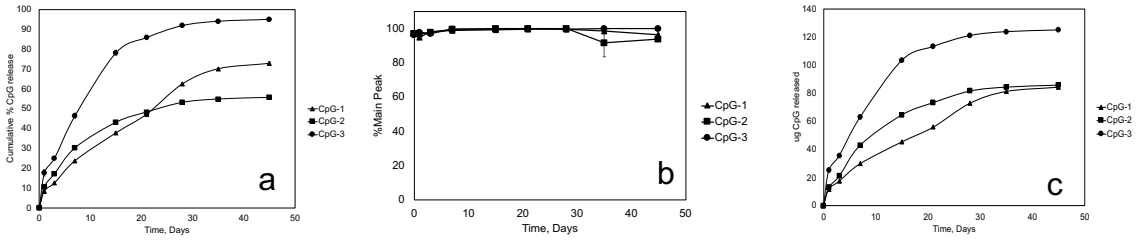

Figure 3-7. In vitro characterization of optimized CpG formulation. *a) Cumulative release percent b) main peak percent and c) µg released of CpG from PLGA implants incubated in PBST. CpG-1,2 and 3 formulations are described in Table 3-3. Data represents mean± SE, n=3.*

Release Buffer	Docetaxel Solubility (avg ug/ml (SEM), n=3)
PBS (0.02% Tween 80)	4.0 (0.1)
PBST + 5% EtOH	6.9 (0.1)
PBST + 15% EtOH	23.3 (0.3)

Table 3-4. Solubility of Docetaxel in PBST with various amounts of ethanol.

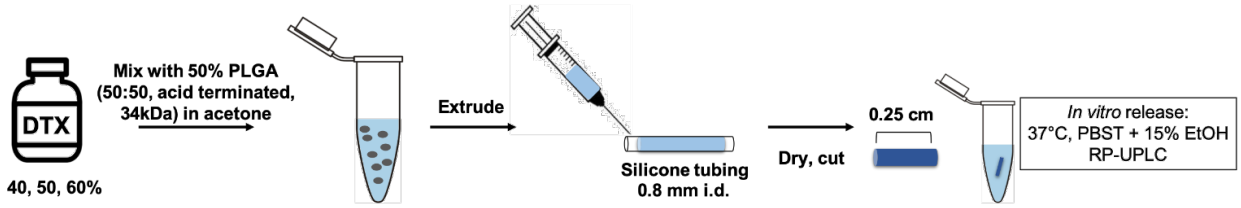

Figure 3-8. Schematic overview of docetaxel PLGA implant formulation.

Formulation	Theoretical DTX loading (%w/w)	DTX Loading (%w/w)	EE%
DTX-40%	40	40.8 (0.6)	102.0 (1.6)
DTX-50%	50	51.0 (0.3)	102.0 (0.7)
DTX-60%	60	62.6 (0.8)	106.0 (1.3)

Table 3-5. Docetaxel loading and encapsulation efficiency. *Data represents mean± SE, n=3.*

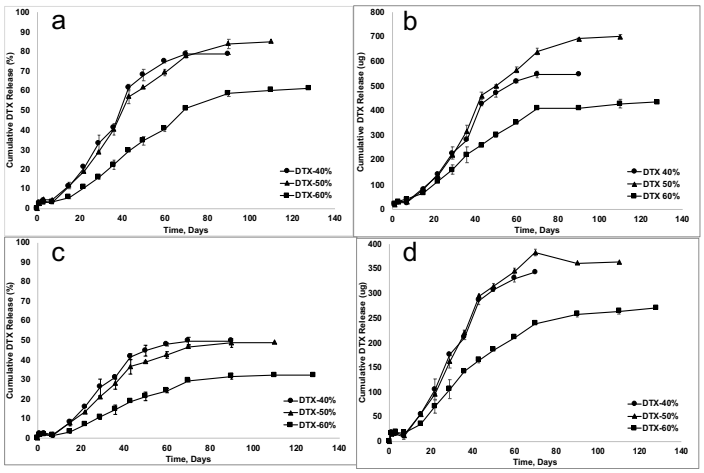

Figure 3-9. In vitro release of docetaxel. *Total cumulative release % and total cumulative μg DTX released from PLGA implants accounting for all peaks (a,b, respectively) and accounting only for the main DTX peak only (c,d, respectively). Release samples were analyzed by RP-C18 UPLC. Data represents mean± SE, n=2.*

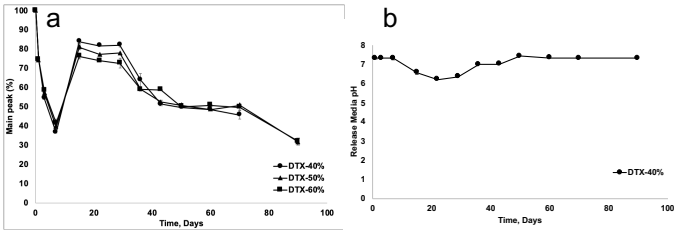

Figure 3-10. In vitro characterization of released docetaxel. *a) %Main peak of docetaxel released from PLGA implants, determined by RP-C18 UPLC. b) pH of release media during incubation. Data represents mean± SE, n=2.*

Chapter 4: In Vitro Degradation and Erosion Behavior of Commercial PLGAs Used for Controlled Drug Delivery

4.1 Abstract

Poly(lactide-*co*-glycolide) (PLGA) is among the most commonly used materials in biomedical applications, especially parenteral controlled drug delivery due to its high biocompatibility, predictable degradation rate, and ease of processing. Besides manufacturing variables of drug delivery vehicles, changes in PLGA raw material properties can also affect product behavior. Accordingly, an in-depth understanding of polymer-related "critical quality attributes" can probably allow for a predictive selection of PLGA performance.

Here, we selected 17 different PLGAs from 5 manufacturers to form drug-free films, implants and microspheres and evaluated differences in their water uptake, degradation, and erosion during *in vitro* incubation as a function of the L/G ratio, molecular weight, end-capping, and formulation geometry. Acid-terminated PLGA 50/50 films from different manufacturers with similar molecular weight and higher glycolic unit blockiness and/or block length values showed faster initial degradation rates. Geometrically larger implants of 75/25, acid-terminated PLGA showed higher water uptake, and ~2-fold faster degradation rates in the first week compared to microspheres of the same polymers, likely due to enhanced effects of acid-catalyzed degradation from PLGA acidic byproducts unable to escape as efficiently from larger geometries. The increased water uptake and degradation in implants appeared to preferentially affect the erosion of glycolic units, whereas microspheres appeared to erode more homogenously, suggesting differences in their hydrolytic mechanisms. Manufacturer differences

such as an increased residual monomer appeared to lead to increased water uptake and increased degradation in poly(lactide) implants.

This dataset of different polymer manufacturers could be useful in selecting a desired PLGA for controlled release applications, and these techniques to further compare differences in less reported properties such as sequence distribution can be used for future analyses of PLGA performance in the field of drug delivery.

4.2 Introduction

Poly(lactide-*co*-glycolide) (PLGA) is frequently used across several applications such as medical devices, tissue engineering, and drug delivery. It is the most commonly investigated biodegradable polymer to achieve long-acting release for a variety of drugs, such as small molecules, peptides, and proteins due to its well-described biocompatibility and ease of processing into numerous distinct formulations such as particulate systems, films, and implantable devices.[15] There are currently 19 FDA-approved drug products that use PLGA to achieve controlled release from weeks to months.[15] Despite patent expirations for many of these medications, there are no generics available due to the complexity of the formulation, such as a lack of understanding of the effects of raw material properties and manufacturing variables on product performance.[227]

After contact with water *in vitro* and *in vivo,* polyesters like poly(lactide) (PLA) and PLGA are degraded via hydrolysis into non-toxic monomers of lactic and glycolic acid which are removed *in vivo* by excretion or the citric acid cycle. An encapsulated drug is typically released from the formulation through a combination of mechanisms among them diffusion over the polymer matrix or water-filled pores, osmotic pressure, or erosion of the polymer itself.[64] The process of polymer degradation and erosion usually begins with an initial water uptake into the formulation that leads to polymer degradation, or a decline of the polymer molecular weight, eventually the polymer molecular weight reduces enough (to ~1 kDa or lower) that the chains become water-soluble oligomers and monomers that can diffuse out of the polymer vehicle.[65] The rate and extent to which these events occur can be affected by changing various properties of the polymer. For example, decreasing the polymer chain molecular weight results in increased hydration and chain mobility which increases the rate of degradation.[228] Elevating the L/G ratio

decreases the rate of degradation and erosion because lactic units are more hydrophobic and sterically hindered to hydrolysis. The most commonly selected polymer properties affecting the rate and extent to which these events occur, are the L/G ratio, molecular weight, and the type of end-capping of the polymer chains.

PLGA is most commonly synthesized by two methods, direct condensation of the acid monomers, or ring-opening polymerization (ROP) of the cyclic dimers, namely lactide and glycolide.[37,52] Direct condensation, or polycondensation, of the two acid monomers, lactic and glycolic acid, is in competition with the depolymerization into the dimers due to the generation of water in the reaction which requires elevated temperatures with high vacuum to control and, thus, can typically only obtain lower molecular weight polymers, typically <50kDa, although with more complicated methods, higher molecular weights can be obtained.[38,229,230] ROP is the most commonly used method for commercial PLA/PLGA synthesis. ROP involves the reaction of lactide and glycolide dimers in the presence of a catalyst and initiator species at around 100-150°C from a couple of minutes to hours.[37,38] The most used and accepted catalyst is stannous octoate and co-initiators are typically OH-bearing molecules such as fatty alcohols, or even "free" lactic and glycolic acid.[47]

During polymer synthesis, glycolide/glycolic acid is more reactive than lactide/lactic acid, so it is not unusual that short "blocks" of glycolic and lactic linkages are formed along the polymer chains rather than a purely random or 'sequenced' distribution.[231] Knowledge of the monomer distribution along the polymer chain is important because the glycolide linkages tend to be more labile towards hydrolysis and, thus, larger lengths would lead to an accelerated degradation and erosion of the polymer, likely accompanied by a faster drug release.[53,54,66,67] For example, Vey et al. determined that the glycolic unit consistently hydrolyzes 1.3 times faster

than the lactic unit across polymer films with varying L/G ratios, submerged in phosphate buffer.[55]

PLA/PLGA that is uncapped has a carboxylic acid at the end of its chain that is hydrophilic and results in increased water uptake, faster hydrolysis and degradation. A capped PLA/PLGA has an alkyl ester at its chain terminus that is more hydrophobic than an uncapped, carboxylic acid end group. When selecting an end-capped polymer from manufacturers, the type of end termination is usually not disclosed, yet it has been shown that longer alkyl chains, which are more hydrophobic, can lead to slower degradation, even when the molecular weight is lower.[42] Polymer selection and changes in source/batch of polymer are only one aspect of the more complex development of long-acting release drug product development along with drug properties, drug-PLGA interactions, included excipients, formulation geometry, and formulation parameters.[11,15,227,232–234] However, better knowledge and control of the relevant macro- (e.g., shape and porosity) and micro-structural (e.g., arrangement of L/G sequence and end-capping) properties of the polymer may help bridge the gap between the effects of raw materials or manufacturing variables and the product performance, allowing for better polymer selection and could potentially increase the number of approved PLGA drug products. Herein, we selected 17 different PLGAs from five manufacturers to form drug-free films, implants and microspheres and investigated differences in their water uptake, degradation, and erosion behaviors during incubation as a function of L/G ratio, molecular weight, end-capping, and formulation geometry. Previously, we also evaluated the sequence distribution of glycolide/glycolic acid and lactide/lactic acid for these polymers and, here, we were able to connect these results with our analyses of *in vitro* performance.

4.3 Materials and methods

4.3.1 Materials

All Expansorb® polymers were provided by Merck KGaA (Germany). Resomer® and Purasorb® polymers, Wako® 7515 and Lactel® DL-PLG B6007-2 were purchased from Sigma Aldrich (US), Corbion (The Netherlands), Wako Pure Chemical Industries, Ltd. (Japan) and Lactel (US), respectively. All polymers used in this investigation were the racemic (D,L) form of lactide or lactic acid and are further described in Table 4-1. Dichloromethane (DCM) was from Merck KGaA. Acetone (99.8%, extra dry, Acros Organics), tetrahydrofuran (THF, HPLC grade) and reusable PTFE Evaporating Dishes were acquired from FisherSci (US) (product no. 02617148). Cicular lever punches, 1.6 cm diameter were obtained from Michaels® Craft Store (US). Platinum-cured silicone tubing (0.5 mm i.d.) was from Cole Parmer (US) (product no. 95802-00). Poly(vinyl alcohol) (PVA, 88% hydrolyzed, molecular weight ~25kDa) was provided by PolySciences, Inc (US) and Merck KGaA. PBS (Gibco) was from the University of Michigan Bioresearch store. 63 cm diameter polypropylene jars were purchased from Grainger, Inc. (US) (product no. 3UCP3 or 32V496). All other chemicals and solvents were of analytical grade and used as received.

4.3.2 Methods

4.3.2.1 Film preparation by solvent casting

Expansorb® DLG 50-2A, Resomer® RG 502H, Expansorb® DLG 50-5A, Resomer® RG 504H, Purasorb® PDLG 5004A, Expansorb® DLG 50-2E, Resomer® RG 502, Expansorb® DLG 75-9E and Lactel® DL-PLG B60072P were prepared as thin films. Polymers were dissolved in THF at 50 mg/mL except for Lactel® DL-PLG B6007-2P, Expansorb® DLG 75-9E, and

Resomer® RG 502 dissolved at 75 mg/mL. 8 mL of the polymer solution was dispersed via a glass pipette into the center of circular, 10 cm diameter, PTFE low form evaporating dish on a leveled surface. Dishes were covered with 2 L beakers to limit but not completely prevent airflow and allowed to dry for 24 h at room temperature under a ventilated chemical hood. Then, films were dried under vacuum (23 in. Hg) at 40°C with desiccant for 48 h. Films were carefully removed from the PTFE dishes using forceps, cut into discs using a 1.6 cm diameter circle lever punch and stored at 4°C until use. The average film thickness was ~53 μm, ranging from 30-78 μm.

4.3.2.2 Implant formulation

Expansorb® DLG 75-2A, Resomer® RG 752H, Purasorb® PDLG 7502A, Wako® 7515, Expansorb® DL 100-2A, Resomer® R 202H, and Purasorb® PDL 02A were prepared as implants similarly as previously described[18]. Polymers were dissolved with acetone at a ratio of 2/1 (w/w, polymer/acetone) and extruded via a 3 mL syringe and a blunt-tip needle into the silicone tubing. Paper clips were placed in the ends of the tubing to prevent the polymer solution from leaking and to compress the mixture to avoid air pockets in the extrudate. Extrusions were dried at room temperature for 48 h followed by drying under vacuum (23 in. Hg) at 40°C with desiccant for 48 h. The silicone tubing was removed from the polymer implants using a razor blade, and the implants were cut into 0.5 cm segments and stored at -20°C until use.

4.3.2.3 Microsphere Formulation

Expansorb® DLG 75-2A, Resomer® RG 752H, Purasorb® PDLG 7502A, and Wako® 7515 were prepared as microspheres similarly as previously described.[235] Polymers were dissolved in DCM at a concentration of 800 mg/mL in a 16 x 100 mm glass test tube for a total volume of 1 mL. An equal volume, 1 mL, of 1% PVA was added to the polymer solution and

thoroughly vortexed at maximum speed for 1 min. The resulting O/W emulsion was immediately added to a 250 mL beaker containing 100 mL of 0.5% PVA and stirred with an overhead stirrer at 600 rpm for 3 h for microsphere hardening and solvent removal. Microspheres were then sieved and collected between 32-63 μm, rinsed with 1 L of distilled water to remove excess PVA, freeze-dried for 2 days and finally stored at -20°C until use.

For the BODIPY uptake experiments, Expansorb® DL 100-2A, Resomer® R 202H, and Purasorb® PDL 02A were formulated as microspheres. Polymers were dissolved at 600 mg/mL and microspheres were fabricated as described above.

4.3.2.4 Incubation conditions

Polymer films, implants, and microspheres were incubated in phosphate-buffered saline (PBS) pH 7.4 at 37°C with low agitation (70 rpm, KS 125 basic shaker, IKA Labortechnik, Germany); thin films were incubated in 30 mL PBS in 63 mm diameter polypropylene jars, implants (0.5 cm) and microspheres (10 mg) were incubated in 1 mL PBS in 2 mL Eppendorf tubes. At predetermined time-points, the incubations were stopped by removing/separating the respective vehicle from the buffer and rinsing it with distilled water. Formulations were then dried at room temperature and under vacuum (23 in. Hg) with desiccant for 72 h.

4.3.2.5 Determination of water content and mass loss

Water content of films and implants (*W(t)*) at time, *t*, was determined during the incubation period by:

$$W(t) = \frac{W_{wet}^{t} - W_{dry}^{t}}{W_{wet}^{t}}, \quad (1)$$

where W_{wet}^{t} and W_{dry}^{t} are the wet and dry formulation weights, respectively, after incubation and drying.

The percent mass loss was calculated according to:

$$\%mass\ loss = \frac{W_0 - W_{dry}^{t}}{W_0} \times 100, \quad (2)$$

where W_0 is the initial weight of the formulation before incubation.

For microsphere water uptake determination, particles were dried and the interparticle water was calculated as previously reported.[232] Briefly, incubated particles were collected on pre-weighed nylon membrane filters washed with distilled water and dried under vacuum for approximately 5 seconds to remove surface water and the wet weight was immediately determined. After drying at room temperature under vacuum for 72 h, the dry weight was recorded. To correct for the interparticle water, dry microspheres were dispersed in PBS at 4°C (where water uptake into microspheres is assumed negligible) and the wet and dry weights were measured after filtering and drying, respectively, as described above. The weight difference between wet and dry particles were used to calculate the fraction of interparticle water (W_{int}), as defined as:

$$W_{int} = \frac{(W_{wet}^{0} - W_{dry}^{0})}{W_{dry}^{0}}, \quad (3)$$

with W_{wet}^{0} and W_{dry}^{0} as the weights of wet microspheres and dry microspheres, respectively, after immediate collection at *t*=0. The water uptake of microspheres at time, *t*, $W_{ms}(t)$ was then determined as defined as:

$$W_{ms}(t) = \frac{(W_{wet}^{t} - W_{dry}^{t} - (W_{dry}^{t} W_{int}^{t}))}{W_{dry}^{t}}, \quad (4)$$

where W_{wet}^{t} and W_{dry}^{t} are the wet and dry microsphere weights after incubation and drying at time *t*. The percent mass loss was calculated as defined according to (2).

4.3.2.6 Determination of relative molecular weight change

Before formulation incubation (day 0) and at each time-point during incubation, formulations were collected after drying and dissolved in THF. The obtained polymer solutions (~4 mg/ml) were then subjected to gel permeation chromatography using two styragel columns (HR 1 and HR 0.5 columns, Waters, US) with a Waters 1525 HPLC system and THF as the elution medium at a flow rate of 1 mL/min and detection by refractive index as previously described.[232] Poly(styrene) standards of known molecular masses were used for calibration. The weight-average molecular weight of polymer samples is reported throughout this study.

4.3.2.7 Determination of dry glass transition temperature (dry T_g)

Raw polymers (0.5-5 mg) were exactly weighed into aluminum pans with a lid and sealed. The dry T_g was determined by a modulated differential scanning calorimetry method as previously described[232] (Discovery, TA instruments, US). A heat/cool/heat cycle was employed in which the temperature was ramped between -20 °C and 90 °C at 3 °C/min, with a modulated amplitude of 1°C/min over 60 seconds. Results were analyzed by the TRIOS software.

4.3.2.8 L/G ratio determination by nuclear magnetic resonance (NMR) spectroscopy

Each PLGA sample (~7 mg) was dissolved in deuterated chloroform ($CDCl_3$) (0.75 mL) and pipetted into a 5 mm × 7 in NMR tube (Aldrich® ColorSpec® NMR tubes, parameter 800 MHz frequency). NMR scanning was performed using a Varian vnmr-500 MHz (11.7 Tesla) Premium Shielded NMR spectrometer running Vnmrj software for ^{1}HNMR. Molar L/G ratios were determined by comparing proton intensities at chemical shifts 5.2 ppm (lactide, one proton) and 4.8 ppm (glycolide, two protons). The L/G molar ratio was converted to the L/G weight ratio. Significant differences were determined by comparing the changes in lactic content by subtracting the lactic content at day 0 from the lactic content determined at each time-point.

4.3.2.9 BODIPY uptake in microparticles

About 10 mg of PLGA microspheres were incubated at 37 °C in 1 mL of PBS containing 0.02% (w/v) Tween-80 (PBST) under mild agitation for 21 days before monitoring the probe uptake. After incubation, 1 mg of the microparticles were separated from PBST solution by a brief centrifugation. Then, 1 mL of BODIPY in PBST (5 μg/mL), which was preincubated at 37°C, was added, and the mixture was incubated at 37°C for 1 day under mild agitation before laser scanning confocal microscopy. Briefly, microspheres were imaged using a Nikon A1 spectral confocal microscope (Japan) to observe dye distribution and microsphere morphology. The images were then analyzed using ImageJ software (National Institutes of Health, US). Normalized dye intensity (I/I_0) – position (r/a) pairs were then fit to the solution of Fick's second law of diffusion using Matlab & Simulink software (Oakdale Engineering, US) to determine the effective solid-state diffusion coefficient of BODIPY (D_{BODIPY}), as described previously.[235]

4.3.2.10 Analysis of erosion rate and onset of erosion from mass loss data

PLGA film erosion was analyzed by two parameters[236], the pseudo-first order apparent rate of erosion (k_{ero}) during the decay phase calculated by:

$$Ln(\%mass\ remaining) = intercept - k_{ero}time, \quad (5)$$

which was typically the last 3-4 time-points, and the onset of erosion (t_{on}) was calculated by:

$$t_{on} = \frac{intercept - ln(100)}{k_{ero}} \quad (6)$$

4.3.2.11 Analysis of degradation rate and half- lives from molecular weight data

The molecular weight (MW) pseudo-first order apparent degradation rate constants, k_{deg}, and half-lives, $t_{1/2}$, were determined by the following:

$$ln(MW) = intercept - k_{deg}time \quad (7)$$

$$t_{1/2} = \frac{ln(2)}{k_{deg}} \quad (8)$$

4.3.2.12 Statistical Analyses

Samples represented independent experiments in triplicate and data represents mean ± standard error (SE). Statistical analyses and regressions were performed using Prism (Graphpad, US). Comparisons were made using unpaired student *t*-tests to determine two-tailed *p*-values. Significance was established at the 95% confidence interval (α <0.05) and all levels of significance are indicated with one asterisk (*). To compare the %lactic content remaining in each formulation during incubation, actual differences relative to their raw polymer starting %lactic content were used for statistical analyses.

4.4 Results and discussion

4.4.1 Effect of polymer molecular weight

Expansorb® DLG 50-2A with Expansorb® DLG 50-5A and Resomer® RG 502H with Resomer® RG 504H (50/50, “low” and “intermediate” molecular weight, acid-terminated

PLGAs) were formulated as thin films. For both comparisons, the water uptake was generally similar by 3 weeks of incubation, but the lower molecular weight films revealed an increased water uptake during the first two weeks (Figure 4-1a,d). In Expansorb® DLG 50-5A and Expansorb® DLG 50-2A films, as the molecular weight decreased, the initial apparent first order rates of degradation increased, 0.072 and 0.092 $days^{-1}$, respectively, and their degradation half-lives decreased, 9.6 and 7.6 days, respectively (Figure 4-1a-c, Table 4-2). The lower molecular weight of Expansorb® DLG 50-2A had a significant effect on the onset of erosion (t_{on}), with a t_{on}=1.3 days compared to Expansorb® DLG 50-5A, t_{on}=11.8 days (Table 4-3). Similar trends were observed with the two Resomer® polymers (Figure 1d-f). These results are expected, as the molecular weight is known to affect the polymer degradation and erosion.[228] We expect the degradation of PLGA to increase with a decline in molecular weight, as the polymer chains become more mobile and time to reach a soluble polymer oligomer shortens. It was previously observed that regardless of the molecular weight, polymer microspheres or implants reach a critical molecular weight, around 10-20 kDa, at which point the formulations collapse and undergo significant constant erosion.[237–239] The starting molecular weight does not appear to influence this critical molecular weight, but the time that it takes to reach the critical molecular weight increases with increasing molecular weight. We observed similar behaviors with our polymer formulations, the critical molecular weight ranged from 5-20 kDa (data not shown) and polymers with similar properties behaved similarly. The time to reach this critical molecular weight for our formulations ranged from 7-28 days with low molecular weight, acid-terminated, 50/50 films and 75/25 implants having a shorter time, and higher molecular weight, 75/25 ester-terminated films as well as PLA, acid-terminated implants taking longer to reach this critical molecular weight. Certainly, almost any desired polymer molecular weight can be achieved with

"fine-tuning" the synthesis process. Here, when investigating the effects of other variables, we are only comparing formulations that have similar starting molecular weights.

4.4.2 Effect of polymer end-capping

The impact of the polymer chain termination was investigated by comparing 50/50, acid-with ester-terminated PLGA films of similar molecular weights within the same manufacturer, either Expansorb® or Resomer®. Ester-terminated Expansorb® DLG 50-2E and Resomer® RG 502 compared to their acid-terminated analogs of similar molecular weights, Expansorb® DLG 50-2A and Resomer® RG 502H, respectively, all showed reduced overall water uptake and slower overall polymer degradation and erosion (Figure 4-2). The onset of erosion and rate of erosion analyses are capturing the tail-end of the erosion vs. time curves, where significant erosion occurs and are not fitted as well for the ester-terminated polymers which did not start significantly eroding until after 21 days. Expansorb® DLG 50-2E films degraded slower than Expansorb® DLG 50-2A, molecular weight degradation rate constants (k_{deg}) were 0.049 and 0.092 days^{-1} and molecular weight half-lives ($t_{1/2}$) were 14.3 and 7.6 days, respectively (Table 4-2). Expansorb® DLG 50-2E films had similar erosion rates compared with Expansorb® DLG 50-2A, k_{ero}=0.047 and 0.048 days^{-1}, respectively, but Expansorb® DLG 50-2A had a much faster onset of erosion than Expansorb® DLG 50-2E: t_{on} values were 1.3 and 13.5 days, respectively. Resomer® RG 502 films had a k_{deg} of 0.032 days^{-1} and a $t_{1/2}$ of 21.4 days (Table 4-2). Resomer® RG 502 films did not start to significantly erode until after 21 days (Figure 4-2) and, thus, analysis of their erosion kinetics was not possible. By contrast, Resomer® RG 502H films had faster degradation and erosion kinetics than their ester-terminated counterparts with k_{deg}=0.127 days^{-1}, $t_{1/2}$=5.5 days, k_{ero}=0.080 days^{-1}, t_{on}=5.5 days (Tables 4-2 and 4-3). In both cases, the lactic content increased significantly faster for the acid-terminated films by either day 7 or day 21

compared to the ester-terminated films (Figure 4-7), further confirming the faster erosion apparent in acid-terminated polymers. The polymer chains equipped with an alkyl ester-end are more hydrophobic and can reduce the polymer hydrolysis rate and onset due to decreased water uptake and lack of acid end-groups available to engage in auto-catalyzed hydrolysis.[44,64,240] Huang et al. showed increasing PLGA carboxylic acid end-groups positively correlated with an increased hydrophobic drug release, and by combining acid- and ester-terminated PLGAs they were able to tailor an intermediate drug release from PLGA films.[240] The type of ester end-capping is not typically reported by polymer manufacturers but has been shown to affect polymer hydrolysis. As an example, Tracy et al., observed a case where differences in the ester end-cap type can overcome differences in molecular weight between PLGA microspheres.[42] The end-cap type can be determined by NMR and would be an interesting future investigation to compare between manufacturers.[44]

4.4.3 Effect of formulation geometry

To investigate the influence of formulation geometry, we compared 75/25, acid-terminated, "low" molecular weight (7-12 kDa) PLGAs, Expansorb® DLG 75-2A, Purasorb® DLG 7502A, Resomer® RG 752H, and Wako® 7515, as implants and microspheres. Geometrically larger implants had increased water uptake (Figure 3a-d), and faster initial degradation (Figure 4-3e-h) in the first week compared to microspheres of the same polymers, likely due to enhanced effects of auto-catalysis from PLGA acidic byproducts unable to escape as efficiently from larger geometries.[64,241,242] As seen in Figure 4-3m-n, the lactic content in microspheres steadily increased over incubation time, from the initial ~75% to 81-86% after 28 days. Implants, however, dramatically increased to ~92-97% lactic content within the first 2 weeks of incubation. Glycolic linkages are known to be labile to hydrolysis[243], but interestingly,

here, the enhanced auto-catalysis in the larger geometry appeared to preferentially affect glycolic linkages. Implants had faster onsets of erosion (Table 4-3), 3-10 days, compared to their microsphere counterparts, 15-23 days, but eventually, implant erosion slowed down resulting in slower overall apparent rate constants than microspheres (Table 4-2). Despite the fact that implants had a faster initial degradation, implants and microspheres had similar erosion profiles over the first month (Figure 4-3i-l), possibly because the degradation products may not have been able to escape due to the larger geometry of implants (0.5 mm diameter x 0.5 cm length) vs. microspheres (32-63 μm). Implants were mostly "poly(lactide)" by two weeks, which would be expected to hydrolyze slower and explains why both the degradation and erosion slowed down after having faster initial rates. Microspheres also have a higher surface area to volume ratio influencing their eventual faster erosion. Typically, the thicker the PLGA device, the faster the degradation.[242] Our results showed that the larger geometry implants resulted in faster initial degradation than microspheres, but an overall slower degradation. Similar results were reported by Witt et al., where PLGA rods initially degraded faster than PLGA microspheres, but eventually slowed down.[236] They also observed that the erosion of the rods was delayed and did not coincide with the faster initial degradation. No analysis was done on the degradation products or differences between the lactic and glycolic degradation, but it is possible that a similar behavior occurred.

4.4.4 Effect of polymer manufacturer

To compare the effects of different manufacturers, we focused on formulations that had the same L/G ratio, end-capping, and similar starting molecular weights to keep all variables as constant as possible. Therefore, *1*) Expansorb® DLG 50-5A, Resomer® RG 504H, and Purasorb® PDLG 5004A films and *2*) Expansorb® DLG 50-2A and Resomer® RG 502H films were

compared. The water uptake between these films was generally very similar (Figure 4-4a,e), but they diverged in their initial first order degradation constants, determined over the first three days of incubation using a least squared linear regression analysis (data not shown). Expansorb® DLG 50-5A and Purasorb® PDLG 5004A both had faster initial degradation rate constants, k_{deg}=0.108 days^{-1} and 0.105 days^{-1}, respectively, than Resomer® RG 504H, k_{deg}=0.078 days^{-1}. Expansorb® DLG 50-2A initial degradation rate constant, k_{deg}=0.13 days^{-1}, was slightly faster than Resomer® RG 502H, k_{deg}=0.108 days^{-1}. Our lab previously analyzed the monomer sequence distribution of these same polymers using high resolution ^{13}CNMR and determined the blockiness (R_c, presence of glycolide linkages), and the block length (L_G, length of the glycolide sequences) by determining relative intensities of the glycolyl and lactyl carbonyls.[244] In the case of Expansorb® DLG 50-5A, Resomer® RG 504H, and Purasorb® PDLG 5004A films, both an increased glycolic blockiness and increased glycolic block length appeared to be influential.[244] Expansorb® DLG 50-5A polymer had a higher glycolic block length, L_G=4.0, than both Purasorb® PDLG 5004A, L_G=3.2, and Resomer® RG 504H, L_G=2.9, polymers. While Purasorb® PDLG 5004A had a slightly lower block length, it had a higher glycolic blockiness, R_c=1.6, than Expansorb® DLG 505A, R_c=0.7, and Resomer® RG 504H, R_c=1.3. Expansorb® DLG 50-2A polymer had higher glycolic block length and blockiness values, L_G=4.2 and R_c=1.9, than Resomer® RG 502H, L_G=3.0 and R_c=1.4.[244] Both the presence of glycolic linkages and the longer length of these glycolic sequences can influence the faster initial rate of degradation. Expansorb® DLG 50-5A films showed an accelerated onset of erosion compared to the other two polymer formulations, Resomer® RG 504H and Purasorb® PDLG 5004A, but a significantly slower overall erosion rate compared to Resomer® RG 504H (Table 4-3), so the faster degradation may have led to a faster initial onset of erosion within the polymer film. Similarly,

Expansorb® DLG 50-2A had a faster onset of erosion but a slower overall rate of erosion compared to Resomer® RG 502H (Table 4-3). Although the erosion profiles (Figure 4-4c,g) do not clearly show these differences due to inherent variability in weighing the degraded films, we have more definitive evidence from ^{1}HNMR determining the lactic content remaining in the samples after incubation. Figure 4-4d,h shows the lactic content remaining in the films after incubation for 7, and 21 or 28 days. Expansorb® DLG 50-5A revealed a higher lactic content, ~59%, than Resomer® RG 504H, ~56%, and Purasorb® PDLG 5004A, ~59%, after 28 days. As the initial lactic content for Purasorb® PDLG 5004A was higher (51%), the changes in lactic content are less significant compared to the other two film polymers. The change of lactic content was less pronounced for Expansorb® DLG 50-2A and Resomer® RG 502H films. In both two cases, the Expansorb® films lost glycolic units faster than the Resomer® films, as expected with their higher glycolic block lengths and faster initial degradation rate. This can also explain why both erosion and degradation rates eventually slow down because these polymers had slightly higher lactic content after the initial glycolic unit loss, which is expected to erode slower. Besides the block length, both the Expansorb® and Purasorb® polymers had higher residual monomers, as reported from their certificates of analysis, than the Resomer® polymers. Expansorb® DLG 50-2A and DLG 50-5A both had 0.5% total residual monomer and Purasorb® PDLG 5004A had 1.3%, while Resomer® RG 502H and 504H had 0.2% and 0.3% total residual monomer, respectively. The residual monomer could potentially contribute to faster degradation due to the increased presence of carboxylic acids and increased plasticization, resulting in enhanced acid-catalyzed hydrolysis, but may not be as influential in smaller geometries (e.g., thin films) since the residual monomer would be expected to efficiently escape the polymer matrix upon hydration.[45,46]

Microspheres and implants of Wako® 7515, a PLGA synthesized by polycondensation[227], consistently degraded faster than the comparable formulations from Expansorb® DLG 75-2A, Resomer® RG 752H and Purasorb® PDLG 7502A, PLGAs synthesized by ring-opening polymerization (Figure 4-3, Table 4-2). The initial apparent first order degradation rate constant, determined from the first 7 days of incubation, of Wako® 7515 microspheres was 0.068 $days^{-1}$ compared to 0.061, 0.060 and 0.052 $days^{-1}$ of Expansorb® DLG 752A, Resomer® RG 752H and Purasorb® PDLG 7502A microspheres, respectively. The initial apparent first order degradation rate constant of Wako® 7515 implants was 0.106 $days^{-1}$ compared to 0.075, 0.086 and 0.082 $days^{-1}$ of Expansorb® DLG 75-2A, Resomer® RG 752H and Purasorb® PDLG 7502A implants, respectively. Wako® 7515 microspheres also had a significantly faster apparent rate of erosion compared to the other three manufacturers, and Wako® 7515 implants showed significantly faster k_{ero} values than Resomer® RG 752H and Purasorb® PDLG 7502A, which is consistent with previous data from our group studying leuprolide-loaded microspheres, where Wako® 7515 microspheres showed faster drug release compared to Resomer® RG 752H microspheres.[227] The glycolic blockiness and block lengths from these four polymers alone do not completely explain the patterns observed. Wako® 7515, the fastest eroding and degrading, had the smallest glycolic block length, L_G=1.4, but a relatively higher blockiness, R_c=0.6. Expansorb® DLG 75-2A had a higher block length, L_G=2.5, but the lowest blockiness, R_c=0.5. Purasorb® PDLG 7502A, had the largest block length, L_G=2.7, but a lower blockiness, R_c=0.5. Resomer® RG 752H, had a higher block length, L_G=2.6, and the highest blockiness, R_c=0.7, yet it consistently degraded and eroded slower. Resomer® RG 752H had the lowest reported total residual monomer, 0.5%, while Expansorb® DLG 75-2A had 0.9%, Purasorb® PDLG 7502A had 1.8%, and Wako residual monomer was unreported. As discussed, this level residual monomer may have minimal

influence, especially in the microspheres, but in the larger geometry implants, the monomers may not diffuse out as easily and may impact the degradation more. We also observed notable differences in the dry glass transition temperatures (T_g) of the polymers (Table 4-1). Resomer® RG 752H had the highest T_g, ~47°C; Expansorb® DLG 75-2A, Purasorb® PDLG 7502A and Wako® 7515 all had lower T_g values of ~40°C, ~42°C and ~41°C, respectively, characteristic of higher polymer chain mobility, another possible function of the residual monomer content. It should be noted that the Expansorb® DLG 75-2A implants and microspheres had a lower starting molecular weight (6 kDa) than the other three polymers which is also related to its lower T_g. There may be multiple variables in their manufacturing processes causing differences in performance, not only the different synthesis methods, polycondensation vs. ROP, but the different types and levels of catalysts and initiators, the reaction temperature and timing conditions, or the purification process, that would require more information and further investigation, ideally with more batches.

High molecular weight, 75/25 ester end-terminated PLGA films across three brands, Expansorb® DLG 75-9E, Lactel® DL-PLG B6007-2, and Resomer® RG 756S were compared. Resomer® RG 756S film preparation resulted in lower starting molecular weights than expected despite careful processing and handling, which resulted in a much higher water uptake while Expansorb® DLG 75-9E and Lactel® DL-PLG B6007-P had similar water uptake profiles (Figure 4-5a). Despite these differences, the three polymer film formulations had similar degradation and erosion behaviors (Figure 5b,c). Degradation rates (0.032-0.038 $days^{-1}$), molecular weight half-lives (18.5-21.6 days), t_{on} values (20.8-23.6 days), and erosion rates (0.01-0.021 $days^{-1}$) (Tables 4-2 and 4-3). All three polymer films eroded slowly, <42%, for the first 42 days (Figure 4-5c). Resomer® RG 756S films had erosion towards the end of the 60 days incubation resulting in a

significantly faster k_{ero} value (Table 4-3). Based on our previous analyses, Resomer® RG 756S polymer had a higher blockiness value, R_c=1.7, compared to both Expansorb® DLG 75-9E polymer, R_c=0.5, and Lactel® DL-PLG B6007-2 polymer R_c=0.6. The higher blockiness may have also contributed to the elevated water uptake[53] as well as a significantly faster loss of lactic units, determined by ^{1}HNMR (Figure 4-5d). Overall, the higher molecular weight, higher L/G ratio, and ester end capping demonstrate how a combination of PLGA properties can be used to dramatically reduce degradation and erosion and would be expected to lead to a slower drug release.

Compared to 75/25, acid-terminated PLGA implants of similar molecular weight, PLA implants typically showed slower degradation and significantly reduced erosion over 56 days, as expected with the 100% racemic lactide polymers. PLA implants, Expansorb® DL 100-2A, Resomer® R 202H, and Purasorb® PDL 02A eroded very slowly, with a small initial erosion phase in the first few weeks followed by a small increase in erosion that resulted in 25-35% mass loss after 56 days of incubation (Figure 4-6). Between the manufacturers, Resomer® R 202H had the slowest water uptake, and slowest degradation and erosion (Figure 4-6, Tables 4-2 and 4-3). Resomer® R 202H had the lowest amount of residual monomer listed on its certificate of analysis, 0.2%, compared to Expansorb® DL 100-2A which had 1.8%, and Purasorb® PDL 02A which had 2.0% of total residual monomer listed. We also previously analyzed the same batch used of Purasorb® PDL 02A by ^{1}HNMR and determined it had some residual glycolide impurity present.[244] Resomer® R 202H also had the highest dry T_g, ~51°C, indicative of its lower residual monomer, while Expansorb® DL 100-2A and Purasorb® PDL 02A revealed T_g values of ~45°C and ~46°C, respectively (Table 4-1). To further characterize these differences, we evaluated the molecular diffusion as a function of incubation time with microspheres incubated with BODIPY

fluorescent dye, which is known to diffuse through solid PLGA over reasonable time scales and can be monitored by laser fluorescence confocal microscopy.[235] Increases in the diffusion coefficient of BODIPY, may be a results of higher polymer chain mobility and polymer hydrolysis rate. Figure 4-6d-g shows the BODIPY diffusion coefficients and representative confocal images of a single microsphere of each of the three polymers. Purasorb® PDL 02A, the fastest degrading polymer, had a significantly greater diffusion coefficient on day 21 of incubation, compared to the other two polymers, and the confocal image further showed how degraded these microspheres became, while Resomer® R 202H, the slowest degrading, was still "intact" by day 21.

We observed differences in sequence distribution, glass transition temperatures, and in reported residual monomer between polymer manufacturers that manifested in differences between their water uptake, degradation, and erosion behaviors when formulated into films, implants and microspheres. These differences may arise from the polymer synthesis process and manufacturing parameters. For example, the ROP method has several variables involved such as the reaction temperature, time, amount of catalyst present, amount of co-initiator present, timing of monomer addition, and the extent of purification. Differences in optimized conditions between manufacturers, or inherent variations between batches within the same manufacturer can lead to deviations in polymer properties that may not be monitored or reported. The amount of catalyst or initiator species present can help to increase the molecular weight quickly, but can also result in residual monomer, or higher chain dispersity. The addition of monomer to the growing chain can be affected by the catalyst used and by the reactivity of each monomer. Glycolic units have a higher reactivity of addition to the growing polymer chain end, both when it is a lactic or glycolic unit, which can result in "blockiness" of lactic or glycolic units.[52,245] Over time, side

reactions including chain back-biting and chain rearrangement can lead to the formation of cyclic dimers and more chain polydispersity or residual monomers.[38] In general, ROP offers better control over the sequence distribution and molecular weight than polycondensation, especially when no catalyst is used in polycondensation.[246] The effects of the monomer sequence have been extensively studied by Meyer et al. and it is clear that the heterogeneity of the sequence, the increased number or lengths of the glycolic linkages, leads to significantly faster swelling and hydrolysis and, thus, polymer erosion.[49,53,243] These studies were done comparing a typical polymer synthesized by ROP to a sequence-controlled polymer, so the differences were very evident. Here, we compared random (co-)polymers, synthesized by ROP, except for Wako® 7515, and their differences in glycolic blockiness and block lengths are less evident. The differences in glycolic sequence that we observed between manufacturers appeared to result in increased *initial* degradation and generally resulted in heterogenous degradation of the glycolic and lactic monomers. This faster initial hydrolysis could potentially lead to a faster initial release of drug which could result in a non-ideal release profile, or dose dumping. We also observed apparent effects of increased residual monomer on water uptake, hydrolysis, and erosion. Although the residual monomers would be expected to diffuse out of smaller geometries quickly, it is possible they are more influential in a larger geometry, as seen in the 75/25 acid-terminated PLGA and in the acid-terminated PLA implants. To better understand the effects of sequence distribution on degradation and erosion behaviors, a larger number of comparisons is needed. Furthermore, it would be interesting to investigate the differences between multiple product batches within the same manufacturer. The data here is a limited example but begins to establish the effects of variations between manufacturers or polymer synthesis methods on PLGA degradation and erosion behavior.

4.5 Conclusion

This work presents data for 17 commercially available PLGA polymers from five different manufacturers. We investigated differences between manufacturers by comparing drug-free films, implants and microspheres with similar L/G ratios, end-capping, and molecular weights. Increased glycolic block lengths in 50/50, acid-terminated PLGA films appeared to increase the initial degradation rate constants. A lower residual monomer in PLA, acid-terminated implants appeared to result in lower water uptake and slower overall degradation and erosion. In 75/25, acid-terminated PLGA implants, the larger geometry had enhanced acid-catalyzed hydrolysis and, thus, increased initial degradation rate constants compared to microspheres. Furthermore, the enhanced acid-catalyzed degradation selectively affected the glycolic units in implants, ^{1}HNMR data showing the implants becoming almost completely "poly(lactide)" within two weeks. A more gradual loss of glycolic monomers occurred in microspheres, suggesting a difference in their hydrolytic mechanisms. Any change in the formulation water uptake, hydrolysis and degradation, or erosion would be expected to also affect drug release since these events are all involved in the mechanism of release. Overall, this work provides a sizeable comparison of commercially available polymers and has investigated differences in less studied variables, such as the glycolic monomer distribution, that can provide a better understanding of selection of polymers for a desired polymer behavior.

Polymer	L/G	End Cap	Molecular Weight, kDa	Inherent Viscosity[a], dL/g	Dry T_g, °C, AVG (SD)	Lot No.
Expansorb® DLG 50-2A	50/50	Acid	13	0.19	41.5 (0.2)	PP10056489
Resomer® RG 502H	50/50	Acid	14	0.22	45.3 (0.1)	BCBZ7916
Expansorb® DLG 50-5A	50/50	Acid	48	0.47	48.0 (0.2)	PP10059967
Resomer® RG 504H	50/50	Acid	52.9	0.57	48.4 (0.1)	BCBX4108
Purasorb® PDLG 5004A	50/50	Acid	29.1	0.37	46.3 (0.4)	1110001124
Expansorb® DLG 50-2E	50/50	Ester	17	0.21	38.0 (0.2)	C100011425
Resomer® RG 502	50/50	Ester	14.7	0.20	43.5 (0.3)	BCCB0256
Expansorb® DLG 75-2A	75/25	Acid	8	0.12	39.8 (0.3)	PP10056560
Resomer® RG 752H	75/25	Acid	13.4	0.22	46.9 (0.1)	BCBw4713
Purasorb® PDLG 7502A	75/25	Acid	NR	0.19	41.9 (0.8)	1802003617
Wako® 7515	75/25	Acid	NR	0.18	41.3 (0.3)	TWO.1257
Expansorb® DLG 75-9E	75/25	Ester	136	0.95	49.9 (0.1)	C100011427
Lactel® DL-PLG B6007-2	75/25	Ester	NR	0.81	45.9 (0.1)	A17-068
Resomer® RG 756S	75/25	Ester	NR	0.90	51.2 (0.2)	BCBZ4420
Expansorb® DL 100-2A	100/0	Acid	11 (0.1)	0.18	45.2 (0.1)	PP10059963
Resomer® R 202H	100/0	Acid	16 (0.1)	0.24	50.9 (0.1)	BCBV6665
Purasorb® PDL 02A	100/0	Acid	14 (0.1)	0.22	46.2 (0.1)	1703003820

Table 4-1. List of polymers used and their properties. *L/G ratio and end-capping as listed by the manufacturer, molecular weight as reported by the manufacturer (determined by gel permeation chromatography), inherent viscosity as reported by the manufacturer, dry glass transition temperature (T_g) as determined by differential scanning calorimetry (n = 2), and the lot number for each polymer used. Similar polymers are shown grouped together. [a]Resomer® inherent viscosity (i.v.): 0.1% in chloroform at 25°C. Expansorb® i.v.: 0.5% chloroform, 25°C. Purasorb® PDLG 5004A i.v.: 0.5 g/dL in chloroform at 25°C. Purasorb® PDLG 7502A, and Purasorb® PDL 02A i.v.: 1 g/dL in chloroform at 25°C. Lactel® i.v.: 0.5 g/dL in chloroform at 30°C. Wako® i.v. method not reported.*

Polymer	Formulation Vehicle	Formulation Starting MW, kDa	k_{deg}, days^{-1}	MW half life, days
Expansorb® DLG 50-2A	Film	10.9 (0.1)	0.092 (0.012) *	7.6 (1.4)
Resomer® RG 502H	Film	12.6 (1.1)	0.123 (0.005)	5.5 (0.3)
Expansorb® DLG 50-5A	Film	35.3 (0.6)	0.086 (0.004)	8.0 (0.6)
Resomer® RG 504H	Film	36.9 (0.1)	0.093 (0.004)	7.5 (0.4)
Purasorb® PDLG 5004A	Film	29.1 (0.2)	0.086 (0.004)	8.1 (0.5)
Expansorb® DLG 50-2E	Film	15.4 (0.1)	0.049 (0.006) *	14.3 (2.6)
Resomer® RG 502	Film	13.2 (0.1)	0.032 (0.004)	21.4 (3.7)
Expansorb® DLG 75-2A	Implant	6.1 (0.1)	0.047 (0.009) *	14.8 (3.9)
Resomer® RG 752H	Implant	10.5 (0.1)	0.067 (0.005) *	10.4 (1.2)
Purasorb® PDLG 7502A	Implant	9.4 (0.2)	0.049 (0.009) *	14.1 (3.6)
Wako® 7515	Implant	12.6 (0.2)	0.078 (0.008) *	8.9 (1.2)
Expansorb® DLG 752A	Microsphere	6.0 (0.2)	0.054 (0.001) *	12.8 (0.5) *
Resomer® RG 752H	Microsphere	11.7 (0.1)	0.057 (0.002) *	12.1 (0.7) * *
Purasorb® PDLG 7502A	Microsphere	9.6 (0.1)	0.050 (0.001) * *	13.9 (0.4) * *
Wako® 7515	Microsphere	13.1 (0.7)	0.076 (0.002) *	9.1 (0.4) *
Expansorb® DLG 75-9E	Film	71.0 (10.5)	0.038 (0.002) *	18.5 (1.5) *
Lactel® DL-PLG B6007-2	Film	79.8 (2.5)	0.035 (0.003)	20.0 (2.8)
Resomer® RG 756S	Film	39.2 (6.5)	0.032 (0.001)	21.6 (1.2)
Expansorb® DL 100-2A	Implant	10.5 (0.1)	0.038 (0.003) *	18.3 (2.3) *
Resomer® R 202H	Implant	15.5 (0.2)	0.035 (0.002) *	20.0 (1.8) *
Purasorb® PDL 02A	Implant	13.7 (0.1)	0.049 (0.002)	14.0 (0.8)

Table 4-2. Formulation vehicle starting molecular weights, apparent first order degradation rate constants and molecular weight half-lives for polymer formulations. *Data represents the mean (standard error), n=3. Statistics represent unpaired t-test; * $p<0.05$.*

Polymer	Formulation Vehicle	t_{on}, days	k_{eros}, days^{-1}
Expansorb® DLG 50-2A	Film	1.3 (0.2) *	0.048 (0.006) *
Resomer® RG 502H	Film	5.5 (0.4)	0.080 (0.004)
Expansorb® DLG 50-5A	Film	11.8 (0.5) *	0.047 (0.002) * *
Resomer® RG 504H	Film	16.4 (1.3)	0.060 (0.003)
Purasorb® PDLG 5004A	Film	15.9 (2.8)	0.076 (0.01)
Expansorb® DLG 50-2E	Film	13.5 (3.2)	0.047 (0.008)
Resomer® RG 502	Film	NA	
Expansorb® DLG 75-2A	Implant	3.0 (0.1) * * *	0.044 (0.001) * * *
Resomer® RG 752H	Implant	9.7 (0.8) *	0.030 (0.002) *
Purasorb® PDLG 7502A	Implant	4.5 (0.1) * *	0.025 (0.001) * *
Wako® 7515	Implant	6.6 (0.8) *	0.042 (0.004) *
Expansorb® DLG 75-2A	Microsphere	14.7 (2.2) * *	0.100 (0.011) *
Resomer® RG 752H	Microsphere	23.1 (1.8)	0.084 (0.005)
Purasorb® PDLG 7502A	Microsphere	21.0 (0.6)	0.086 (0.002) * * *
Wako® 7515	Microsphere	20.9 (5.8)	0.154 (0.03) *
Expansorb® DLG 75-9E	Film	20.8 (6.1)	0.010 (0.002) *
Lactel® DL-PLG B6007-2	Film	21.8 (10.0)	0.011 (0.003)
Resomer® RG 756S	Film	23.6 (7.0)	0.021 (0.006)
Expansorb® DL 100-2A	Implant	19.4 (0.8)	0.014 (0.003)
Resomer® R 202H	Implant	NA	
Purasorb® PDL 02A	Implant	22.9 (6.2)	0.014 (0.003)

Table 4-3. Apparent erosion rates and onsets for polymer formulations. *Data represents average (standard error), n=3. Statistics represent unpaired t-test, *p<0.05. NA = Not applicable, erosion not significant enough to analyze kinetics.*

.

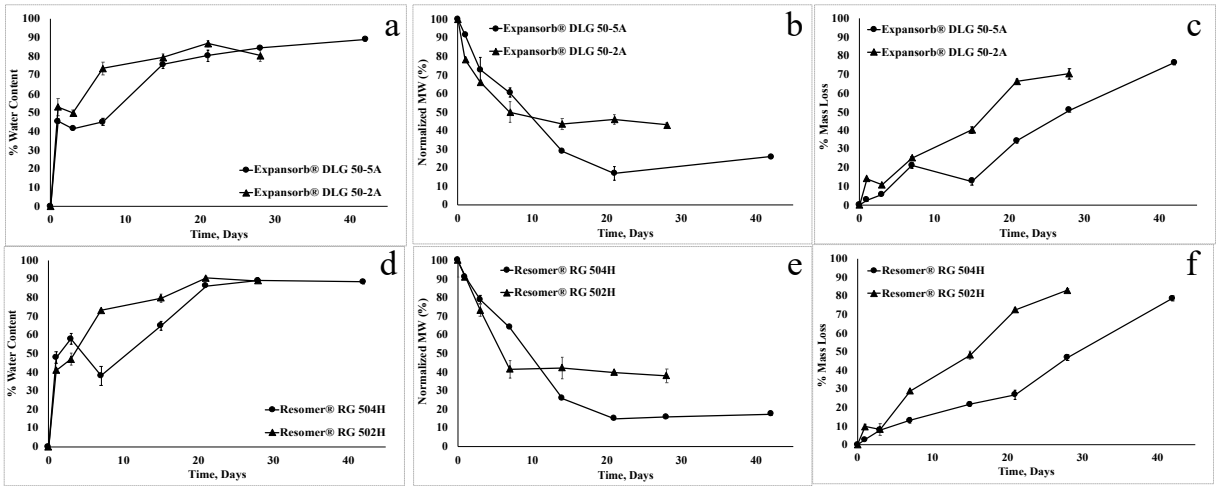

Figure 4-1. Effect of molecular weight on erosion behavior in 50/50 acid-terminated PLGA films. *Kinetics of water content, molecular weight (MW) loss as determined by gel permeation chromatography, and mass loss are represented for Expansorb® (a-c) and Resomer® (d-f) films, respectively. Data represents mean ± standard error (SE), n=3.*

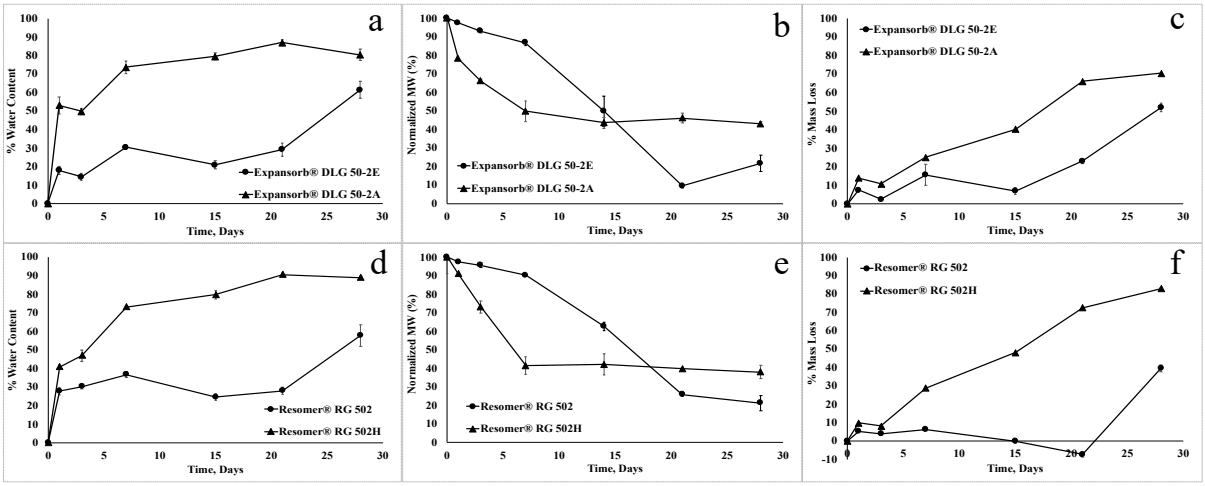

Figure 4-2. Effect of end-capping on erosion behavior in 50/50 PLGA films. *Kinetics of water content, molecular weight (MW) loss as determined by gel permeation chromatography, and mass loss are represented for Expansorb® (a-c) and Resomer® (d-f) PLGA films, respectively. Data for Expansorb® DLG 50-2A and Resomer® RG 502H were reproduced from Figure 4-1. Data represents mean ± standard error (SE), n=3.*

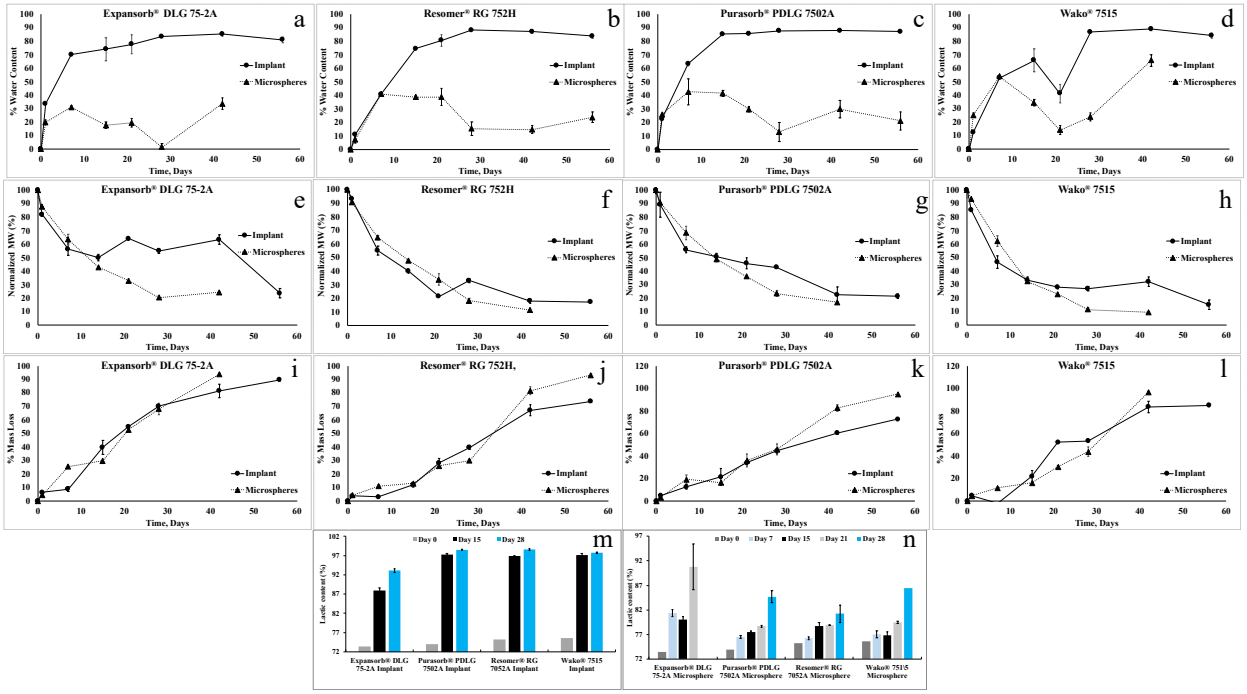

Figure 4-3. Effect of formulation size and geometry on erosion behavior and lactic content, in acid-terminated 75/25 PLGA implants and microspheres. *Kinetics of water content (a-d), molecular weight (MW) loss as determined by gel permeation chromatography (e-h), and mass loss (i-l) were determined for Expansorb® (a,e,i), Purasorb® (b,f,j), Resomer® (c,g,k) and Wako® (d,h,l) PLGA formulations, respectively. The remaining lactic content was determined for microspheres (j) and implants (k) by ^{1}HNMR. Data represents mean ± standard error (SE), n=3.*

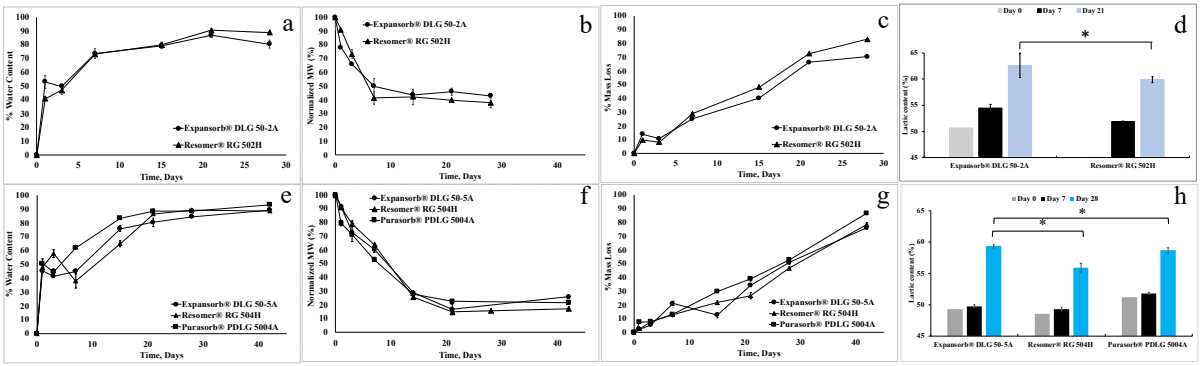

Figure 4-4. Effect of manufacturer on the erosion behavior and lactic content of 50/50 acid-terminated PLGA films. *Kinetics of water content (a, e), molecular weight (MW) loss as determined by gel permeation chromatography (b, f, j), mass loss (c, g), and lactic content (d, h) are shown for two sets of comparable Expansorb® and Resomer® polymers in a-d and e-h, respectively, and for Purasorb (i-l). Data for Expansorb® DLG 50-2A, Expansorb® DLG 50-5A, Resomer® RG 502H, and Resomer® RG 504H were reproduced from Figure 4-1. The remaining lactic content was determined by ^{1}HNMR and actual differences relative to their raw polymer starting %lactic content were used for statistical analyses. Data represents mean ± standard error (SE), n=3. Statistics represent unpaired t-test; * $p \leq 0.05$.*

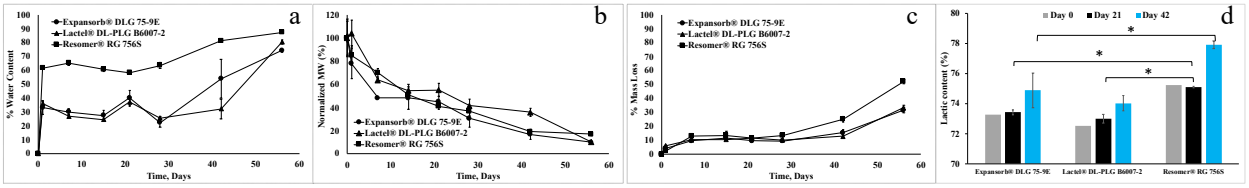

Figure 4-5. Effect of manufacturer on the erosion behavior and lactic content of 75/25 ester-terminated PLGA films. *Kinetics of water content (a), molecular weight (MW) loss as determined by gel permeation chromatography (b), mass loss (c), and lactic content (d) are shown. The remaining lactic content was determined by ^{1}HNMR and actual differences relative to their raw polymer starting %lactic content were used for statistical analyses. Data represents mean ± standard error (SE), n=3. Statistics represent unpaired t-test; * $p<0.05$.*

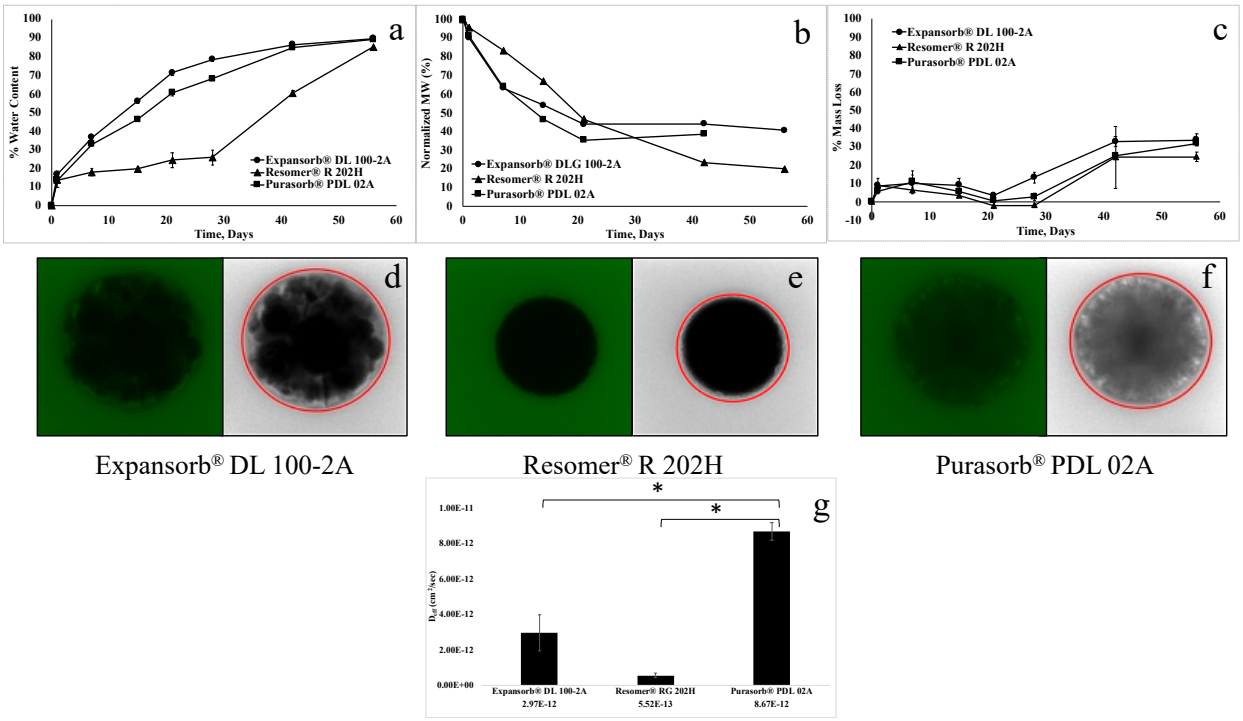

Figure 4-6. Effect of manufacturer on the erosion behavior of acid-terminated PLA implants. *Kinetics of water content (a), molecular weight (MW) loss as determined by gel permeation chromatography (b), and mass loss (c) were determined for Expansorb®, Resomer®, and Purasorb® implants. Data represents mean ± standard error (SE), n=3. Representative confocal images of microspheres after 21 days of incubation (d-f) and effective BODIPY diffusion coefficients and are shown (g). Data represents mean ± standard error (SE), n=4. Statistics represent unpaired t-test; *p<0.05.*

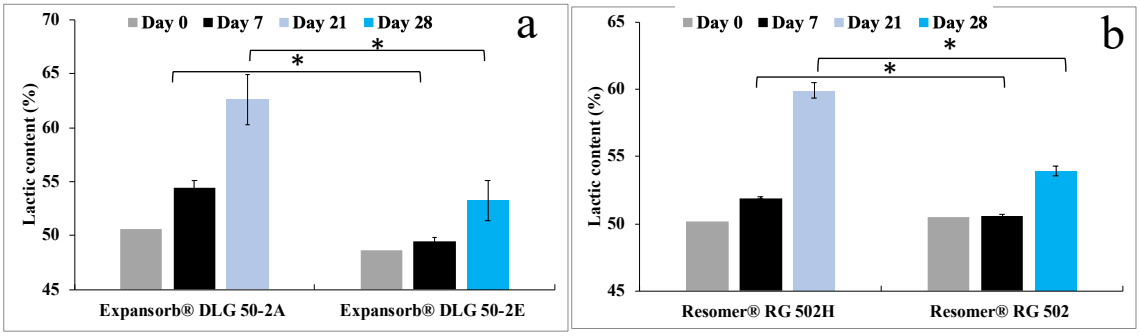

Figure 4-7. Lactic content remaining in 50/50 acid- and ester-terminated PLGA films as a function of incubation time*. The remaining lactic content was determined by [1]HNMR and actual differences relative to their raw polymer starting %lactic content were used for statistical analyses. Data represents mean ± standard error (SE), n=3. Day 21 was used in place of day 28 for Resomer® RG 502H and Expansorb® DLG 50-2A due to significant film mass loss. Statistics represent unpaired t-test, *p<0.05.*

Chapter 5: Conclusions, Significance, and Future Outlook

The work presented in this thesis discusses poly(lactic-co-glycolic acid) (PLGA) as a biodegradable delivery system for specialized drugs and excipients of interest in brain cancer treatment. Implants, microspheres and thin films were examined. Currently, there are no long-acting release products for drug molecules larger than 5,000 Da such as proteins and monoclonal antibodies (mAbs), likely due to instability issues during encapsulation and during long-term release from PLGA. Most currently reported long-term controlled release approaches for mAbs are insufficient in one or more aspect to be translated into a successful product. We identified several desired criteria for a successful long-acting-release product, namely, a high loading allowing for relevant therapeutic levels, a low initial burst release to avoid dose dumping, a slow and controlled release >2 months to avoid multiple injections, complete release (>80%) of the total loaded mAb to avoid instability of unreleased mAb, retained structure to avoid loss of activity or potential immune reactions, high activity or released mAb for optimal therapeutic efficacy, and proof of in vivo efficacy. Here, we have shown using stabilizing excipients, such as trehalose, to protect during cryomicronization and lyophilization, and $MgCO_3$ as an antacid to protect from the acidic microclimate that occurs during PLGA degradation, we can prevent instability of encapsulated monoclonal antibodies and maintain their structure and in vivo activity. We found in order to balance the necessary high level of stabilizing excipients, achieve a high loading of mAb, and sustain the release over 2 months with a low initial burst, it was crucial to implement a drug-free PLGA coating around the drug-loaded core implant.

Glioblastoma (GBM) is a devastating disease that has a poor prognosis and is challenged by an immunosuppressive tumor environment with few treatment options due to the blood brain and blood tumor barriers which do not allow for successful treatment with mAb therapeutics without extensive systemic toxicities, and thus a local sustained release option is a viable option for improved outcomes as has been used in the Gliadel® BCNU slow release wafers. Our PLGA implants delivering immune checkpoint inhibitors, anti-PD-1 or anti-CTLA-4, combined with radiation, demonstrated improved survival after implantation in an intracranial murine GL26 GBM model. Long-term survivors from the initial treatment group underwent a contralateral tumor cell rechallenge and had improved survival compared to treatment-naïve mice, exhibiting the production of a long-term immunological memory from our initial treatment. Glioblastoma tumors are highly heterogenous and have a high rate of recurrence, often in the same area of the original tumor. Here we also developed PLGA implants delivering CpG ODN and docetaxel to offer a multi-faceted approach for treating GBM. CpG is a TLR9-agonist and will help to initiate an immune response. Docetaxel is an apoptosis-inducing agent that will induce tumor-cell death and help to improve the tumor penetration of itself and other therapeutics by reducing the abnormal solid tumor stress present in GBM. Here, we have formulated implants delivering CpG, with albumin, a porosigen and buffering agent, and $MgCO_3$, an antacid. CpG was released over ~40 days and showed retained TLR9 binding activity in vitro. Docetaxel was successfully formulated in PLGA implants at a high loading (40-60%) and slowly released >80% of the total docetaxel for >100 days. Our PLGA implants capable of delivering both immune checkpoint inhibitors, CpG, and docetaxel are an advantageous approach not only for their local controlled release, but with the advancement of surgical capabilities, they are able to be inserted through a trocar syringe without the need for invasive surgery. Our in vivo work is lacking extensive

controls to compare to the current standard of care, or to systemic controls. In the future, we will test our combined therapeutic approach to treat glioblastoma against proper controls and also further characterize the immunological responses. Future work would include implanting combinations of all four implants in a subcutaneous GBM tumor model and comparing our local controlled release delivery option to systemic or even, locally injected controls. We will further evaluate the best candidate in an intracranial GBM model to better represent the disease state and to evaluate the elicited immune response and enhancement of tumor penetration of our drugs after including docetaxel, a tumor penetration enhancing agent.

Another great application of our mAb PLGA implants is intraocular delivery of anti-VEGF for the treatment of wetAMD. Anti-VEGF therapies, such as Avastin®, are used on and off-label to treat wetAMD by monthly or twice-monthly, intravitreal injections. To achieve a more applicable, patient-compliant therapeutic option for intraocular administration, we need to adjust our implants to <0.5 mm diameter. We first approached this by reducing the diameter of the silicone tubing used while keeping our mAb-loaded core formulation the same to retain the stabilizing effects of our added excipients. The smaller diameter implants required additional PLGA coating in order to achieve slow and controlled release of stabile bevacizumab for ~50 days, likely due to the now shorter lateral distance that the mAb has to traverse to release from the PLGA matrix. Next, we investigated the efficiency of our coating process by using a PLGA-glucose STAR (STAR) polymer to coat the linear PLGA, mAb-loaded core implant. One coating of the STAR polymer was not able to slowly sustain the release of bevacizumab, so we applied a second coating. The second coating of the STAR polymer resulted in incomplete release and increased water uptake and ultimately increased instability of bevacizumab realized by a decrease in the monomer content. This investigation showed the importance of the environment

inside the implant for the stability of the mAb; the acidic biproducts of PLGA degradation need to be able to efficiently escape in order to prevent acid-induced instability. To achieve the full potential of our mAb implants for intravitreal applications, more research will be done to reduce the implant diameter even further while still maintaining our slow and continuous release of stabile mAb. This could be approached by finding a more suitable tubing that still allows for acetone evaporation to occur, or by trying other options such as compression molding or twin-screw extruders to have better control over our implant diameter.

Although PLGA is the most commonly investigated polymer for controlled release due to its ease of processing, biocompatibility, and successful use in FDA approved products, there have not been more than ~19 approved products using PLGA since the first approval in 1980s, and no generic products available in the U.S. The process of approval for PLGA-based drug products could be improved by better knowledge of available commercial PLGAs and the effects of changing their properties and batch variations that may cause detrimental setbacks for reproducibility. Here, we performed a sizeable comparison into in vitro degradation and erosion of commercial PLGAs as a function of L/G ratio, MW, end-capping, manufacturer, and formulation geometry. Most notable, we found that the increased auto-catalysis preferentially affected the loss of glycolic units over lactic units in 75/25, acid-capped PLGA implants compared to microspheres. To our knowledge, this is the first time such an effect has been demonstrated, and the strong preferential loss of glycolic acid units could be predicted to be responsible for PLGA specimens retaining mass much longer than predicted. Also significant, we found that comparable PLGAs from different manufacturers could differ in their performance. Higher glycolic sequence blockiness or block lengths, led to increased initial degradation and faster erosion of glycolic units in 50/50, acid-capped PLGA films. Manufacturer

differences such as an increased acid number and increased residual monomer appeared to lead to increased water uptake and increased degradation in PLA implants. These studies have provided insight into effects of changes in PLGA source and the effects of lesser-reported properties such as sequence distribution. This work would be improved by further investigating more lot numbers within one PLGA product to further confirm our findings and to compare the effects on encapsulated drug release. The work could also provide insight as to PLGA selection when translating the PLGA dosage forms for treatment in brain cancer.

References

1. Tanaka, S., Louis, D. N., Curry, W. T., Batchelor, T. T. & Dietrich, J. Diagnostic and therapeutic avenues for glioblastoma: no longer a dead end? *Nat Rev Clin Oncol* **10**, 14–26 (2013).
2. Gately, L., McLachlan, S., Dowling, A. & Philip, J. Life beyond a diagnosis of glioblastoma: a systematic review of the literature. *J. Cancer Surviv.* (2017).
3. Lowenstein, P. R. & Castro, M. G. Evolutionary basis of a new gene-and immune-therapeutic approach for the treatment of malignant brain tumors: from mice to clinical trials for glioma patients. *Clin. Immunol.* **189**, 43–51 (2018).
4. Wang, P. P., Frazier, J. & Brem, H. Local drug delivery to the brain. *Adv Drug Deliv Rev* **54**, 987–1013 (2002).
5. Liu, H. L. *et al.* Blood-brain barrier disruption with focused ultrasound enhances delivery of chemotherapeutic drugs for glioblastoma treatment. *Radiology* **255**, 415–425 (2010).
6. Groothuis, D. R. The blood-brain and blood-tumor barriers: a review of strategies for increasing drug delivery. *Neuro Oncol* **2**, 45–59 (2000).
7. Castro, M. G., Baker, G. J. & Lowenstein, P. R. Blocking Immunosuppressive Checkpoints for Glioma Therapy: The More the Merrier! *Clin. Cancer Res.* **20**, 5147 LP – 5149 (2014).
8. Kamran, N. *et al.* Immunosuppressive myeloid cells' blockade in the glioma microenvironment enhances the efficacy of immune-stimulatory gene therapy. *Mol. Ther.*

25, 232–248 (2017).

9. Sakuishi, K. *et al.* Targeting Tim-3 and PD-1 pathways to reverse T cell exhaustion and restore anti-tumor immunity. *J. Exp. Med.* **207**, 2187–2194 (2010).
10. Spain, L., Diem, S. & Larkin, J. Management of toxicities of immune checkpoint inhibitors. *Cancer Treat. Rev.* (2016).
11. Zhu, G., Mallery, S. R. & Schwendeman, S. P. Stabilization of proteins encapsulated in injectable poly (lactide-co-glycolide). *Nat. Biotechnol.* **18**, 52–57 (2000).
12. Gaozhong, Z. & Schwendeman, S. P. Stabilization of proteins encapsulated in cylindrical poly(lactide-co- glycolide) implants: Mechanism of stabilization by basic additives. *Pharm. Res.* **17**, 351–357 (2000).
13. Zhou, T., Lewis, H., Foster, R. E. & Schwendeman, S. P. Development of a multiple-drug delivery implant for intraocular management of proliferative vitreoretinopathy. *J. Control. Release* (1998).
14. Schwendeman, S. P., Shah, R. B., Bailey, B. A. & Schwendeman, A. S. Injectable controlled release depots for large molecules. *J. Control. Release* **190**, 240–253 (2014).
15. Park, K. *et al.* Injectable, long-acting PLGA formulations: Analyzing PLGA and understanding microparticle formation. *J. Control. Release* **304**, 125–134 (2019).
16. Lupron Depot® package insert. Available from: http://www.rxabbvie.com/pdf/lupronuro_pi.pdf.
17. Jiang, W. & Schwendeman, S. P. Stabilization and controlled release of bovine serum albumin encapsulated in poly (D, L-lactide) and poly (ethylene glycol) microsphere blends. *Pharm. Res.* **18**, 878–885 (2001).
18. Kang, J. & Schwendeman, S. P. Comparison of the effects of Mg (OH) 2 and sucrose on

the stability of bovine serum albumin encapsulated in injectable poly (D, L-lactide-co-glycolide) implants. *Biomaterials* **23**, 239–245 (2002).

19. Ding, A. G., Shenderova, A. & Schwendeman, S. P. Prediction of microclimate pH in poly(lactic-co-glycolic acid) films. *J Am Chem Soc* **128**, 5384–5390 (2006).
20. Zhong, Y. *et al.* Rescue of SCID murine ischemic hindlimbs with pH-modified rhbFGF/Poly(DL-lactic-co-glycolic acid) implants. *J. Control. Release* (2007).
21. Jiang, W. & Schwendeman, S. P. Stabilization of tetanus toxoid encapsulated in PLGA microspheres. *Mol. Pharm.* **5**, 808–817 (2008).
22. Reinhold, S. E., Desai, K. G. H., Zhang, L., Olsen, K. F. & Schwendeman, S. P. Self-Healing Microencapsulation of Biomacromolecules without Organic Solvents. *Angew. Chemie-International Ed.* **51**, 10800–10803 (2012).
23. Shah, R. B. & Schwendeman, S. P. A biomimetic approach to active self-microencapsulation of proteins in PLGA. *J. Control. Release* **196**, 60–70 (2014).
24. Tee, B. C. *et al.* Reconstructing jaw defects with MSCs and PLGA-encapsulated growth factors. *Am. J. Transl. Res.* **8**, 2693 (2016).
25. Uhrich, K. E., Cannizzaro, S. M., Langer, R. S. & Shakesheff, K. M. Polymeric systems for controlled drug release. *Chem Rev* **99**, 3181–3198 (1999).
26. Major, I. & Fuenmayor, E. The production of solid dosage forms from non-degradable polymers. *Curr. Pharm.* 2738–2760 (2016).
27. Friend, D. R. Intravaginal rings: Controlled release systems for contraception and prevention of transmission of sexually transmitted infections. *Drug Deliv. Transl. Res.* **1**, 185–193 (2011).
28. Abdullah, K. *et al.* Drug-Eluting Stents for Treatment of Peripheral Artery Disease. *Am. J.*

Cardiovasc. Drugs **18**, 175–180 (2018).

29. Gray, W. A. *et al.* A polymer-coated, paclitaxel-eluting stent (Eluvia) versus a polymer-free, paclitaxel-coated stent (Zilver PTX) for endovascular femoropopliteal intervention (IMPERIAL): a randomised, non-inferiority trial. *Lancet* **392**, 1541–1551 (2018).
30. Bodick, N. *et al.* An intra-articular, extended-release formulation of triamcinolone acetonide prolongs and amplifies analgesic effect in patients with osteoarthritis of the knee: a randomized clinical trial. *J. Bone Joint Surg. Am.* **97**, 877–888 (2015).
31. Jain, R. A. The manufacturing techniques of various drug loaded biodegradable poly(lactide-co-glycolide) (PLGA) devices. *Biomaterials* **21**, 2475–2490 (2000).
32. Malafaya, P. B., Silva, G. A. & Reis, R. L. Natural–origin polymers as carriers and scaffolds for biomolecules and cell delivery in tissue engineering applications. *Adv. Drug Deliv. Rev.* **59**, 207–233 (2007).
33. Go, A. & Langer, R. Modeling monomer release from bioerodible polymers. *J. Control. Release* **33**, 55–69 (1995).
34. Heller, J., Barr, J., Ng, S. Y., Abdellauoi, K. S. & Gurny, R. Poly (ortho esters): synthesis, characterization, properties and uses. *Adv. Drug Deliv. Rev.* **54**, 1015–1039 (2002).
35. Langer, R. & Chasin, M. Biodegradable polymers as drug delivery systems. *Inf. Heal. Care* (1990).
36. Makadia, H. K. & Siegel, S. J. Poly Lactic-co-Glycolic Acid (PLGA) as Biodegradable Controlled Drug Delivery Carrier. *Polym.* **3**, 1377–1397 (2011).
37. Avgoustakis, K. Polylactic-co-glycolic acid (PLGA). *Encycl Biomater Biomed Eng. Taylor Fr. Milt.* 2259–2269 (2008).
38. Ren, J. *Biodegradable poly (lactic acid): synthesis, modification, processing and*

applications. (Springer Science & Business Media, 2011).

39. Dijkstra, P. J., Du, H. & Feijen, J. Single site catalysts for stereoselective ring-opening polymerization of lactides. *Polym. Chem.* **2**, 520–527 (2011).

40. Dechy-Cabaret, O., Martin-Vaca, B. & Bourissou, D. Controlled ring-opening polymerization of lactide and glycolide. *Chem. Rev.* **104**, 6147–6176 (2004).

41. Hyon, S.-H., Jamshidi, K. & Ikada, Y. Synthesis of polylactides with different molecular weights. *Biomaterials* **18**, 1503–1508 (1997).

42. Tracy, M. A. *et al.* Factors affecting the degradation rate of poly(lactide-co-glycolide) microspheres in vivo and in vitro. *Biomaterials* **20**, 1057–1062 (1999).

43. Korhonen, H., Helminen, A. & Seppälä, J. V. Synthesis of polylactides in the presence of co-initiators with different numbers of hydroxyl groups. *Polymer (Guildf).* **42**, 7541–7549 (2001).

44. Samadi, N. *et al.* The effect of lauryl capping group on protein release and degradation of poly (d, l-lactic-co-glycolic acid) particles. *J. Control. Release* **172**, 436–443 (2013).

45. Hyon, S., Jamshidi, K. & Ikada, Y. Effects of residual monomer on the degradation of DL-lactide polymer. *Polym. Int.* **46**, 196–202 (1998).

46. Schliecker, G., Schmidt, C., Fuchs, S., Wombacher, R. & Kissel, T. Hydrolytic degradation of poly (lactide-co-glycolide) films: effect of oligomers on degradation rate and crystallinity. *Int. J. Pharm.* **266**, 39–49 (2003).

47. Braun, D., Cherdron, H., Rehahn, M., Ritter, H. & Voit, B. *Polymer synthesis: theory and practice: fundamentals, methods, experiments*. (Springer Science & Business Media, 2012).

48. Nomura, N., Ishii, R., Yamamoto, Y. & Kondo, T. Stereoselective Ring-Opening

Polymerization of a Racemic Lactide by Using Achiral Salen–and Homosalen–Aluminum Complexes. *Chem. Eur. J.* **13**, 4433–4451 (2007).

49. Washington, M. A. *et al.* The impact of monomer sequence and stereochemistry on the swelling and erosion of biodegradable poly (lactic-co-glycolic acid) matrices. *Biomaterials* **117**, 66–76 (2017).

50. Stanford, M. J. & Dove, A. P. Stereocontrolled ring-opening polymerisation of lactide. *Chem. Soc. Rev.* **39**, 486–494 (2010).

51. Thakur, K. A. M., Kean, R. T., Hall, E. S., Kolstad, J. J. & Munson, E. J. Stereochemical aspects of lactide stereo-copolymerization investigated by 1H NMR: a case of changing stereospecificity. *Macromolecules* **31**, 1487–1494 (1998).

52. Lendlein, A. & Sisson, A. *Handbook of biodegradable polymers: isolation, synthesis, characterization and applications*. (John Wiley & Sons, 2011).

53. Li, J., Rothstein, S. N., Little, S. R., Edenborn, H. M. & Meyer, T. Y. The effect of monomer order on the hydrolysis of biodegradable poly (lactic-co-glycolic acid) repeating sequence copolymers. *J. Am. Chem. Soc.* **134**, 16352–16359 (2012).

54. Li, J., Stayshich, R. M. & Meyer, T. Y. Exploiting sequence to control the hydrolysis behavior of biodegradable PLGA copolymers. *J. Am. Chem. Soc.* **133**, 6910–6913 (2011).

55. Vey, E. *et al.* Degradation kinetics of poly (lactic-co-glycolic) acid block copolymer cast films in phosphate buffer solution as revealed by infrared and Raman spectroscopies. *Polym. Degrad. Stab.* **96**, 1882–1889 (2011).

56. English, J. P. Method of making biodegradable polymeric implants. (2002).

57. Schwendeman, S. P. Recent advances in the stabilization of proteins encapsulated in injectable PLGA delivery systems. *Crit Rev Ther Drug Carr. Syst* **19**, 73–98 (2002).

58. Fu, K., Klibanov, A. M. & Langer, R. Protein stability in controlled-release systems. *Nat. Biotechnol.* **18**, 24–25 (2000).

59. Zoladex (R) [package insert]. AstraZeneca Pharmaceuticals LP, WIlmington, DE.; 2009.

60. Ozurdex(R) [FDA package insert]. Allergen, Inc Irvine, CA; 2014.

61. Repka, M. A. *et al.* Pharmaceutical applications of hot-melt extrusion: part I. *Drug Dev. Ind. Pharm.* **33**, 909–926 (2007).

62. Chang, R. S. & Schwendeman, S. PLGA depots for controlled release of bevacizumab (Doctoral Dissertation). *retrieved from deepblue.lib.umich.edu* (University of Michigan, 2016).

63. Xichen Zhang *et al.* A mechanistic study of antibiotic release from biodegradable poly (d, 1-lactide) cylinders. *J. Control. Release* **31**, 129–144 (1994).

64. Fredenberg, S., Wahlgren, M., Reslow, M. & Axelsson, A. The mechanisms of drug release in poly(lactic-co-glycolic acid)-based drug delivery systems--a review. *Int J Pharm* **415**, 34–52 (2011).

65. Farrar, D. Modelling of the degradation process for bioresorbable polymers. in *Degradation rate of bioresorbable materials* 183–206 (Elsevier, 2008).

66. Badi, N., Chan-Seng, D. & Lutz, J. Microstructure control: an underestimated parameter in recent polymer design. *Macromol. Chem. Phys.* **214**, 135–142 (2013).

67. Chen, X. & Ooi, C. P. Hydrolytic degradation and drug release properties of ganciclovir-loaded biodegradable microspheres. *Acta Biomater.* **4**, 1046–1056 (2008).

68. Zhang, X., Wyss, U. P., Pichora, D., Amsden, B. G. & Goosen, M. F. A. Controlled release of albumin from biodegradable poly (DL-lactide) cylinders. *J. Control. Release* **25**, 61–69 (1993).

69. Kim, H., Park, S., Kim, D. J. & Park, J. New Coating Method for Sustained Drug Release: Surface Modification of ePTFE Grafts by inner coating PLGA. *Bull. Korean Chem. Soc.* **35**, 1333–1336 (2014).

70. Zhu, X. & Braatz, R. D. A mechanistic model for drug release in PLGA biodegradable stent coatings coupled with polymer degradation and erosion. *J. Biomed. Mater. Res. Part A* **103**, 2269–2279 (2015).

71. Wang, X., Venkatraman, S. S., Boey, F. Y. C., Loo, J. S. C. & Tan, L. P. Controlled release of sirolimus from a multilayered PLGA stent matrix. *Biomaterials* **27**, 5588–5595 (2006).

72. Weiner, L. M., Surana, R. & Wang, S. Monoclonal antibodies: versatile platforms for cancer immunotherapy. *Nat. Rev. Immunol.* **10**, 317–327 (2010).

73. Padlan, E. A. Anatomy of the antibody molecule. *Mol Immunol* **31**, 169–217 (1994).

74. Weiner, G. J. Monoclonal antibody mechanisms of action in cancer. *Immunol. Res.* **39**, 271–278 (2007).

75. Grainger, D. W. Controlled-release and local delivery of therapeutic antibodies. *Expert Opin Biol Ther* **4**, 1029–1044 (2004).

76. Opdivo (R) [package insert].Bristol-Myers Squibb Company, Princeton, NJ; 2016.

77. Yervoy (R) [package insert]. Bristol-Myers Squibb Company, Princeton, NJ; 2015.

78. Adams, G. P. & Weiner, L. M. Monoclonal antibody therapy of cancer. *Nat. Biotechnol.* **23**, 1147–1157 (2005).

79. Daugherty, A. L. & Mrsny, R. J. Formulation and delivery issues for monoclonal antibody therapeutics. *Adv Drug Deliv Rev* **58**, 686–706 (2006).

80. Hmiel, L. K., Brorson, K. A. & Boyne 2nd, M. T. Post-translational structural

modifications of immunoglobulin G and their effect on biological activity. *Anal Bioanal Chem* **407**, 79–94 (2015).

81. Baynes, B. M. & Trout, B. L. Rational design of solution additives for the prevention of protein aggregation. *Biophys. J.* **87**, 1631–1639 (2004).

82. Yamaguchi, Y. & SpringerLink (Online service). Immunotherapy of Cancer An Innovative Treatment Comes of Age. IX, 358 p. 46 illus., 8 illus. in color

83. Sharma, P. & Allison, J. P. The future of immune checkpoint therapy. *Science (80-.).* **348**, 56–61 (2015).

84. Philips, G. K. & Atkins, M. Therapeutic uses of anti-PD-1 and anti-PD-L1 antibodies. *Int Immunol* **27**, 39–46 (2015).

85. Thomas, A. A., Ernstoff, M. S. & Fadul, C. E. Immunotherapy for the treatment of glioblastoma. *Cancer J* **18**, 59–68 (2012).

86. Pardoll, D. M. The blockade of immune checkpoints in cancer immunotherapy. *Nat Rev Cancer* **12**, 252–264 (2012).

87. Keytruda (R) [package insert]. Merck & Co., Inc., Whitehouse Station, NJ; 2017.

88. Shirota, H. & Klinman, D. M. Chapter 9 - CpG Oligodeoxynucleotides as Adjuvants for Clinical Use. in *Immunopotentiators in Modern Vaccines* 163–198 (Elsevier Ltd, 2017). doi:10.1016/B978-0-12-804019-5.00009-8

89. Akira, S. & Takeda, K. Toll-like receptor signalling. *Nat. Rev. Immunol.* **4**, 499–511 (2004).

90. Bachem. Oligonucleotide Trends January 2020. (2020). Available at: https://www.bachem.com/service-support/newsletter/oligonucleotide-trends-january-2020/.

91. Pogocki, D. & Schöneich, C. Chemical stability of nucleic acid–derived drugs. *J. Pharm. Sci.* **89**, 443–456 (4AD).

92. Kodra, J. T., Kehler, J. & Dahl, O. Stability of oligodeoxynucleoside phosphorodithioates and phosphorothioates in aqueous ammonia. *Nucleic Acids Res.* **23**, 3349–3350 (1995).

93. Mueller, M., Reichardt, W., Koerner, J. & Groettrup, M. Coencapsulation of tumor lysate and CpG-ODN in PLGA-microspheres enables successful immunotherapy of prostate carcinoma in TRAMP mice. *J. Control. Release* **162**, 159–166 (20AD).

94. Ali, O. A. *et al.* The efficacy of intracranial PLG-based vaccines is dependent on direct implantation into brain tissue. *J. Control. Release* **154**, 249–257 (2011).

95. Mohajer, M., Khameneh, B. & Tafaghodi, M. Preparation and characterization of PLGA nanospheres loaded with inactivated influenza virus, CpG-ODN and Quillaja saponin. *Iran. J. Basic Med. Sci.* **17**, 722–726 (9AD).

96. Nikitczuk, K. P., Schloss, R. S., Yarmush, M. L. & Lattime, E. C. PLGA-polymer encapsulating tumor antigen and CpG DNA administered into the tumor microenvironment elicits a systemic antigen-specific IFN-γ response and enhances survival. *J. Cancer Ther.* **4**, 280–290 (1AD).

97. Ebrahimian, M. *et al.* Induction of a balanced Th1/Th2 immune responses by co-delivery of PLGA/ovalbumin nanospheres and CpG ODNs/PEI-SWCNT nanoparticles as TLR9 agonist in BALB/c mice. *Int. J. Pharm.* **515**, 708–720 (30AD).

98. San Román, B., Gómez, S., Irache, J. M. & Espuelas, S. Co-encapsulated CpG oligodeoxynucleotides and ovalbumin in PLGA microparticles; an in vitro and in vivo study. *J. Pharm. Pharm. Sci.* **17**, 541 (2014).

99. Román, B. S. *et al.* Co-encapsulation of an antigen and CpG oligonucleotides into PLGA

microparticles by TROMS technology. *Eur. J. Pharm. Biopharm.* **70**, 98–108 (2008).

100. Martínez Gómez, J. M. *et al.* A Protective Allergy Vaccine Based on CpG- and Protamine-Containing PLGA Microparticles. *Pharm. Res.* **25**, 710 (3AD).

101. Fischer, S. *et al.* Concomitant delivery of a CTL-restricted peptide antigen and CpG ODN by PLGA microparticles induces cellular immune response. *J. Drug Target.* **17**, 652–661 (2009).

102. Sohail, M. F. *et al.* Advancements in the oral delivery of Docetaxel: challenges, current state-of-the-art and future trends. *Int. J. Nanomedicine* **13**, 3145 (2018).

103. Thiesen, J. & Krämer, I. Physico-chemical stability of docetaxel premix solution and docetaxel infusion solutions in PVC bags and polyolefine containers. *Pharm. World Sci.* **21**, 137–141 (1999).

104. Taxotere(R) [package insert]. Sanofi-Aventis, Bridgewater, NJ; 2013.

105. Perez, E. A. Microtubule inhibitors: Differentiating tubulin-inhibiting agents based on mechanisms of action, clinical activity, and resistance. *Mol. Cancer Ther.* **8**, 2086–2095 (1AD).

106. Jordan, M. A. & Wilson, L. Microtubules as a target for anticancer drugs. *Nat. Rev. Cancer* **4**, 253–265 (4AD).

107. Kapoor, D. N. *et al.* PLGA: a unique polymer for drug delivery. *Ther. Deliv.* **6**, 41–58 (2015).

108. Ong, B. Y. S. *et al.* Paclitaxel delivery from PLGA foams for controlled release in post-surgical chemotherapy against glioblastoma multiforme. *Biomaterials* **30**, 3189–3196 (2009).

109. Musumeci, T. *et al.* PLA/PLGA nanoparticles for sustained release of docetaxel. *Int. J.*

Pharm. **325**, 172–179 (2006).

110. Fonseca, C., Simoes, S. & Gaspar, R. Paclitaxel-loaded PLGA nanoparticles: preparation, physicochemical characterization and in vitro anti-tumoral activity. *J. Control. release* **83**, 273–286 (2002).

111. Immordino, M. L. *et al.* Preparation, characterization, cytotoxicity and pharmacokinetics of liposomes containing docetaxel. *J. Control. Release* **91**, 417–429 (2003).

112. Musumeci, T. *et al.* Pharmaceutical Nanotechnology PLA / PLGA nanoparticles for sustained release of docetaxel. **325**, 172–179 (2006).

113. Desai, K. G. H., Mallery, S. R. & Schwendeman, S. P. Effect of formulation parameters on 2-methoxyestradiol release from injectable cylindrical poly (DL-lactide-co-glycolide) implants. *Eur. J. Pharm. Biopharm.* **70**, 187–198 (2008).

114. Omuro, A. & LM, D. Glioblastoma and other malignant gliomas: A clinical review. *JAMA* **310**, 1842–1850 (2013).

115. Lim, M., Xia, Y., Bettegowda, C. & Weller, M. Current state of immunotherapy for glioblastoma. *Nat. Rev. Clin. Oncol.* 1 (2018).

116. Guerin, C., Olivi, A., Weingart, J. D., Lawson, H. C. & Brem, H. Recent Advances in Brain Tumor Therapy: Local Intracerebral Drug Delivery by Polymers. *Invest. New Drugs* **22**, 27–37 (2004).

117. McDannold, N., Arvanitis, C. D., Vykhodtseva, N. & Livingstone, M. S. Temporary disruption of the blood-brain barrier by use of ultrasound and microbubbles: safety and efficacy evaluation in rhesus macaques. *Cancer Res* **72**, 3652–3663 (2012).

118. Fakhoury, M. Drug delivery approaches for the treatment of glioblastoma multiforme. *Artif Cells Nanomed Biotechnol* **44**, 1365–1373 (2016).

119. Shankar, G. M. *et al.* Genotype-targeted local therapy of glioma. *Proc. Natl. Acad. Sci.* 201805751 (2018).

120. Van Tellingen, O. *et al.* Overcoming the blood–brain tumor barrier for effective glioblastoma treatment. *Drug Resist. Updat.* **19**, 1–12 (2015).

121. Pardridge, W. M. The blood-brain barrier: bottleneck in brain drug development. *NeuroRx* **2**, 3–14 (2005).

122. Gliadel (R) [package insert]. Arbor Pharmaceuticals, LLC, Atlanta, GA; 2013.

123. Attenello, F. J. *et al.* Use of Gliadel (BCNU) wafer in the surgical treatment of malignant glioma: A 10-year institutional experience. *Ann. Surg. Oncol.* **15**, 2887–2893 (2008).

124. Buonerba, C. *et al.* A comprehensive outlook on intracerebral therapy of malignant gliomas. *Crit. Rev. Oncol. Hematol.* **80**, 54–68 (2011).

125. Lin, S. H. & Kleinberg, L. R. Carmustine wafers: localized delivery of chemotherapeutic agents in CNS malignancies. *Expert Rev. Anticancer Ther.* **8**, 343–359 (2008).

126. Khawar, I. A., Kim, J. H. & Kuh, H.-J. Improving drug delivery to solid tumors: priming the tumor microenvironment. *J. Control. Release* **201**, 78–89 (2015).

127. Narita, Y. Bevacizumab for glioblastoma. *Ther. Clin. Risk Manag.* **11**, 1759 (2015).

128. Kim, M. M., Umemura, Y. & Leung, D. Bevacizumab and glioblastoma: Past, present, and future directions. *Cancer J.* **24**, 180–186 (2018).

129. Buahin, K. G. & Brem, H. Interstitial chemotherapy of experimental brain tumors: comparison of intratumoral injection versus polymeric controlled release. *J. Neurooncol.* **26**, 103–110 (1995).

130. Debinski, W. & Tatter, S. B. Convection-enhanced delivery for the treatment of brain tumors. *Expert Rev. Neurother.* **9**, 1519–1527 (2009).

131. Kim, J. E. & Lim, M. The role of checkpoints in the treatment of GBM. *J. Neurooncol.* **123**, 413–423 (7AD).

132. Ampie, L., Woolf, E. C. & Dardis, C. Immunotherapeutic advancements for glioblastoma. *Front Oncol* **5**, 12 (2015).

133. Berghoff, A. S. *et al.* Programmed death ligand 1 expression and tumor-infiltrating lymphocytes in glioblastoma. *Neuro Oncol* **17**, 1064–1075 (2015).

134. Parsa, A. T. *et al.* Loss of tumor suppressor PTEN function increases B7-H1 expression and immunoresistance in glioma. *Nat Med* **13**, 84–88 (2007).

135. Nduom, E. K. *et al.* PD-L1 expression and prognostic impact in glioblastoma. *Neuro Oncol* **18**, 195–205 (2016).

136. Jacobs, J. F. *et al.* Regulatory T cells and the PD-L1/PD-1 pathway mediate immune suppression in malignant human brain tumors. *Neuro Oncol* **11**, 394–402 (2009).

137. El Andaloussi, A. & Lesniak, M. S. An increase in CD4+CD25+FOXP3+ regulatory T cells in tumor-infiltrating lymphocytes of human glioblastoma multiforme. *Neuro Oncol* **8**, 234 (7AD).

138. Garcia-Fabiani, M. B. *et al.* Immunotherapy for gliomas: shedding light on progress in preclinical and clinical development. *Expert Opin. Investig. Drugs* 1–26 (2020). doi:10.1080/13543784.2020.1768528

139. Zeng, J. *et al.* Anti-PD-1 blockade and stereotactic radiation produce long-term survival in mice with intracranial gliomas. *Int. J. Radiat. Oncol. Biol. Phys.* (2013).

140. Belcaid, Z. *et al.* Focal radiation therapy combined with 4-1BB activation and CTLA-4 blockade yields long-term survival and a protective antigen-specific memory response in a murine glioma model. *PLoS One* **9**, e101764 (2014).

141. Scheetz, L. *et al.* Synthetic high-density lipoprotein nanodiscs for personalized immunotherapy against gliomas. *Clin. Cancer Res.* (2020).

142. Reardon, D. A. *et al.* Glioblastoma eradication following immune checkpoint blockade in an orthotopic, immunocompetent model. *Cancer Immunol. Res.* **4**, 124–135 (2016).

143. Sampson, J. H. *et al.* Preliminary safety and activity of nivolumab and its combination with ipilimumab in recurrent glioblastoma (GBM): CHECKMATE-143. *J. Clin. Oncol.* **33**, 3010 (20AD).

144. Meng, Y. *et al.* Expression of TLR9 within human glioblastoma. *J. Neurooncol.* **88**, 19–25 (2008).

145. Deng, S. *et al.* Recent advances in the role of toll-like receptors and TLR agonists in immunotherapy for human glioma. *Protein Cell* **5**, 899–911 (2014).

146. Leng, L., Jiang, T. & Zhang, Y. TLR9 expression is associated with prognosis in patients with glioblastoma multiforme. *J. Clin. Neurosci.* **19**, 75–80 (2012).

147. Wang, C. *et al.* TLR9 expression in glioma tissues correlated to glioma progression and the prognosis of GBM patients. *BMC Cancer* **10**, 415 (2010).

148. Carpentier, A. *et al.* Intracerebral administration of CpG oligonucleotide for patients with recurrent glioblastoma: a phase II study. *Neuro. Oncol.* **12**, 401–408 (2010).

149. Andaloussi, A. El, Sonabend, A. M., Han, Y. & Lesniak, M. S. Stimulation of TLR9 with CpG ODN enhances apoptosis of glioma and prolongs the survival of mice with experimental brain tumors. *Glia* **54**, 526–535 (2006).

150. Meng, Y. *et al.* Successful combination of local CpG-ODN and radiotherapy in malignant glioma. *Int. J. cancer* **116**, 992–997 (2005).

151. Mangsbo, S. M. *et al.* Enhanced tumor eradication by combining CTLA-4 or PD-1

blockade with CpG therapy. *J. Immunother.* (2010).

152. Carpentier, A. F., Xie, J., Mokhtari, K. & Delattre, J.-Y. Successful Treatment of Intracranial Gliomas in Rat by Oligodeoxynucleotides Containing CpG Motifs. *Clin. Cancer Res.* **6**, 2469 LP – 2473 (2000).

153. Jang, S. H., Wientjes, M. G. & Au, J. L.-S. Enhancement of paclitaxel delivery to solid tumors by apoptosis-inducing pretreatment: effect of treatment schedule. *J. Pharmacol. Exp. Ther.* **296**, 1035–1042 (2001).

154. Jang, S. H., Wientjes, M. G., Lu, D. & Au, J. L.-S. Drug Delivery and Transport to Solid Tumors. *Pharm. Res.* **20**, 1337–1350 (2003).

155. Au, J. L.-S. & Wientjes, G. Methods and compositions for enhancing delivery of therapeutic agents to tissues. (2007).

156. Wang, J., Lu, Z., Gao, Y., Wientjes, M. G. & Au, J. L. S. Improving delivery and efficacy of nanomedicines in solid tumors: role of tumor priming. *Nanomedicine* **6**, 1605–1620 (2011).

157. Au, J. L.-S., Panchal, N., Li, D. & Gan, Y. Apoptosis: A New Pharmacodynamic Endpoint. *Pharm. Res.* **14**, 1659–1671 (1997).

158. Lu, D., Wientjes, M. G., Lu, Z. & Au, J. L.-S. Tumor priming enhances delivery and efficacy of nanomedicines. *J. Pharmacol. Exp. Ther.* **322**, 80–88 (2007).

159. Tsai, M., Lu, Z., Wientjes, M. G. & Au, J. L.-S. Paclitaxel-loaded polymeric microparticles: quantitative relationships between in vitro drug release rate and in vivo pharmacodynamics. *J. Control. Release* **172**, 737–744 (2013).

160. Kuh, H.-J., Jang, S. H., Wientjes, M. G., Weaver, J. R. & Au, J. L.-S. Determinants of Paclitaxel Penetration and Accumulation in Human Solid Tumor. *J. Pharmacol. Exp.*

Ther. **290**, 871–880 (1999).

161. Kadiyala, P. *et al.* High Density Lipoprotein-Mimicking Nanodiscs for Chemo-Immunotherapy against Glioblastoma Multiforme. *ACS Nano* (2019).

162. Lindsley, C. W. New 2017 Data and Statistics for Pharmaceutical Products. *ACS Chem. Neurosci.* **9**, 1518–1519 (2018).

163. Roopenian, D. C. & Akilesh, S. FcRn: The neonatal Fc receptor comes of age. *Nat. Rev. Immunol.* **7**, 715–725 (2007).

164. Ljubimova, J. Y. *et al.* Covalent nano delivery systems for selective imaging and treatment of brain tumors. *Adv. Drug Deliv. Rev.* **113**, 177–200 (2017).

165. Hosoya, K., Tomi, M. & Tachikawa, M. Strategies for therapy of retinal diseases using systemic drug delivery: relevance of transporters at the blood–retinal barrier. *Expert Opin. Drug Deliv.* **8**, 1571–1587 (2011).

166. Tanaka, S., Louis, D. N., Curry, W. T., Batchelor, T. T. & Dietrich, J. Diagnostic and therapeutic avenues for glioblastoma: no longer a dead end? *Nat Rev Clin Oncol* **10**, 14–26 (2013).

167. Brahmer, J. R. *et al.* Management of immune-related adverse events in patients treated with immune checkpoint inhibitor therapy: American Society of Clinical Oncology Clinical Practice Guideline. *J. Clin. Oncol.* **36**, 1714–1768 (2018).

168. Maxwell, R., Jackson, C. M. & Lim, M. Clinical Trials Investigating Immune Checkpoint Blockade in Glioblastoma. *Curr. Treat. Options Oncol.* **18**, 51 (8AD).

169. Chappelow, A. V & Kaiser, P. K. Neovascular age-related macular degeneration: potential therapies. *Drugs* **68**, 1029–1036 (2008).

170. Kulkarni, A. D. & Kuppermann, B. D. Wet age-related macular degeneration. *Adv. Drug*

Deliv. Rev. **57**, 1994–2009 (2005).

171. Singh, A. D. Gene- and Cell- Based Treatment Strategies for the Eye. 43–60 (2015).

172. Syed, B. A., Evans, J. B. & Bielory, L. Wet AMD market. *Nat. Rev. Drug Discov.* 1–2 (2012).

173. Lucentis(R) (ranibizumab injection) [FDA package insert]. San Francisco, CA: Genentech, Inc; 2014.

174. Eylea (TM) (aflibercept) [FDA package insert]. Tarrytown, NY; Regeneron Pharmaceuticals, Inc.; 2011.

175. Falavarjani, K. G. & Nguyen, Q. D. Adverse events and complications associated with intravitreal injection of anti-VEGF agents: a review of literature. *Eye (Lond).* **27**, 787–94 (2013).

176. Droege, K. M. *et al.* Adherence to ranibizumab treatment for neovascular age-related macular degeneration in real life. *Graefe's Arch. Clin. Exp. Ophthalmol.* **251**, 1281–1284 (2013).

177. Mu, H. *et al.* Multivesicular liposomes for sustained release of bevacizumab in treating laser-induced choroidal neovascularization. *Drug Deliv.* **25**, 1372–1383 (2018).

178. Ghosh, J. G. *et al.* Long-acting protein drugs for the treatment of ocular diseases. *Nat. Commun.* **8**, 1–10 (2017).

179. Badiee, P. *et al.* Ocular implant containing bevacizumab-loaded chitosan nanoparticles intended for choroidal neovascularization treatment. *J. Biomed. Mater. Res. - Part A* **106**, 2261–2271 (2018).

180. Bertens, C. J. F., Gijs, M., van den Biggelaar, F. J. H. M. & Nuijts, R. M. M. A. Topical drug delivery devices: A review. *Exp. Eye Res.* **168**, 149–160 (2018).

181. Van De Weert, M., Hennink, W. E. & Jiskoot, W. Protein instability in poly(lactic-co-glycolic acid) microparticles. *Pharm. Res.* **17**, 1159–1167 (2000).

182. Baumann, M. D. *et al.* An injectable drug delivery platform for sustained combination therapy. *J. Control. Release* **138**, 205–213 (2009).

183. Stanwick, J. C., Baumann, M. D. & Shoichet, M. S. In vitro sustained release of bioactive anti-NogoA, a molecule in clinical development for treatment of spinal cord injury. *Int. J. Pharm.* **426**, 284–290 (2012).

184. Wang, J., Chua, K. M. & Wang, C. H. Stabilization and encapsulation of human immunoglobulin G into biodegradable microspheres. *J. Colloid Interface Sci.* **271**, 92–101 (2004).

185. Rahimian, S. *et al.* Polymeric microparticles for sustained and local delivery of antiCD40 and antiCTLA-4 in immunotherapy of cancer. *Biomaterials* **61**, 33–40 (2015).

186. Koutsopoulos, S. & Zhang, S. Two-layered injectable self-assembling peptide scaffold hydrogels for long-term sustained release of human antibodies. *J. Control. release* **160**, 451–458 (2012).

187. Mordenti, J. *et al.* Intraocular pharmacokinetics and safety of a humanized monoclonal antibody in rabbits after intravitreal administration of a solution or a PLGA microsphere formulation. *Toxicol. Sci. an Off. J. Soc. Toxicol.* **52**, 101–106 (1999).

188. Li, F., Hurley, B., Liu, Y., Leonard, B. & Griffith, M. Controlled release of bevacizumab through nanospheres for extended treatment of age-related macular degeneration. *Open Ophthalmol. J.* **6**, 54 (2012).

189. Lance, K. D. *et al.* In vivo and in vitro sustained release of ranibizumab from a nanoporous thin-film device. *Drug Deliv. Transl. Res.* **6**, 771–780 (2016).

190. Cossé, A., König, C., Lamprecht, A. & Wagner, K. G. Hot melt extrusion for sustained protein release: matrix erosion and in vitro release of PLGA-based implants. *AAPS PharmSciTech* **18**, 15–26 (2017).

191. Tian, W. M. *et al.* Hyaluronic acid hydrogel as Nogo-66 receptor antibody delivery system for the repairing of injured rat brain: in vitro. *J. Control. Release* **102**, 13–22 (2005).

192. Andrew, J. S. *et al.* Sustained release of a monoclonal antibody from electrochemically prepared mesoporous silicon oxide. *Adv. Funct. Mater.* **20**, 4168–4174 (2010).

193. Schweizer, D., Schönhammer, K., Jahn, M. & Göpferich, A. Protein–polyanion interactions for the controlled release of monoclonal antibodies. *Biomacromolecules* **14**, 75–83 (2012).

194. Adamson, P. *et al.* Single ocular injection of a sustained-release anti-VEGF delivers 6 months pharmacokinetics and efficacy in a primate laser CNV model. *J. Control. Release* **244**, 1–13 (2016).

195. Tyagi, P., Barros, M., Stansbury, J. W. & Kompella, U. B. Light-activated, in situ forming gel for sustained suprachoroidal delivery of bevacizumab. *Mol. Pharm.* **10**, 2858–2867 (2013).

196. Gregoritza, M., Messmann, V., Abstiens, K., Brandl, F. P. & Goepferich, A. M. Controlled antibody release from degradable Thermoresponsive hydrogels cross-linked by Diels–Alder chemistry. *Biomacromolecules* **18**, 2410–2418 (2017).

197. Sousa, F., Cruz, A., Pinto, I. M. & Sarmento, B. Nanoparticles provide long-term stability of bevacizumab preserving its antiangiogenic activity. *Acta Biomater.* **78**, 285–295 (2018).

198. Giannos, S. A., Kraft, E. R., Zhao, Z. Y., Merkley, K. H. & Cai, J. Formulation Stabilization and Disaggregation of Bevacizumab, Ranibizumab and Aflibercept in Dilute Solutions. *Pharm. Res.* **35**, 1–15 (2018).

199. Jain, N. K. & Roy, I. Effect of trehalose on protein structure. *Protein Sci.* (2009).

200. Jain, N. K. & Roy, I. Trehalose and protein stability. *Curr. Protoc. Protein Sci.* (2010).

201. Hadar, J. *et al.* Method matters: Development of characterization techniques for branched and glucose-poly (lactide-co-glycolide) polymers. *J. Control. Release* **320**, 484–494 (2020).

202. Kang, J. & Schwendeman, S. P. Pore Closing and Opening in Biodegradable Polymers and Their Effect on the Controlled Release of Proteins. *Mol. Pharm.* **4**, 104–118 (2006).

203. Liu, L. *et al.* Silicone oil microdroplets and protein aggregates in repackaged bevacizumab and ranibizumab: Effects of long-term storage and product mishandling. *Investig. Ophthalmol. Vis. Sci.* **52**, 1023–1034 (2011).

204. Murillo, R. M. & Martinez, A. *Animal models of brain tumors*. *Rodent Glioma Models: Intracranial Stereotactic Allografts and Xenografts* (Humana Press ; Springer, 2013).

205. FDA Oncologic Drugs Advisory Committee. *Opdivo/Nivolumab Label*. *FDA Label* (2015).

206. Yervoy(R) (ipilimumab) [FDA package insert]. Princeton, NJ: Bristol-Myers Squibb Company; 2011.

207. Postow, M. A., Sidlow, R. & Hellmann, M. D. Immune-Related Adverse Events Associated with Immune Checkpoint Blockade. *N. Engl. J. Med.* **378**, 158–168 (2018).

208. Krieg, A. M. Antitumor applications of stimulating toll-like receptor 9 with CpG oligodeoxynucleotides. *Curr. Oncol. Rep.* **6**, 88–95 (2004).

209. Carpentier, A. F., Auf, G. & Delattre, J.-Y. CpG-oligonucleotides for cancer immunotherapy: review of the literature and potential applications in malignant glioma. *Front Biosci* **8**, e115–e127 (2003).

210. Lollo, G. *et al.* Development of multifunctional lipid nanocapsules for the co-delivery of paclitaxel and CpG-ODN in the treatment of glioblastoma. *Int. J. Pharm.* (2015).

211. Castro, M. G. *et al.* Current and future strategies for the treatment of malignant brain tumors. *Pharmacol. Ther.* (2003).

212. Yesilirmak, N., Ozdemir, E. S. & Altinors, D. D. Effect of dexamethasone intravitreal implant in a corneal graft rejection. *Int. J. Ophthalmol.* **9**, 475–477 (2016).

213. Ozurdex(R) [FDA Package Insert]. Irvine, CA: Allergan; 2014.

214. Pang, C. E., Mrejen, S., Hoang, Q. V., Sorenson, J. A. & Freund, K. B. Association between needle size, postinjection reflux, and intraocular pressure spikes after intravitreal injections. *Retina* **35**, 1401–1406 (2015).

215. Thackaberry, E. A. *et al.* Evaluation of the toxicity of intravitreally injected PLGA microspheres and rods in monkeys and rabbits: Effects of depot size on inflammatory response. *Investig. Ophthalmol. Vis. Sci.* **58**, 4274–4285 (2017).

216. Saltzman, W. M. & Radomsky, M. L. Drugs released from polymers: diffusion and elimination in brain tissue. *Chem. Eng. Sci.* **46**, 2429–2444 (1991).

217. Haller, M. F. & Saltzman, W. M. Localized delivery of proteins in the brain: Can transport be customized? *Pharm. Res.* (1998).

218. Mak, M., Fung, L., Strasser, J. F. & Saltzman, W. M. Distribution of drugs following controlled delivery to the brain interstitium. *J. Neurooncol.* **26**, 91–102 (1995).

219. Kuai, R., Ochyl, L. J., Bahjat, K. S., Schwendeman, A. & Moon, J. J. Designer vaccine

nanodiscs for personalized cancer immunotherapy. *Nat. Mater.* **16**, 489–496 (4AD).

220. Kemper, E. M., Verheij, M., Boogerd, W., Beijnen, J. H. & Van Tellingen, O. Improved penetration of docetaxel into the brain by co-administration of inhibitors of P-glycoprotein. *Eur. J. Cancer* **40**, 1269–1274 (2004).

221. Lam, Y. W. F., Chan, C. Y. J. & Kuhn, J. G. Pharmacokinetics and pharmacodynamics of the taxanes. *J. Oncol. Pharm. Pract.* **3**, 76–93 (1997).

222. Normand-Sdiqui, N. & Akhtar, S. Oligonucleotide delivery: Uptake of rat transferrin receptor antibody (OX-26) conjugates into an in vitro immortalised cell line model of the blood–brain barrier. *Int. J. Pharm.* **163**, 63–71 (1998).

223. Akhtar, S. & Agrawal, S. In vivo studies with antisense oligonucleotides. *Trends Pharmacol. Sci.* **18**, 12–18 (1997).

224. Zlomke, C., Barth, M. & Mäder, K. Polymer degradation induced drug precipitation in PLGA implants–Why less is sometimes more. *Eur. J. Pharm. Biopharm.* **139**, 142–152 (2019).

225. Zhang, X. Controlled release of testosterone and estradiol- 17p from biodegradable cylinders. **29**, 157–161 (1994).

226. Kumar, D. *et al.* Isolation and characterization of degradation impurities in docetaxel drug substance and its formulation. *J. Pharm. Biomed. Anal.* **43**, 1228–1235 (2007).

227. Zhou, J. *et al.* Effect of Manufacturing Variables and Raw Materials on the Composition-Equivalent PLGA Microspheres for 1-Month Controlled Release of Leuprolide. *Mol. Pharm.* **17**, 1502–1515 (2020).

228. Park, T. G. Degradation of poly (D, L-lactic acid) microspheres: effect of molecular weight. *J. Control. Release* **30**, 161–173 (1994).

229. Hu, Y., Daoud, W. A., Cheuk, K. K. L. & Lin, C. S. K. Newly developed techniques on polycondensation, ring-opening polymerization and polymer modification: Focus on poly (lactic acid). *Materials (Basel).* **9**, 133 (2016).

230. Gao, Q., Lan, P., Shao, H. & Hu, X. Direct synthesis with melt polycondensation and microstructure analysis of poly (L-lactic acid-co-glycolic acid). *Polym. J.* **34**, 786–793 (2002).

231. Braun, D., Cherdron, H., Ritter, H. & service), S. (Online. *Polymer Synthesis: Theory and Practice Fundamentals, Methods, Experiments*. *Polymer Synthesis: Theory and Practice Fundamentals, Methods, Experiments* (Springer Berlin Heidelberg : Imprint: Springer, 2001).

232. Shi, N.-Q. *et al.* Microencapsulation of luteinizing hormone-releasing hormone agonist in poly (lactic-co-glycolic acid) microspheres by spray drying. *J. Control. Release* (2020).

233. Zhang, Y., Sophocleous, A. M. & Schwendeman, S. P. Inhibition of peptide acylation in PLGA microspheres with water-soluble divalent cationic salts. *Pharm. Res.* **26**, 1986–1994 (2009).

234. Zhang, Y. & Schwendeman, S. P. Minimizing acylation of peptides in PLGA microspheres. *J. Control. Release* **162**, 119–126 (2012).

235. Doty, A. C. *et al.* Mechanistic Analysis of Triamcinolone Acetonide Release from PLGA Microspheres as a Function of Varying In vitro Release Conditions. *Eur. J. Pharm. Biopharm.* **113**, 24–33 (2017).

236. Witt, C. & Kissel, T. Morphological characterization of microspheres, films and implants prepared from poly (lactide-co-glycolide) and ABA triblock copolymers: is the erosion controlled by degradation, swelling or diffusion? *Eur. J. Pharm. Biopharm.* **51**, 171–181

(2001).

237. Husmann, M., Schenderlein, S., Lück, M., Lindner, H. & Kleinebudde, P. Polymer erosion in PLGA microparticles produced by phase separation method. *Int. J. Pharm.* **242**, 277–280 (2002).

238. Bodmer, D., Kissel, T. & Traechslin, E. Factors influencing the release of peptides and proteins from biodegradable parenteral depot systems. **1**, (1992).

239. Spenlehauer, G., Vert, M., Benoit, J. P. & Boddaert, A. In vitro and in vivo degradation of poly (D, L lactide/glycolide) type microspheres made by solvent evaporation method. *Biomaterials* **10**, 557–563 (1989).

240. Huang, C. L. *et al.* Modulating drug release from poly (lactic-co-glycolic acid) thin films through terminal end-groups and molecular weight. *Polym. Degrad. Stab.* **98**, 619–626 (2013).

241. Alexis, F. Factors affecting the degradation and drug-release mechanism of poly(lactic acid) and poly[(lactic acid)-co-(glycolic acid)]. *Polym. Int.* **54**, 36–46 (2005).

242. Grizzi, I., Garreau, H., Li, S. & Vert, M. Hydrolytic degradation of devices based on poly (DL-lactic acid) size-dependence. *Biomaterials* **16**, 305–311 (1995).

243. Washington, M. A. *et al.* Monomer sequence in PLGA microparticles: Effects on acidic microclimates and in vivo inflammatory response. *Acta Biomater.* **65**, 259–271 (2018).

244. Sun, J., Walker, J., Beck-Broichsitter, M. & Schwendeman, S. P. Characterization of Commercial PLGAs by NMR Spectroscopy. *Submitted* (2020).

245. Qian, H., Wohl, A. R., Crow, J. T., Macosko, C. W. & Hoye, T. R. A strategy for control of "random" copolymerization of lactide and glycolide: application to synthesis of PEG-b-PLGA block polymers having narrow dispersity. *Macromolecules* **44**, 7132–7140 (2011).

246. Masutani, K. & Kimura, Y. PLA synthesis. From the monomer to the polymer. (2014).